MINISTRY OF EDUCATION & TRAINING

LE QUY DON TECHNICAL UNIVERSITY

NGUYEN THI HUYEN

ULTRA-WIDE BAND SIGNAL PROCESSING METHODS FOR POSITIONING BURIED OBJECTS

A Thesis for the Degree of Doctor of Philosophy

HA NOI - 2021

MINISTRY OF EDUCATION & TRAINING

LE QUY DON TECHNICAL UNIVERSITY

NGUYEN THI HUYEN

ULTRA-WIDE BAND SIGNAL PROCESSING METHODS FOR POSITIONING BURIED OBJECTS

A Thesis for the Degree of Doctor of Philosophy

Specialization: Electronic Engineering
Specialization code: 9 52 02 03

SUPERVISORS
1. Assoc. Prof. PHAM THANH HIEP
2. Assoc. Prof. VU VAN SON

HA NOI - 2021

ASSURANCE

I hereby declare that this thesis was carried out by myself under the guidance of my supervisors. The presented results and data in the thesis are reliable and have not been published anywhere in the form of books, monographs or articles. The references in the thesis are cited in accordance with the university's regulations.

Hanoi, Nov. 15th, 2021

Author

Nguyen Thi Huyen

ACKNOWLEDGEMENTS

This work would not have been possible without the support of my colleagues, friends, and mentors. Specifically, I would like to thank my advisors, Assoc. Prof. Pham Thanh Hiep and Assoc. Prof. Vu Van Son for their excellent guidance and generous support throughout my Ph.D course. I am very grateful to have their trust in my ability, and I have often benefited from their insight and advice.

Besides my advisors, my sincere thanks go to my lecturers in Faculty of Radio Electronic Engineering, especially my colleagues in Department of Circuit Theory and Measurement who share a variety of difficulties for me to have more time to concentrate on researching.

Finally but not least, my gratitude is for my family members who support my studies with strong encouragement and sympathy. Especially, my deepest love is for my parents, and two little sons Tien Dung, Tien Son who are always my endless inspiration and motivation for me to overcome all obstacles. Without their invaluable helps, this work would have never been completed.

Author

Nguyen Thi Huyen

TABLE OF CONTENTS

LIST OF ABBREVIATIONS

Abbreviation	Definition
AOA	Angle Of Arrival
AWGN	Additive White Gaussian Noise
CFST	Correlation Function Separation Technique
CWFM	Continuous Wave Frequency Modulation
DS-UWB	Direct Sequence-Ultra-Wide Band
GPR	Ground Penetrating Radar
EIRP	Effective Isotropic Radiated Power
FCC	Federal Communications Commission
IFT	Inverse Fourier Transform
IR- UWB	Impulse Radio Ultra-Wide Band
LFSR	Linear Feedback Shift Register
LMFA	Levenberg-Marquardt Fletcher Algorithm
MSE	Mean Square Error
NDT	Non-Destructive Testing
OOK	On-Off Keying
PAM	Pulse Amplitude Modulation
PPM	Pulse Position Modulation
RF	Radio Frequency

RSSI	Received Signal Strength Indicator
RTLS	Real Time Location System
PN	Pseudo random Noise
PSD	Power Spectrum Density
SNR	Signal to Noise Ratio
TDOA	Time Difference Of Arrival
TH	Time Hopping
TOA	Time Of Arrival
TH-BPSK	Time Hopping- Binary Phase Shift Keying
TH-PPM	Time Hopping- Pulse Position Modulation
UWB	Ultra-Wide Band
UWB-PPM	Ultra-Wide Band-Pulse Position Modulation
UWB-PPM-ATS	Ultra-Wide Band-Pulse Position Modulation-Additional Time Shift
UWB-PST	Ultra-Wide Band-Pulse Shifting Technique
WSN	Wireless Sensor Network

LIST OF FIGURES

LIST OF TABLES

LIST OF SYMBOLS

Symbol	Meaning
$\mathbf{x}$	x vector
$\mathbf{X}$	X matrix
$\mathbf{X}^T$	The transpose of $\mathbf{X}$
$\widehat{X}$	The estimated value of X
$s(t)$	The transmitted signal
$r(t)$	The received signal
pw	The impulse width
T_c	Chip width
N_p	Number of transmitted pulses
η	The path loss exponent
ε	The relative permitivity of environment
λ	The damping factor
$g(t)$	The Gaussian pulse
Z_{ob}, or x_T	The horizontal position of the buried object
d_{ob}, or d_T	The vertical position of the buried object
x_D, or Z_D	The horizontal position of the device
δZ, or δx	The movement step of the device
α	The rotation angle of the device's antenna
τ	The traveling time

μ_p	The time normalization factor of the Gaussian pulse
T_r	The pulse repetition period
T_{PPM}	The time shift associated with binary PPM
ζ	The additional time shift
$R(\tau)$	The correlation function
δ_d	The relative error of estimated distance
$\mathbf{J}$	The Jacobian matrix
∂	The partial derivatives

INTRODUCTION

Motivation

In recent years, studying on non-destructive evaluation have been a burning issue of many research groups. The purpose of the non-destructive testing like soils, concretes, and other materials is to detect and locate the fault structures, buried objects in the evaluated environment. The discovery of the buried objects including cracks by non-destructive evaluation has several benefits in life as used in solving the consequences of war, rescuing trapped victims, and overcoming construction problems.

Various techniques have been developed for buried objects detection, such as acoustic and vibration techniques [4], [5], [6], [7], radio-frequency identification (RFID)/sensor techniques [8], infrared thermography [9], magnetic flux leakage method [10], eddy current technique [11], as well as ground penetrating radar (GPR) [12], [13], [14]. Among these non-destructive techniques, GPR is widely used because it can locate both non-metallic and metallic objects without prior knowledge.

In the GPR systems, the penetration and resolution of the system depend mainly on the signal bandwidth. Traditional systems use a narrow signal frequency band to modulate a sinusoidal carrier signal. The narrow bandwidth makes the information capacity of the radio system

limited. This information capacity is especially essential for radiolocation systems in which the lifetime of the targets is limited. Therefore, narrowband radio systems have practically exhausted the information opportunities in range resolution and target characteristics. To solve this problem, a new radar system was developed to transmit signals with ultra-wide bandwidth (UWB).

For practical purposes, the UWB radar means radio detection and ranging systems which use signal bandwidths greater than 500 MHz to measure distances with spatial resolutions $\Delta r < 30$ cm. Combining the ability of range determination with a fine resolution and the material's penetrating ability of electromagnetic waves can provide a wide range of remote sensing capabilities. The UWB radar generally implied short-range devices that use impulse or continuous wave frequency modulation (CWFM) signals in the range of $0.5 \div 10$ GHz. The non-destructive materials testing radars operate at extremely high frequencies signal from 30 to 300 GHz. UWB radars measure distances by detecting reflected signals with matched filters based on the transmitted signal format. Also, these systems can find hidden objects with a strong electrical contrast to the surrounding medium, such as rebars, pipes, and conduits. To increase the accuracy in distance measurements and the spatial resolution through multiple-layer medium, it is require to find new methods for UWB signal processing for the UWB radar system.

In the literature, several methods for locating buried objects and measuring the electrical properties of materials have been reported. These methods can be classified into inverse electromagnetic problem [15] with

optimization techniques like gradient descent optimization [16], genetic algorithm [17]; radar image processing [18], [19]; the mean square error (MSE) method to estimate buried object parameters [3]. However, the solution of inverse electromagnetic methods is inherently non-unique by virtue of the equivalence principle [20]. The images of underground objects in radar image processing methods heavily depend on the propagation velocity. Hence, the determination of the relative permittivity of the environment is necessary, but the relative permittivity cannot be determined only based on the images. The MSE -based method can calculate the relative permittivity by minimizing the absolute differences between the measured reflection coefficient and the theoretical reflection coefficient. However, in this method, the parameters of the buried object (the depth, the thickness) are frequency dependent, this is inconsistent with the reality. The size of the solution domain in the MSE method is exponentially increased by the number of the unknown parameters, causing large errors. Moreover, for environments with many reflective layers, the estimation of the total reflection coefficient is very complicated.

In general, the position of the target is determined based on the parameters of the reflected signal such as received signal strength index (RSSI), angle of arrival (AOA), time of arrival (TOA) methods [21]. With the AOA method, a common technique to estimate the AOA parameter is to employ multiple antennas in the form of an antenna array. Then the differences in arrival times of an incoming signal at different antenna elements can be used to obtain the AOA information based on the known array geometry. However, for UWB systems, time differ-

ences cannot be represented by phase shifts and both TOA and AOA parameters are based on the time delay but AOA estimation commonly requires multiple antenna elements lead to more complex UWB receiver side [1]. Therefore, timing-related parameters, especially TOA, are commonly preferred for UWB positioning systems. However, the TOA-based positioning method depends strongly on the determination of the delay time of the reflected signal corresponding to the peak of the correlation function. The estimation error of the TOA parameter depends on the transceiver synchronization and the determining correlation peak. In order to increase the accuracy in locating the buried objects and determining the relative permittivity, several signal processing methods applied to transmitted and received UWB signals were proposed. The investigated distance and the position of buried object were determined by analyzing the reflected signal combined with the Gauss-Newton and Lavenberg-Martquardt estimation algorithms.

The proposed methods in this thesis are different from the existing techniques in four ways. Firstly, the bandwidth of the used UWB signals is chosen relatively to the investigated distance. Secondly, by enhancing the UWB signal with pulse position modulation (UWB-PPM), the accuracy of distance measurement in a multi-layer medium (heterogeneous environment) is significantly improved. Thirdly, the objects buried adjacent to each other in a single-layer medium (homogeneous environment) are distinguished and located by using separation of the correlation function and spectrum of the received signal in the impulse radio UWB (IR-UWB) system. Finally, the multi-buried objects in a heterogeneous

environment are located by shifting the transmitted pulse's position with different movements. Different from previous techniques that have been used in position estimation such as lateration, triangulation, multilateration, geometric principles, etc., in this thesis, the non-linear estimation methods such as Gauss-Newton, Lavenberg-Marquardt are applied. Incorporating these methods into the existing UWB GPR designs enhances the accuracy of the buried object locations.

Research Objectives

The research content focuses on signal processing methods with three main objectives listed as follows.

- To evaluate the quality of UWB technology in comparison with others in positioning through simulation systems to show the advantages of using UWB technology.
- To develop the algorithms of estimating the location of buried objects in the homogeneous, heterogeneous environments using the time of arrival, received signal strength methods combined with the modified modulation technique for UWB signals.
- To improve the resolution in positioning the buried objects in the heterogeneous environments, the shifted pulses and correlation separation techniques combined with the non-linear estimation algorithm are applied to UWB signals.

Motivated by the application potentials of UWB-based positioning systems in the non-destructive environments, based on the advantages

of UWB technology, and the extant points of the previous researches; this work proposes the signal processing methods for enhancing the accuracy of locating buried objects, and increasing the resolution and detection distance for UWB positioning systems. The specific objectives of the thesis research can be summarized as follows.

- To evaluate the performance of the distance estimation methods such as received signal strength indicator (RSSI), and time of arrival (TOA) in UWB penetrating systems.
- In order to improve the accuracy of the estimation of propagation distance, a method of enhancing the pulse position modulation techniques with UWB signal, called UWB-PPM-ATS, is proposed.
- To locate multiple buried objects in the homogeneous medium, a novel method based on the correlation function separation combined with the Levenberg-Marquardt called CFST was proposed. In addition, a method of UWB pulses shifting named UWB-PST was proposed for locating multi-buried objects in the heterogeneous environments.

Research areas

- UWB technology, positioning techniques, and mathematical approaches of signal processing.
- Statistical estimation methods such as Gauss-Newton, Levenberg-Marquardt, etc.
- Detection theory and complexity evaluation.

Research method

In this thesis, both the theoretical analysis and the computer simulation are implemented to evaluate the performance of the considered systems.

- The analytical methods are used to process the transmitted and received signals, the correlation function, and the parameters in the estimation model of the proposed systems.
- The computer simulation is applied to validate the analytical results and to make a comparison between the performance of the proposed and other previous systems.

Thesis contribution

In this thesis, the UWB signal processing methods in penetration radar UWB systems are proposed for measuring the distances and locating buried objects in environments such as dry sand, soil, concrete, etc. This model can also be used to probe a wall with different layers of construction materials. The major contributions of the thesis can be summarized as follows.

- To calculate the pulse width and the length of pseudo random noise (PN) sequence (used to modulate UWB signals) relative to the distance/size of the investigated range for improving the accuracy of distance estimation. This contribution is presented in [J1], [J2], and [C2].
- To construct a system model for positioning a single buried object

in a homogeneous environment (single layer) using IR-UWB system. A novel method for positioning multi-buried objectives based on the correlation function separation technique (CFST) combined with the non-linear least square Levenberg—Marquardt is proposed. This contribution is presented in [J5].

- In order to increase the accuracy of measuring the distance, an enhanced ultra-wide band pulse position modulation technique, called UWB -PPM -ATS is proposed and compared with other techniques such as conventional UWB-PPM, UWB- OOK. This contribution is presented in [J4].

- To propose a method of shifting transmitted pulses applied in the UWB system for enhancing the accuracy of locating multiple buried objects in heterogeneous environments (multi-layers) named UWB pulse shifting technique (UWB-PST). This contribution is presented in [J3].

Thesis structure

The thesis is organized in three chapters as follows.

- Chapter 1: Overview of UWB technology

  This chapter presents background knowledge of UWB technology, methods of generating UWB signals, advantages and disadvantages of UWB technology, and the model of a penetrating UWB system used for measuring the distance. In particular, it presents a comprehensive review of recent researches on UWB and buried object

positioning methods, and outlines some challenging issues that promote the contributions of this work in the subsequent chapters. The research objectives and methods in the thesis are also presented in this chapter. The content of this chapter is published in [C2],[J1].

- Chapter 2: Determination of the propagation distance using UWB penetrating system.

  In this chapter, the method of applying RSSI combined with Gauss-Newton algorithm for IR-UWB system to determine the propagation distance and the position of a buried object is proposed. However, due to the rapid attenuation of the signal, this method is only applicable for short-range detection and homogeneous medium. In the heterogeneous medium, to increase the ability of detection of the received UWB signal and thereby increase the accuracy of distance estimation, the UWB-PPM-ATS method is proposed. In the UWB-PPM-ATS method, the position of UWB pulse is modulated by PN sequence with an optimal additional time shift. This makes the error of distance estimation significantly reduced. Performance comparisons between the proposed system and the related ones are provided using numerical and simulation results especially in lossy transmission environments. The results of this chapter are published in [C1], [J2], [J4].

- Chapter 3: Correlation function separation and shifted pulse-based buried objects positioning methods.

  In this chapter, the methods used to locate the buried objects by the

correlation function separation technique, called CFST and pulse shifting technique, named UWB-PST, for UWB systems are proposed. Our analysis indicates that, based on the values of the correlation function of the received UWB signals and the nonlinear estimation method LMF, the characteristics of the environment and the location of buried objects can be determined. The CFST method may be applied to locate the single buried object, and multi-buried objects are close to each other. In addition, the accuracy of positioning multi-buried objects in the heterogeneous medium can be improved by using the UWB-PST. The performance of the UWB systems is assessed by positioning errors. The proposed methods have significantly improved the accuracy of locating buried objects. However, the environment under consideration is limited as the dry medium, and has two layers. The results of this chapter are published in [J3], [J4], [J5].

Chapter 1
OVERVIEW OF UWB TECHNOLOGY

1.1. Introduction to UWB technology

Ultra-wide band (UWB) is a new technology with outstanding features in many applications such as communications, position, medical, and so on. Before 2001, the applications of UWB are limited to military only; since 2002, the Federal Communications Commission (FCC) has gradually allowed commercialization of the UWB frequency bands, making it possible for anyone to use its properties. The FCC controls the frequency range of UWB technology in the US from 3.1 GHz to 10.6 GHz. However, in the European Union, the frequency band is divided into two parts: from 3.4 GHz to 4.8 GHz and from 6 GHz to 8.5 GHz. The UWB's radiated power requirement is very strict and it cannot interfere with previous radio equipments.

Since the first US patent for UWB was proposed in 1973, the field of impulse communication has moved in a new direction. Other applications, such as traffic control, micro-level systems, and water level measurement have also been developed. The US Department of Defense is considered to use the term Ultra-Wide band firstly. Then, UWB standards were developed by IEEE in the form of IEEE 802.15.3 and the high data rate versions IEEE 802.15.3a standards are currently in use.

After 1990, commercial products of UWB technology began to appear, companies like Time Domain and especially Xtreme Spectrum were established around the idea of communication using UWB technology. In 2002, UWB has become a promising technology by FCC in wireless communications with widespread research interests in the World.

According to the definition given by the FCC, the UWB signal is characterized by a very wide bandwidth when compared to conventional, narrow band (NB) signals. A UWB signal is defined as having an absolute bandwidth of at least 500 MHz or a measurement bandwidth ratio of -10 dB greater than or equal to 20%. As indicated in Fig. 1.1, the absolute band is defined as the difference between f_H and f_L at -10 dB:

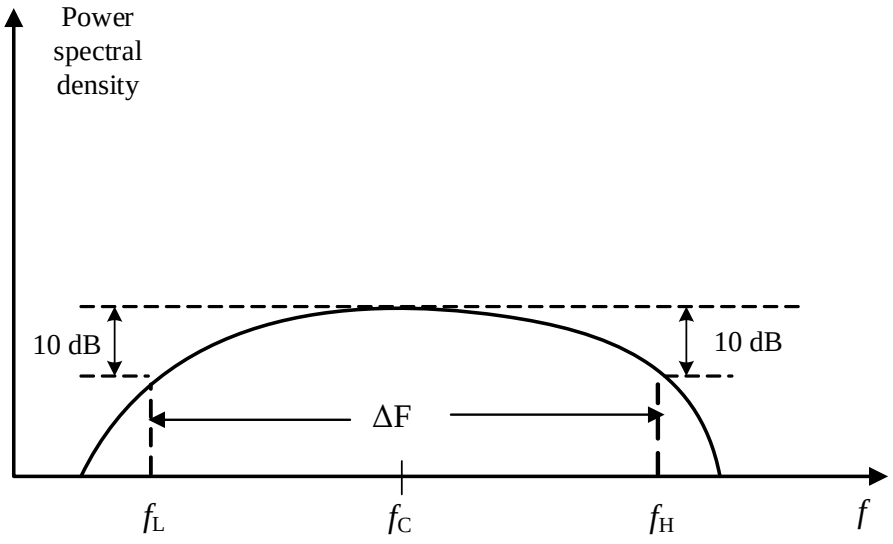

Figure 1.1: Absolute bandwidth of UWB signal [1].

$$\Delta F = f_H - f_L, \tag{1.1}$$

The bandwidth ratio is determined by:

$$B_{frac} = \frac{\Delta F}{f_c}, \tag{1.2}$$

where f_c is the center frequency defined by:

$$f_c = \frac{f_H + f_L}{2}. \tag{1.3}$$

Because UWB signals occupy a very large spectrum and they should be used in existing narrow band systems without causing significant interferences to those systems, a series of rules of UWB systems is regulated by FCC. Accordingly, UWB systems must transmit impulse or non-sinusoidal wave signals below a certain energy level in order to avoid interferences with older systems in the same frequency spectrum. Specifically, the average power spectral density (PSD) shall not exceed -41.3 dBm/MHz on the frequency range of 3.1 to 10.6 GHz and must be lower outside this range depending on the specific application [22]. Fig. 1.2 illustrates the FCC limits for indoor systems.

1.1.1. Applications of UWB technology

In recent years, the rapid development of UWB signaling technologies has been tested on commercial applications from wireless to remote sensing networks, tracking devices, and penetrating radars. In particular, the UWB technology makes major improvements in three wireless applications such as communications, radar, and measurement positioning.

- *UWB technology in communications*

  Communication applications can be divided into two areas: low and

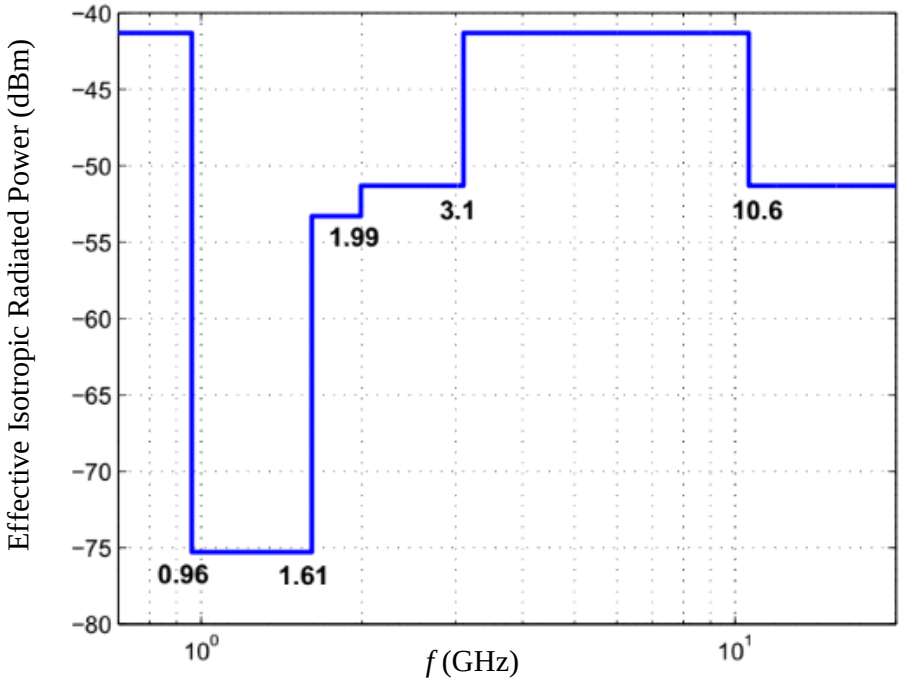

Figure 1.2: The EIRP limits for UWB systems in indoor environments are set by the FCC [1].

high data rates [23]. Both require low power and high capacity, which are typical features of UWB technology. Using UWB and RF techniques with large available bandwidth, UWB communication channels have become feasible.

- *UWB technology in positioning*

  Including UWB technology for locating indoor environment, and for detecting and locating in non-destructive mediums, many advanced techniques and technologies have been introduced for indoor positioning with the high accuracy and reliability. However, these technologies still face many challenges depending on environmental factors and technological limitations.

  Radio frequency (RF)-based positioning technologies have many ad-

vantages over the others [24] which use ultrasonic [25], optical [26] and infrared devices [27]. Both RF narrow band and wide band systems have been implemented for short-range/real-time indoor positioning systems. RF technologies are often used because they have the good ability of penetration, a large coverage area, and reduced hardware costs. In RF technologies, UWB technology has emerged as a viable candidate for pinpointing the position because UWB signals can be used to measure distances with centimeter errors due to the high resolution [28].

In addition, the high-speed data transmission is possible for the ultra-wide bandwidth of the UWB signals. In contrast, the limited channel capacity of narrow band systems leads to unreliability and poor signal quality. Meanwhile, the impulse radio UWB technology (IR-UWB) is one of the common physical layer transmission techniques using the base band propagating UWB pulses with a very narrow pulse (nanoseconds) [29]. The positioning system is based on IR-UWB technology for high accuracy, low complexity implementation and longer battery life, making it a better and more economical option in many applications [30] [31].

- With the material penetration ability of electromagnetic waves, UWB technology can be used in positioning buried objects in non-destructive environments such as in dry ground, concrete, etc. or used to check the perfection of structures such as bridges, pillars, aircraft wings, fuselages, and so on. The research scope of the thesis focuses on

UWB signal processing methods to increase the resolution in locating buried objects in non-destructive structural environments such as dry sand, bricks, etc.

1.1.2. *UWB technology for measuring the distance and positioning buried objects*

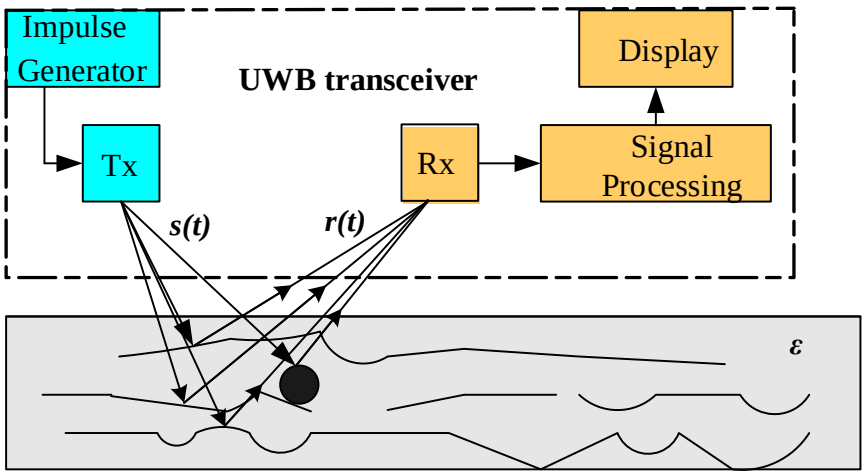

Figure 1.3: The principle of measuring and positioning buried objects with the UWB system.

A system using UWB technology for measuring the distance and positioning buried object is illustrated in Fig. 1.3, where ε is the relative permittivity (dielectric constant) of environment. $s(t)$ denotes the transmitted pulse signal, and $r(t)$ is the received signal with:

$$r(t) = \sum_i r_i(t) + \sum_k r_{kob}(t) + n(t), \tag{1.4}$$

$$r_i(t) = A_i A(d_i) s(t - \tau_i), \tag{1.5}$$

$$r_{kob}(t) = A_{kob} A(d_k) s(t - \tau_{kob}), \tag{1.6}$$

where $r_i(t)$, A_i represent the reflected signal and the reflection coefficient from the boundary between the i^{th} layer and $(i-1)^{th}$ layer, respectively;

$A(d_i)$ is the attenuation of amplitude respect to the penetrated distance d_i; τ_i is the delay time of UWB pulse, also called as the propagation or traveling time. $r_{kob}(t)$, A_{kob} and τ_{kob} are the reflected signal, reflection coefficient at the surface and the traveling time of $r_{kob}(t)$ from the k^{th}-buried object, respectively. $n(t)$ represents the additive white Gaussian noise (AWGN).

In the UWB system, $s(t)$ is generated based on Gaussian [32] or Hermite [33] functions and their derivatives. The Gaussian type is mathematically described by Eq. (1.7) [34] and shown in Fig. 1.4. Comparing

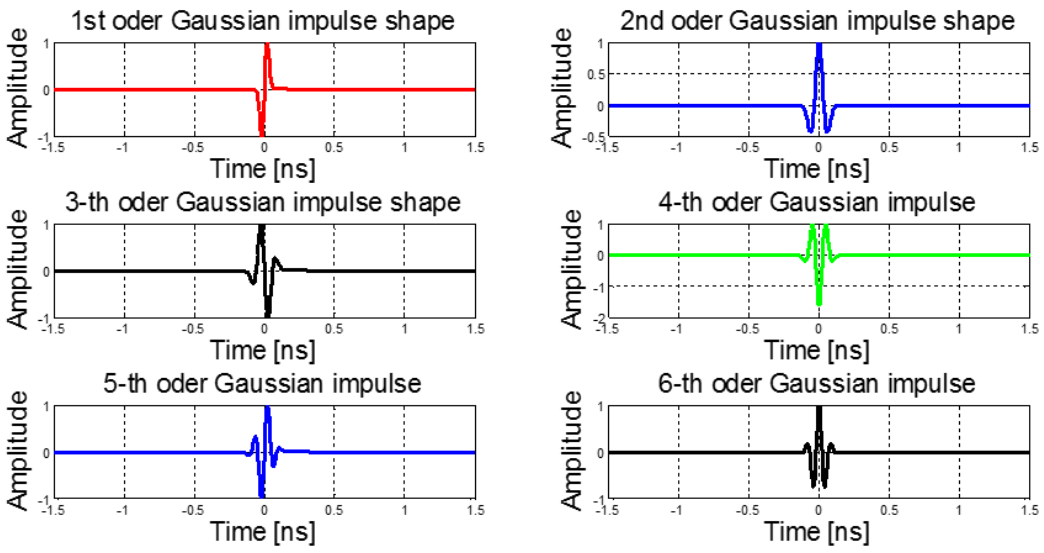

Figure 1.4: The Gaussian pulse shapes.

to Gaussian pulses, the Hermite pulse is useful for parallel data transmission with high data rates, however it is hard to achieve in the real world [35]. Therefore, the UWB signals generated based on Gaussian pulses are applied in this thesis. A typical Gaussian pulse usually takes

the form [32]:

$$g(t) = A_p e^{-2\pi(\frac{t}{\mu_p})^2}, \tag{1.7}$$

where μ_p is a factor which influences the amplitude and the width of Gaussian pulse, also called time normalization factor, the width of a pulse becomes narrower when μ_p reduces. The n^{th} derivative of Gaussian pulse, named n^{th}-order monocycle, is

$$g_n(t) = A_{np} \frac{d^n}{dt^n} e^{-2\pi(\frac{t}{\mu_p})^2}, \tag{1.8}$$

The selected Gaussian pulse shape must met FCC requirements about power and frequency range used and those requirements for the effective isotropic radiated power (EIRP) of transmitted signals are shown in Fig. 1.5 and the PSD is determined by Eq. (1.9).

$$|PSD_n(f)| = A_{np} \left(\frac{(\sqrt{\pi} f \mu_p)^2}{n} \right)^n e^{-(\sqrt{\pi} f \mu_p)^2 + n} \tag{1.9}$$

According to the pulse shapes in Fig. 1.4 and their PSD in Fig. 1.5, the UWB signals used in this thesis restricts on the second-order (see Eq. (1.10)) and the fourth-order (see Eq. (1.11)) Gaussian monocycles; the remaining pulse shapes are used for comparison.

$$g_2(t) = A_{2p} \big[1 - 4\pi \big(\frac{t}{\mu_p} \big)^2 \big] e^{-2\pi(\frac{t}{\mu_p})^2}, \tag{1.10}$$

$$g_4(t) = A_{4p} \left[-12\pi + 96\pi^2 \left(\frac{t}{\mu_p} \right)^2 - 64\pi^3 \left(\frac{t}{\mu_p} \right)^4 \right] e^{-2\pi.\left(\frac{t}{\mu_p}\right)^2}. \tag{1.11}$$

1.1.3. Modulation techniques for the UWB signals

A sequence of UWB signal pulses can be generated by Gaussian pulses (commonly referred to as IR-UWB single pulse) or modulated according to different modulation types. General modulation techniques used

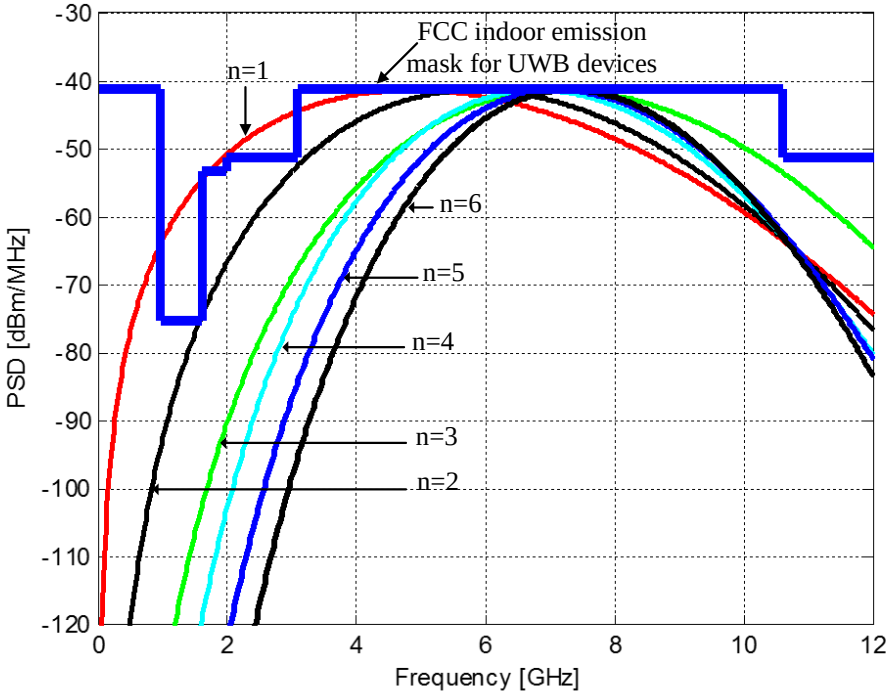

Figure 1.5: The PSD of the different derivatives of Gaussian pulses.

for UWB signals include pulse amplitude modulations (PAMs), On-Off Keying (OOK), and pulse position modulation (PPM) [36]. In addition, using time hopping sequence (TH) to create TH-PPM, TH-BPSK signal types [2]; direct sequence UWB (DS-UWB) [37] or designing a generator circuit which generates the 4-th and 5-th order derivatives of Gaussian pulses in TH-QPSK system [38] are also used. Each modulation technique has a different application range, the choice of suitable modulation configuration not only increases the efficiency of the system implementation, maximizes the benefits of ultra-wide bandwidth, but also reduces the complexity of the system.

The forms of IR-UWB, TH-PPM, TH-BPSK, and DS-UWB signals

are described in the Eqs. (1.12) to (1.15) and shown in Fig. 1.6.

$$s_{IR}(t) = \sqrt{P} \sum_{i=0}^{N_p} g(t - iT_r), \tag{1.12}$$

$$s_{TH-BPSK}(t) = \sqrt{P} \sum_{i=0}^{N_p} p_i g(t - iT_r - c_i T_c), \tag{1.13}$$

$$s_{TH-PPM}(t) = \sqrt{P} \sum_{i=0}^{N_p} g(t - iT_r - c_i T_c - p_i T_{PPM}), \tag{1.14}$$

$$s_{DS}(t) = \sqrt{P} \sum_{i=0}^{N_p - 1} p_i g(t - iT_c), \tag{1.15}$$

where P, T_c, p_i are the transmit power, chip width, and $i-$th component

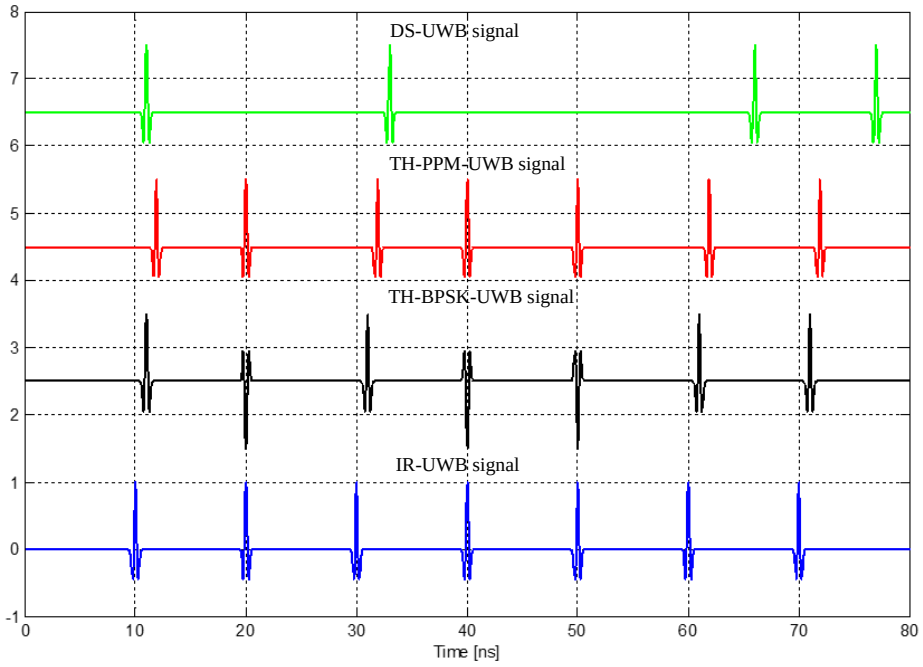

Figure 1.6: The shapes of modulated UWB signals with PN sequence of 1010011 and the 4^{th}-order Gaussian pulse.

of a pseudo random noise (PN) sequence with the length of N_p (N_p also is the number of transmitted pulses with IR-UWB signal), respectively; $g(t)$ is Gaussian pulse; T_r is the repetitive period of the pulse; $p_i \in$

$\{1, -1\}$ with TH-BPSK UWB signal and $p_i \in \{0, 1\}$ with TH-PPM UWB signal; and T_{PPM} is the time shift associated with PPM signal; c_i represents the TH code. In communications technology, p_i in TH-PPM and TH-BPSK is data bit; while in the positioning application, p_i is the component of the PN sequence, which is used to change the timing of the corresponding UWB pulse. The PN sequence is typically generated by a Linear Feedback Shift Register (LFSR), also known as a Linear Sequence Shift Register [39]. The TH code is also pseudo random sequence, so it is also denoted by the PN sequence.

In the distance measurement systems using UWB technology, for improving the processing time and reducing the mean distance measuring error, the UWB modulated signals are used. Besides that, the spreading sequences play an important role in determining the penetrating distance of UWB system because they decide the properties and ranging performance of the system. The errors of estimated distance becomes smaller as the length of the PN sequence used in the UWB system increases [40], [41]. However, with a longer PN sequence length, the processing of distance estimation algorithm takes longer time. Hence, the PN sequence length should be changed in accordance with the detectable distance to optimize the processing time of the system.

1.2. The UWB system model used for investigating and positioning buried objects

Various systems are used in positioning such as the Global Positioning System (GPS) [42], the indoor location system [43], etc. To detect buried

objects in environments such as underground, brick, concrete, etc., penetrating radar systems are used very commonly. The investigated environments are classified into homogeneous and heterogeneous environments. A homogeneous medium is understood here as a single-layer with the constant relative permittivity, or in other words, the wave-propagation velocity in this medium is constant. A heterogeneous medium is one with many layers of different dielectric constants and wave propagation velocities. An illustrative example of a homogeneous and heterogeneous medium is shown in Fig 1.7. In this figure, d_i, ε_i are respectively the depth and the relative permittivity corresponding to the i^{th} layer, and Layer 0 is free space with $\varepsilon = 1$.

In addition, the receiving (Rx) antenna is placed beside the transmitting (Tx) antenna in a monostatic radar configuration [42][43]. The monostatic configuration means the transmitting and receiving antennas are the same, or are aligned along the perpendicular to the surface of the probed region. The transmitting and receiving antennas are located close to each other and should be ensured a high electromagnetic decoupling between antennas. The reflection from the surface of the border of transmitter and medium to the receiver is easily eliminated by placing transceiver antennas close to the surface of the environment. Accordingly, the reflected signals from the surface was rejected during the signal processing, only the reflected signals with the time delay after that was considered.

To describe the distance measurement procedure, let us consider a UWB system model with a homogeneous environment as illustrated in

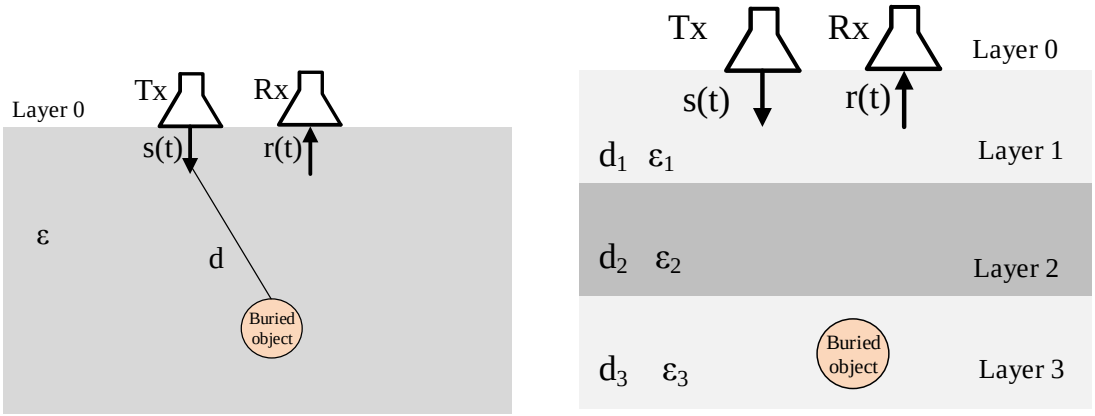

Figure 1.7: The homogeneous (a) and the heterogeneous (b) mediums

Fig. 1.8. In this model, the UWB pulse is modulated by a PN sequence. With the IR-UWB signal, the PN sequence are not used.

The transmitted signal $s(t)$ goes through an environment with the relative permittivity of ε. The reflected (scattered) signals from the buried object are captured by the receiving antenna. Both the Tx and Rx antennas are directional to maintain an illumination area that is smaller than the transverse area of the buried object.

The distance can be estimated by the delay (traveling) time denoted by τ and calculated from the maximum value of $R(\tau)$:

$$R(\tau) = \int_{-\infty}^{\infty} r(t)\omega(t-\tau)dt. \tag{1.16}$$

$\omega(t)$ is the reference signal at the receiver which is $g(t)$ with IR-UWB and TH-BPSK UWB [44], $g(t) - g(t - T_{PPM})$ with PPM and TH-PPM UWB [45]. So the traveling time is:

$$\tau = \text{Arg}\max_{\tau}\{\text{R}(\tau)\}. \tag{1.17}$$

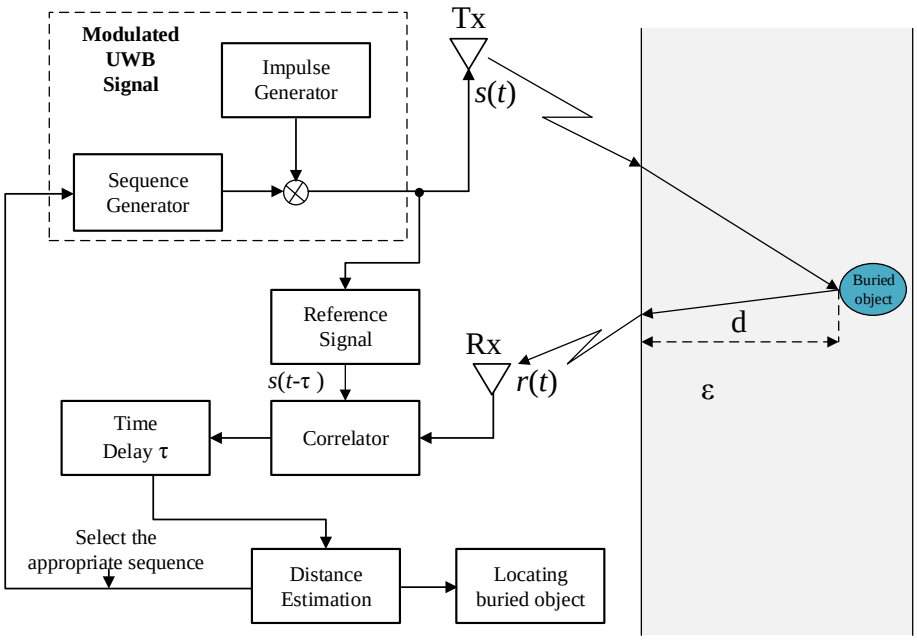

Figure 1.8: The block diagram of the distance estimation configuration using UWB technology.

Because the traveling time of signal is twice propagation time from the transceiver antenna to the buried object, hence the depth d is given by [46]:

$$d = \frac{c\tau}{2\sqrt{\varepsilon}}. \tag{1.18}$$

The waveform and cepstrum (results from taking the inverse Fourier transform (IFT) of the logarithm of the estimated spectrum of a signal [47]) of the received signal can be shown in Fig. 1.9.

For each distance value of d, PN sequence has an optimal length denoted as N_{opt}. The optimum criterion here is the minimum length of the PN (TH) sequence while ensuring that the error of estimated distance is within allowed ranges. The method of determining N_{opt} is proposed in research [C2] and is named the adaptive length of the ranging distance,

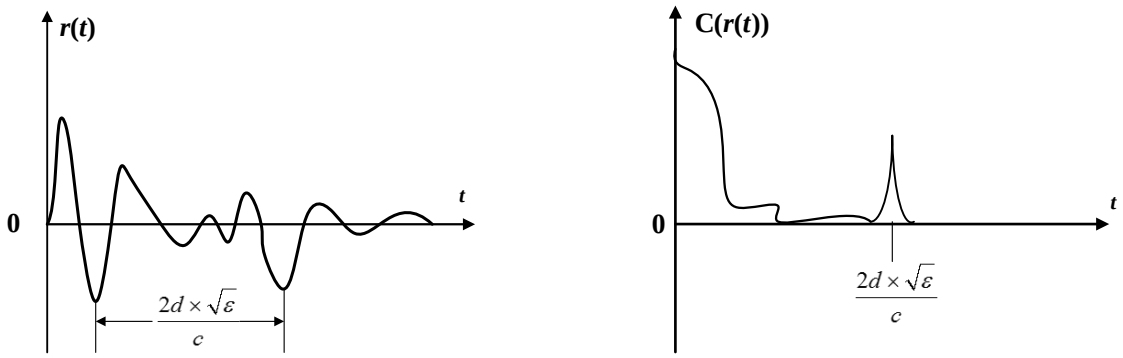

(a) The received signal waveform. (b) The cepstrum of received signal.

Figure 1.9: The received signal waveform (a) and cepstrum (b).

or called the linear searching method and shown in Fig. 1.10.

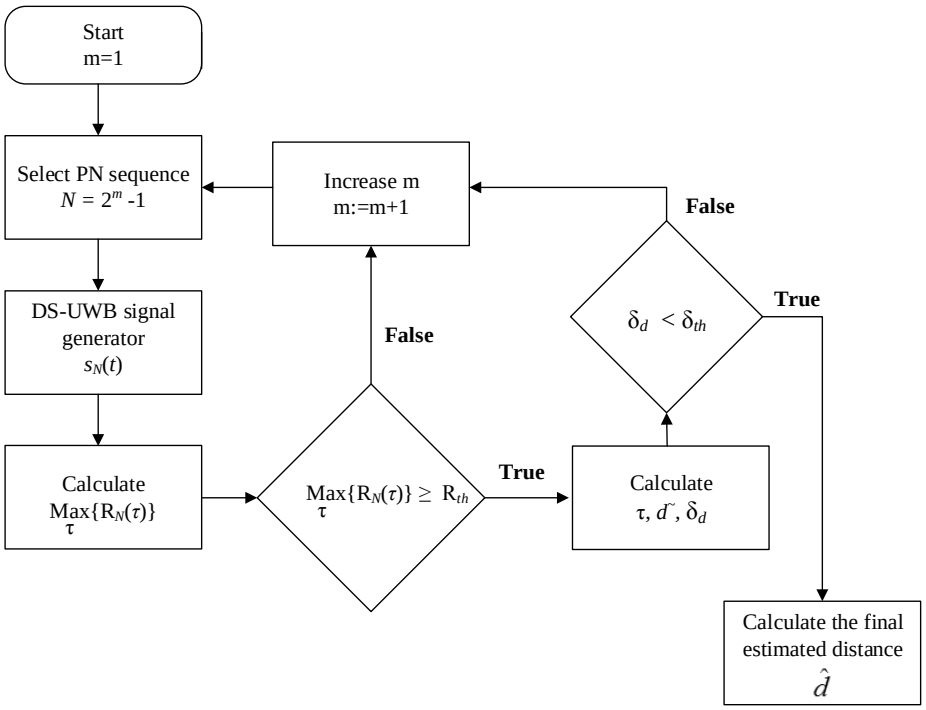

Figure 1.10: The algorithm of searching PN (TH) sequence length and estimating distance.

The searching is started with the shortest sequence (length of PN sequence equal three) and increase the length one-by-one. The maximum value of the correlation function $R_N(\tau)$ is calculated according to the

length of the PN sequence, τ, and compared with the threshold value R_{th} which is set with a false alarm probability of 0.01 of radar system [48]. This threshold value is calculated by the depth of buried object (usually using the ideal value of the correlation function). If the maximum value of $R_N(\tau)$ is larger than R_{th}, the estimation of delay time $\hat{\tau}$ is obtained as below.

$$\hat{\tau} = \arg\max_{\tau}\{R_N(\tau)\}, \tag{1.19}$$

Otherwise, the comparison procedure resumes with a longer PN sequence and newly transmitted signal $s_{DS}(t)$. Once a delay time is calculated, the depth $\tilde{d}$ of buried object is estimated according Eq. (1.18). To achieve a more accurate distance estimate, the standard deviation δ_d of the K distance estimates is compared with a certain threshold δ_{th} (δ_{th} is chosen equal to 2% the maximum detectable range [49]). If δ_d is less than δ_{th}, the final distance estimate $\hat{d}$ and the minimum length of PN sequence are determined; otherwise, the searching process is repeated with increasing m by 1.

This PN sequence are used to modulate the transmitted signal, and to determine the depth of buried object. By using the PN sequence with minimum length, the data processing time of system can be reduced. The results of the calculation of the PN sequence length according to the penetration depth of the UWB signal with the investigated medium as sand dry are shown in the Fig. 1.11. In addition, to increase the accuracy of distance estimation in a homogeneous environment, a variable impulse width method for the IR-UWB penetrating system is proposed in [J1]

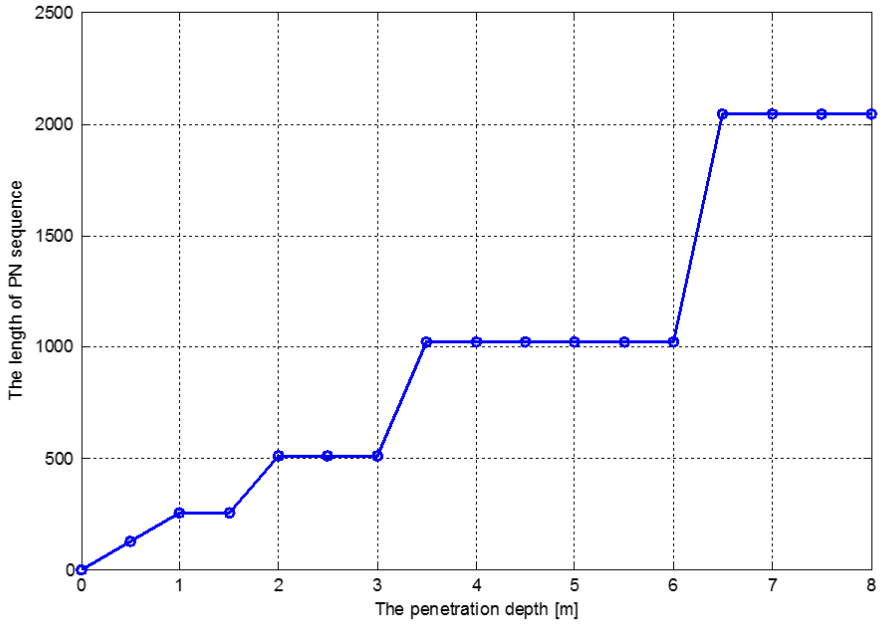

Figure 1.11: The spreading sequence length according to the penetration depth in the sand dry environment.

and the results are illustrated in Fig. 1.12.

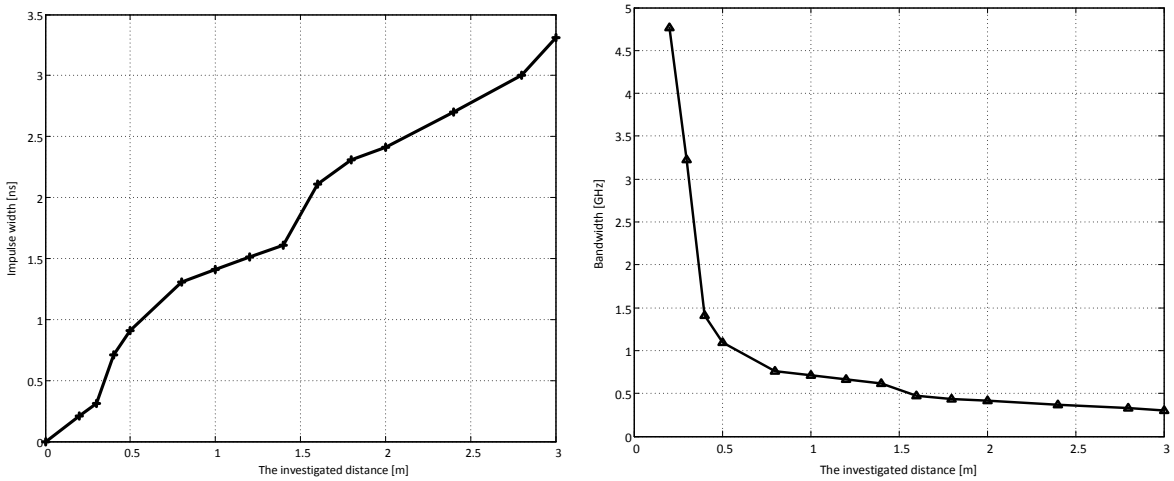

(a) (b)

Figure 1.12: The width of impulse (a) and the bandwidth (b) according to the investigated distance

1.3. Evaluation of positioning systems using UWB technology

The performance of the positioning UWB systems is evaluated based on the positioning error. This error is estimated by averaging the absolute differences between the estimated result and the actual value of the penetrated distances, and has the form:

$$\Delta d = \frac{1}{K}\sum_{k=1}^{K} \mid \hat{d}_k - d_0 \mid, \tag{1.20}$$

where $\hat{d}_k$ is the estimated distance calculated from the traveling time corresponding to the k^{th} transmitted pulse, and d_0 is the actual distance, K is the number of the transmitted pulses. In addition, the relative error is often used to evaluate the accuracy of measurements, and is defined as follows.

$$\delta d(\%) = \frac{1}{K}\sum_{k=1}^{K} \frac{\mid \hat{d}_k - d_0 \mid}{d_0} \times 100\%. \tag{1.21}$$

An example of a comparison between the UWB signal types used to measure the same distance in a homogeneous medium with a dielectric constant of $\varepsilon = 2.5$ (dry sand) [50] is shown in Fig. 1.13. In this figure, the relative errors of estimated distances in the DS-UWB with a suitable PN sequence are less than 5% of the actual distance. For example, the average error is about 0.042 m at the depth of 5 m. In comparison with the IR-UWB system, the DS-UWB and TH-BPSK system are more accurately detect the received signal for multiplication of impulses by PN sequence. As a result, the average of the estimation errors in DS-UWB and TH-BPSK systems is smaller than IR-UWB ones.

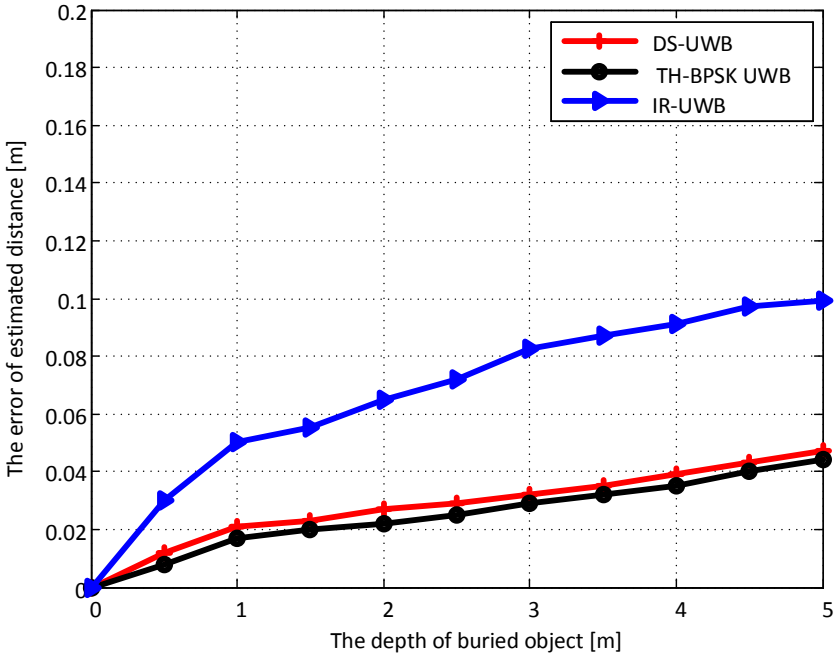

Figure 1.13: The errors of estimated distances of the different UWB systems.

In the following chapters of the thesis, UWB signals are applied to locate the buried objects in 2-D space. The performance of these systems are assessed in terms of the positioning error in the same way.

1.4. The related works

UWB is an effective technology in both high-speed communications and high-resolution measurements. UWB-based measuring techniques used to resolve three main purposes: propagation distance determination, non-destructive evaluation, and the buried object location. The thesis focuses on researching UWB applications in measuring distance and locating buried objects by non-destructive techniques.

1.4.1. The related studies abroad

Research and development in the domain of UWB technology [51], especially for target data collection, accurate locating, and tracking applications, have been received great interests in the recent years [52]. With the high spatial resolution ranging, the UWB-based penetration system is one of the potential candidates for the non-destructive testing (NDT). There are many systems of locating and detecting buried objects, in which the most popular one could be penetrating radar systems; for example, the ground penetrating radar (GPR) [12] [13]. Some other methods are also used for locating underground buried objects likes magnetic flux leakage [10], acoustic methods [6], [7], laser Doppler multi-beam differential vibration sensor for acoustic detection of buried objects [53]. To make the identification of targets much easier, the machine learning method using sparse whitened non-negative matrix factorization [54] can be used. Furthermore, the positioning accuracy is improved by using a model of 2-D reduction convolutional neural networks with unsupervised score-based bounding box regression combined with a non-maximum suppression algorithm [55]. In addition, with underwater medium, the detection of buried objects in shallow sea with large bandwidth and low frequency electromagnetic waves proposed in [56] can overcome the limitations of acoustic waves and blue-green lasers.

The resolution and detection distance of the non-destructive techniques which are used in the penetrating systems strongly depend on the signal shapes, the system bandwidth, and the material of the buried ob-

jects (plastic or metal) as well as information of environmental properties (relative permittivity). In the above mentioned systems, the UWB GPR systems have been applied extensively to detect the subsurface objects, locate buried pipes and utility installations in the construction industry [57], [58], [19], and investigate concrete structures for determination of reinforcing bar locations, air voids, and the quality of concrete [59], etc. The distance and position of buried objects can be determined by the UWB GPR in a short-range based on processing scanned images and measuring the reflected signals. Hence, the performance of UWB GPR system depends mainly on the method of the received signal processing. They can provide a high image resolution and efficient data processing when using reverse domain conversion techniques [60], or using wide band chaotic signals based on time domain correlation and back-projection algorithm [61], or other methods depending on the purpose of measuring distances or non-destructive testing, or positioning buried objects.

For the purpose of measuring the propagation distance, techniques for determining distance between radiating objects in multi-path wireless power delivery environments were proposed in [62]. In addition, to increase the accuracy, various modulation techniques were used for UWB signals such as PAMs, OOK, PPM [36], TH-PPM, TH-BPSK [2] and TH-QPSK [38]. Each modulation technique has a different application range. A simple peak detection based on a non-coherent UWB receiver was proposed in [63] for low data rate wireless sensor networks (WSN) and IoT applications. This approach has improved receiver performance

with TH-PPM UWB signals. Furthermore, to reduce the complexity of the TH-UWB receiver, in [64], a channel shortening equalizer design method was proposed based on an eigen filter using a new objective function, whereby the proposed system has dramatically reduced the power of channel impulse response, spectral distortion, multi-access interference and noise power, etc. Therefore, different UWB signal modulation types have considerably affected the quality and application of the UWB system.

In those modulation techniques, the PPM technique is one of the widely used configurations in UWB systems. Studies on UWB-PPM in wireless communication networks mainly focus on solutions to reducing the conflicts in multi-user access systems. For example, Zhao in [65] proposed an M-ary PPM modulation configuration for the UWB (M-PPM) system indicated that this system has significantly improved performance compared to systems using direct spreading sequences in the environments with a low signal to noise (SNR) ratio. In [66], Vinod Venkatesan et al. proposed the application of a direct spreading sequence with the optimized UWB-PPM technique for multi-access systems. Their method reduced the impact of multi-access interferences (MAI) as well as significantly reduced the floor error compared to the orthogonal signal configuration at a large SNR ratio. In addition, several studies on improving the quality of the receiver for UWB-PPM signals presented in [67] [68] [69]. The combination of PPM symbols and time of arrival (TOA) estimation algorithm using the Sub-Nyquist IR-UWB signal in the IR-UWB device was discussed in [70]. Turbo codes for

PPM-IR UWB signals to improve the PSD power signal density [71], and randomizing the pulses to improve the UWB system [72] were proposed. In the thesis, the UWB-PPM technique with an optimal time shift was proposed for the penetration system to increase the detection capability and the accuracy in measuring distance and positioning buried objects.

For testing purposes, material penetrating systems using UWB technology to examine non-destructive environments were discussed in [73], [74], the results indicated that these system can detect imperfect structures of metal. Furthermore, the estimation of the layer's thickness based on the processing of the GPR's data with the optimized techniques (such as neural networks) was discussed in [75], [76].

For locating purposes, UWB indoor positioning systems were presented in [30], [77], [43] to exploit two-way flight time for the distance determination. As a result, the transceiver location based on Pozyz inner algorithm with a range accuracy of 320 $\pm$ 30mm was computed [77]. The UWB and IEEE 802.15. 4 radios with nonlinear Bayesian filters can be used to estimate distances and position nodes by RSSI in WSN networks in [78], [79]. In the range-based localization systems, the position of a sensor node can be estimated by using lateration, or trilateration, or multilateration technique [80], [81]; however, these techniques are not applicable to locate buried objects in penetrating systems. In underground environment, to locate personnel in coal mines, the time difference of arrival (TDOA) algorithm was proposed for the UWB wireless sensor network in [82], and this system can achieve high-precision positioning

in real-time. The existence of the buried object can be detected using the GPR scan [83], [13] or combined with the spectral analysis of the radar data [84]. In [3], buried object characteristics (the depth, thickness, and frequency-dependent permittivity) were determined by measuring the reflection coefficient with the buried object using the mean square error (MSE) method.

1.4.2. The domestic studies

In Vietnam, there are several studies on through-wall radar imaging of Tang el al in [85], [86]. In these papers, in order to process and reconstruct received images for wall clutter mitigation, a sparse Bayesian learning [85] and a matrix completion [86] were proposed. In fact, the authors worked with the received images and their methods aimed to improve quality of the received scenes. That can be considered as a final step of signal processing. In addition, the Faster-RCNN framework for the detection of underground buried objects (hyperbola reflections) in B-scan GPR images was proposed in [87]. Due to the lack of real data for training, their method used radargrams simulated from different configurations using the GPRMax toolbox and could provide significant improvements compared to classical computer vision methods. Besides, the solution to extend the bandwidth for antennas used in GPR systems was proposed by Vo Chung Ha et al. in [88], with the use of the proposed antenna's structure, the bandwidth of GPR system is extended at 900 MHz.

Further more, to the best of my knowledge, I have not found any other

research groups in Vietnam which study on the properties of investigated medium (soil, concrete) using radio waves.

1.4.3. Research objectives of the thesis

From the above analysis, when using UWB technology for measuring distance, non-destructive testing, positioning buried objects, it is the most important to develop a suitable signal processing method for the improvement of system performance.

The thesis focuses on the methods of processing UWB signals for measuring distances and locating buried objects. Distance measuring techniques in free space such as RSSI and TOA were proposed for measuring the penetration depth with penetrating UWB systems in [C1], [J1]. In [J1], the solution of changing the impulse width of the UWB signal adaptively with the investigated depth was proposed. In addition, to increase the accuracy of penetration distance measurements, the system using DS-UWB signal with a variable PN sequence length was proposed in [C2]. These researches were applied for the homogeneous investigated environments. With the heterogeneous environments, in order to increase the ability of accurate detection of the reflected UWB signal and thereby increase the accuracy of distance estimation, a UWB PPM technique with an optimal additional time shift, called UWB-PPM-ATS was proposed in [J4].

For the positioning purpose, in the methods based on radar image processing, the images of underground objects heavily depend on the propagation velocity or the relative permittivity of medium. Hence, in

signal processing of these systems, to increase the accuracy, the determination of the relative permittivity of the environment is necessary, but the relative permitivity cannot be determined only based on the images. Using the MSE method, the frequency-dependent permittivity can be estimated, however, the convergence of MSE algorithm is highly dependent on the chosen adaptation step. Moreover, in the case of a heterogeneous medium with multiple layers, the estimation of the reflection coefficient is very complicated.

Different from previous studies, the thesis proposed two estimation methods: the correlation function separation technique (CFST) combined with Levenberg-Marquardt algorithm for locating nearby buried objects in the homogeneous medium and UWB pulse shifting technique (UWB-PST) for locating the multi-buried objects in the heterogeneous medium. The CFST method can be used to locate and distinguish the adjacent buried objects and improve the resolution of the penetrating systems [J5]. Also, with the UWB-PST proposed in [J3], the accuracy of locating multi-buried objects in heterogeneous environments is significantly improved.

In summary, the thesis proposed novel UWB signal processing methods applied for IR-UWB and modulated UWB signals to increase the accuracy of measuring penetration distance and locating buried objects. The proposed methods were used in positioning a single and multiple buried objects in the homogeneous, and heterogeneous environments. The results of the proposed methods were performed by mathematical analysis and simulation using Matlab software. The performance of

proposed systems are evaluated by the positioning errors in comparison with the actual values and with conventional systems. Furthermore, these methods can be used for non-destructive testing to determine the quality, integrity of materials, probing a wall with different layers of construction materials, and locating buried objects such as detecting the locations of underground cables, water pipes, etc.

1.5. Summary

This chapter presents background knowledge of UWB technology, methods of generating UWB signals, advantages and disadvantages of UWB technology, and the model of a penetrating UWB system used for measuring the distance. In particular, it presents a comprehensive review of recent researches on UWB and buried object positioning methods, and outlines some challenging issues that promote the contributions of this work in the subsequent chapters. The research objectives and methods in the thesis are also presented in this chapter.

Chapter 2
DETERMINATION OF THE PROPAGATION DISTANCE USING UWB PENETRATING SYSTEM

To determine the propagation distance using electromagnetic waves, the parameters related to the distance between the target and the transceiver such as the time of arrival (TOA), the angle of arrival (AOA), receiver signal strength indicator (RSSI), etc. need to be calculated. In addition, the distance also can be determined based on the channel model [89], and the Friis transmission equation [62]. In the propagation environments like free space, indoors, the distance measuring methods based on TOA, AOA, RSSI provide a high accuracy [90]. However, for other transmission mediums such as soils, concrete, etc. due to the dielectric characteristics of the transmission medium, the AOA based method is difficult to be applied, and TOA and RSSI based methods can be applied with certain assumptions about environment.

The method of determining propagation distances in a well-known characteristic medium was presented in Section 1.2. However, in many practical applications, the penetrating system operates with a prior unknown environment. The methods of determining distances in an unknown homogeneous environment by RSSI and TOA, and localizing objects by the nonlinear estimation method Gauss-Newton are described in detail in this Chapter. In addition, to increase the accuracy in de-

termining distances in heterogeneous environments, an enhanced pulse position modulation technique for UWB signal, called UWB-PPM-ATS was proposed. The results in this chapter were presented in the papers [C1], [J2], [J4].

2.1. Analysis of a UWB penetrating system

Consider a detection and localization system using UWB technology illustrated in Fig. 2.1. The investigated medium is heterogeneous with

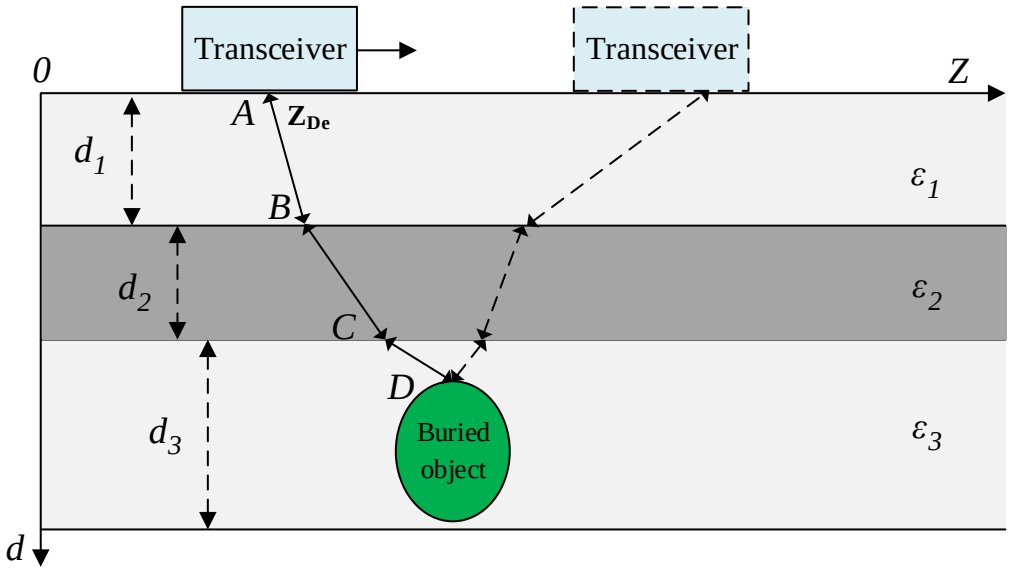

Figure 2.1: The penetrating UWB system.

three layers, whose thickness and relative permittivities are d_1, d_2, d_3 and ε_1, ε_2, ε_2, respectively. The penetrating system operates by transmitting UWB signals into the investigated medium and receiving the reflected pulses as they encounter discontinuities. The discontinuity could be a boundary or interface between materials with different dielectrics or it could be a subsurface of the buried object. As seen in Fig. 2.1, the

UWB signal propagates from point $A \rightarrow B \rightarrow C \rightarrow D$ and reflected backwards from D to A, and the propagation distance of the signal equal to $2(AB + BC + CD)$. The strength of the received signals or their corresponding arrival times can be used to calculate the location of the discontinuity (layer thickness and the position of buried object). This section solves the first problem in positioning technique: determining the transmission distance which is the thickness of the layers in the investigated environment.

In Fig. 2.1, the transmitted signal is a sequence of UWB pulses, which are IR-UWB pulses $s(t)$, takes the form:

$$s(t) = \sqrt{P} \sum_{i=0}^{N-1} g(t - iT_r), \tag{2.1}$$

where $g(t)$ is the impulse signal (Gaussian monocycle) with repetition period T_r, and P is the transmitted power of the impulse. The transmitted waveform is normalized as bellow.

$$B_s \int_{-\infty}^{\infty} g^2(t)dt = B_s \int_{-\infty}^{\infty} |G(f)|^2 df = 1, \tag{2.2}$$

with B_s is the occupied bandwidth of the waveform and $G(f)$ is the Fourier transform of $g(t)$. In general, the received signal $r(t)$ is presented as in Eq. (1.4).

In this model, any distorted effects that antennas and channels introduce in UWB communication are removed from consideration. Based on the parameters of the received signal, the propagation distance can be determined based on the value of traveling time or RSSI as indicated in Fig. 2.2. In the procedure of distance estimation, if the traveling time

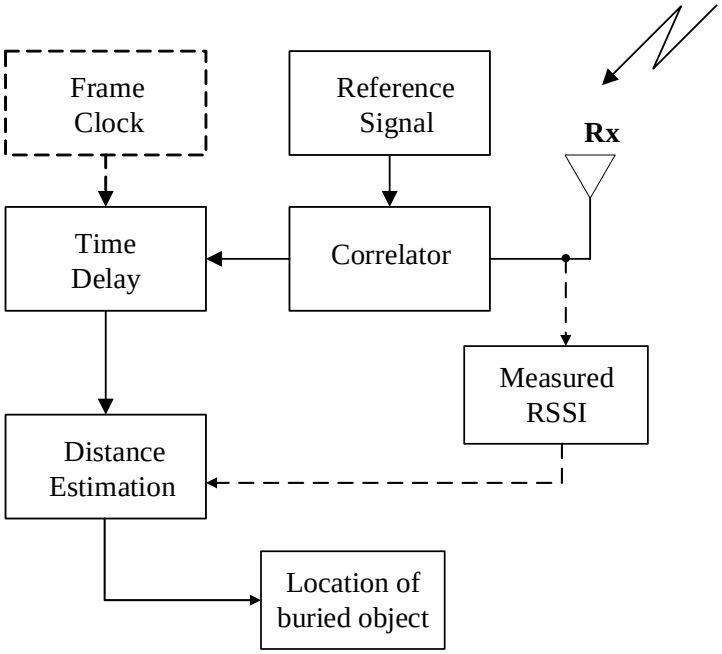

Figure 2.2: Block diagram of distance estimation procedure in the UWB system.

is used, the received signal is fed to the *Correlator* to calculate the time delay and estimate the distance; and if RSSI is used, the received signal is fed to the *Measured RSSI* and the distance is estimated.

2.2. Determination of the propagation distance based on RSSI

2.2.1. Evaluation of RSSI ranging performance

In the penetrating system, the propagation distance is the distance from the transceiver to the buried object with the homogeneous medium, and is the sum of propagation distances through the layers with the heterogeneous medium (see Fig. 2.1). Those distance are estimated by RSSI as follows.

$$d = \frac{1}{2} \times 10^{\left(\frac{P_{Tx}-RSSI}{10\eta}\right)}[m]. \tag{2.3}$$

where P_{Tx}[dBm] is transmitted power, the factor $1/2$ for the case of the

transmit and receive antennas at the same location, so that the distance from the transmitter to the discontinuity point and then reflected back to the receiver is twice the actual distance from the transceiver to the buried object.

According to Eq. (2.3), the value of d is completely determined if η is known. The error of estimated distance depends on the estimated value of η, which is denoted by $\hat{\eta}$, and is calculated as follows.

$$e_d = \hat{d} - d = \frac{1}{2} \times 10^{\left(\frac{P_{Tx} - RSSI}{10\hat{\eta}}\right)} - d[m]. \tag{2.4}$$

The relation between the error of estimated distance with $\hat{\eta}$ is as shown in Fig. 2.3, where the actual value of d is calculated for $\eta = 3$ and $P_{Tx} = -5.4$ [dBm] [91]. Fig. 2.3 indicates that the error of estimated distance depends on the distances d and $\hat{\eta}$, when $\hat{\eta}$ is lower than η, the negative range errors occur and vice versa. In order to obtain $|e_d| < 5cm$ at the range of 80 cm, η has to be estimated with an accuracy of ± 0.5. Hence, the accuracy of path loss exponent estimation is very important for more accurate distance estimation.

The propagation distance and the path loss exponent η of the transmission medium are estimated by the Gauss-Newton algorithm.

2.2.2. Gauss-Newton method

The Gauss-Newton method is used to estimate the path loss exponent and the location of the buried object by using RSSI. To describe the Gauss-Newton method, let us consider a scenario with a circular buried object with radius R in a homogeneous environment with the path loss

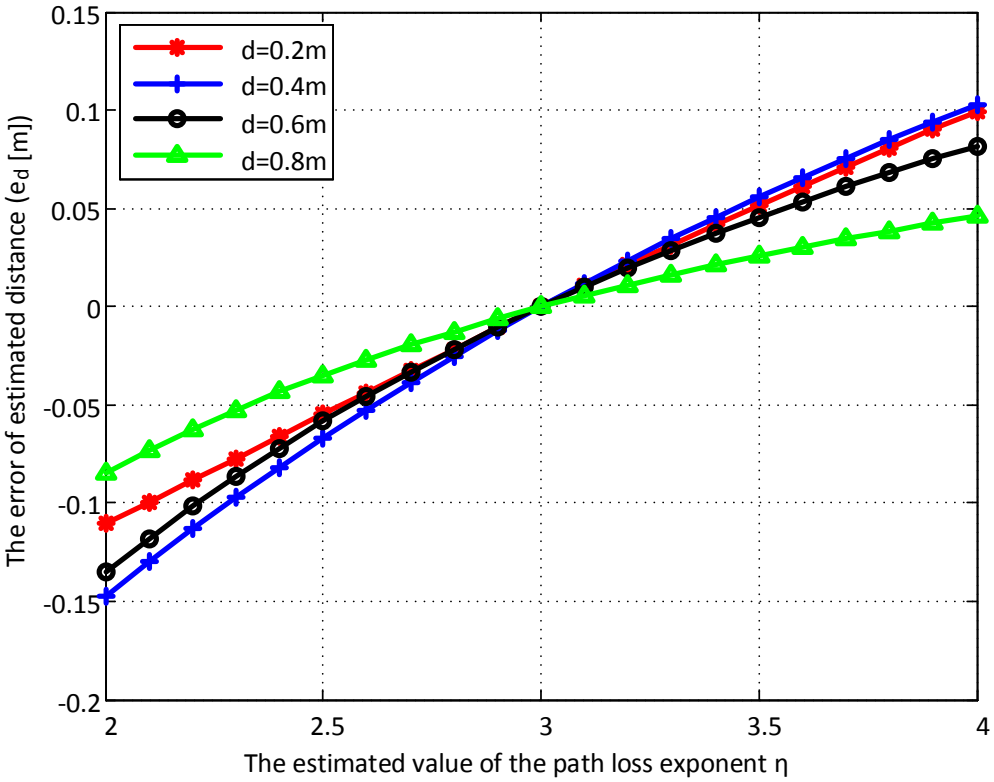

Figure 2.3: The error of estimated distance according to different values of $\hat{\eta}$ for specific distances d from the buried object to the UWB transceiver.

exponent η as shown in Fig. 2.4. In this figure, the position of buried object is defined by coordinates of (Z_{ob}, d_1), and (Z_{ob}, d_2) in the 2-D space, Z_{ob} is the coordinate at the center of the object, and the radius is $R = (d_2 - d_1)/2$. The transceiver antennas is set at position of $(Z_{De}, 0)$. To determine the path loss exponent and the location of buried object, the UWB transceiver transmits and receives UWB signals while moving along the Z-direction, and measures the RSSI in each movement step. The propagation distance is determined by RSSI as explained in previous section. Its value depends on the position Z_{De} of the device and is

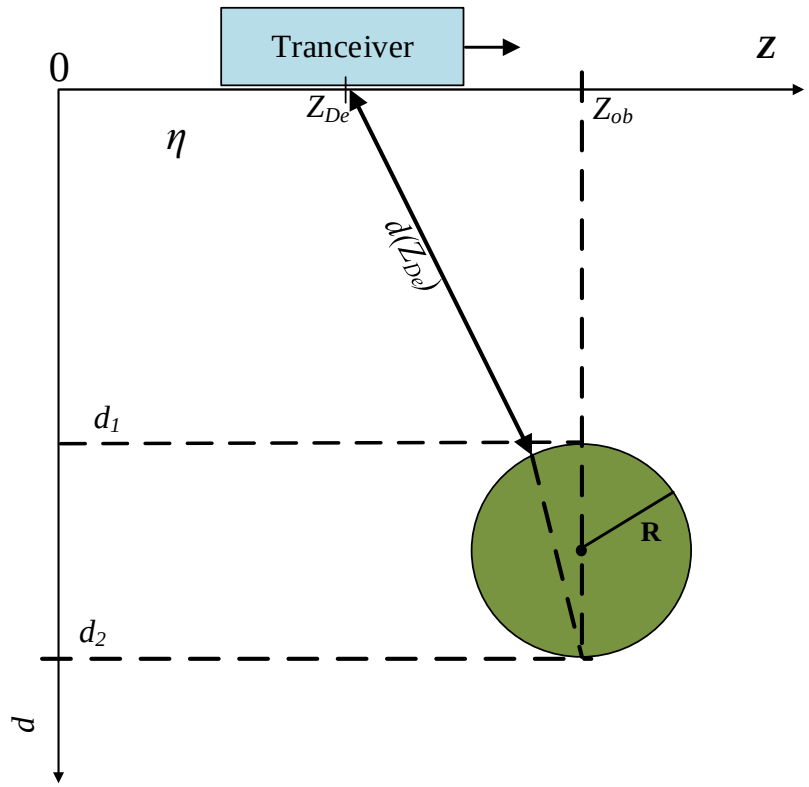

Figure 2.4: A scenario with a circular buried object.

denoted as $d(Z_{De})$ can be approximately equal to:

$$d(Z_{De}) \approx \left(\frac{d_1}{d_2} \sqrt{d_2^2 + (Z_{De} - Z_{ob})^2} \right), \tag{2.5}$$

The parameters Z_{ob}, d_1, d_2 and η of the system in Fig. 2.4 are assigned as elements of the vector $\mathbf{r} = (Z_{ob}, d_1, d_2, \eta)$, and estimated so that the deviation function reaches the minimum value, that is:

$$\widehat{\mathbf{r}} *_{op} = \arg\min_{\mathbf{r}} \left\{ \left(\mathbf{d} - \widehat{d}(Z_{De}, \widehat{\mathbf{r}}) \right)^2 \right\}, \tag{2.6}$$

where $\widehat{\mathbf{r}} = (\widehat{Z_{ob}}, \widehat{d}_1, \widehat{d}_2, \widehat{\eta})$, and $\widehat{d}(Z_{ob}, \widehat{\mathbf{r}})$ is given by:

$$\widehat{d}(Z_{De}, \widehat{\mathbf{r}}) \approx \frac{\widehat{d}_1}{\widehat{d}_2} \sqrt{\widehat{d}_2^{\,2} + \left(Z_{ob} - \widehat{Z}_{De} \right)^2}. \tag{2.7}$$

From Eqs. (2.3) and (2.7), Eq. (2.6) is rewritten as follows.

$$\widehat{\mathbf{r}}*_{op} = arg\min_{\mathbf{r}}\left\{\frac{1}{2}\times 10^{\frac{P_{Tx}-RSSI(Z_{De})}{10\widehat{\eta}}} - \frac{\widehat{d}_1}{\widehat{d}_2}\sqrt{\widehat{d}_2{}^2 + \left(Z_{ob}-\widehat{Z}_{De}\right)^2}\right\}^2. \quad (2.8)$$

The cost function is defined as:

$$E(\widehat{\mathbf{r}}) = \sum_{i=1}^{N}\left\{\frac{1}{2}\times 10^{\frac{P_{Tx}-RSSI(Z_{Dei})}{10\widehat{\eta}}} - \frac{\widehat{d}_1}{\widehat{d}_2}\sqrt{\widehat{d}_2{}^2 + \left(\widehat{Z}_{ob}-Z_{Dei}\right)^2}\right\}^2, \quad (2.9)$$

where N is the number of movements of the device (number of RSSI measurements). The value of vector $\widehat{\mathbf{r}}*_{op}$ can be estimated by the Gauss-Newton method with the calculation steps as follows.

Step 1: *Initialize parameters*

The elements of vector $\mathbf{r}$ are assigned to any non-negative value (usually zero values).

Step 2: *Update the parameter values*

In each iteration, the value of vector $\mathbf{r}$ is updated as:

$$\widehat{\mathbf{r}}^{k+1} = \widehat{\mathbf{r}}^{(k)} + \Delta^{(k)}, \quad (2.10)$$

where:

$$\Delta^{(k)} = \left(\mathbf{J^T J}\right)^{-1}\mathbf{J^T E}(\widehat{\mathbf{r}}^{(\mathbf{k})}), \quad (2.11)$$

$\mathbf{J}$ is the Jacobian matrix:

$$\mathbf{J} = \left[\frac{\partial E\left(\widehat{\mathbf{r}}^{(k)}\right)}{\partial \widehat{d}_1}, \frac{\partial E\left(\widehat{\mathbf{r}}^{(k)}\right)}{\partial \widehat{d}_2}, \frac{\partial E\left(\widehat{\mathbf{r}}^{(k)}\right)}{\partial \widehat{Z}_{ob}}, \frac{\partial E\left(\widehat{\mathbf{r}}^{(k)}\right)}{\partial \widehat{\eta}}\right]. \quad (2.12)$$

Step 3: *Check the stop condition*

If the cost function has the minimum value, the algorithm stops and produces the estimated results. Otherwise, the algorithm repeats from Step 2. The Gauss–Newton algorithm may converge slowly or not at

all if the initial guess is far from the minimum [92]. Therefore, for any initialization value, the estimated results are obtained after a certain number of iterations.

The parameter for Matlab simulation is summarized as follows. The center frequency and bandwidth of UWB system in this case are 5 GHz, $\Delta F = 2$ GHz, respectively. The transmitted power of the selected system is -5.4 dBm [91]. The Gauss-Newton method was used to estimate the path loss exponent and location of the buried object by using RSSI and TOA of reflected signals. The simulation results are obtained after 50 iterations, and shown in Table 2.1 (including absolute and relative errors calculated by the Eq. (1.20)) and Fig. 2.5. The errors of the RSSI and TOA-based method are calculated by Eq. (1.19). These errors include the error in the calculation of RSSI (or TOA) and the Gauss-Newton method error.

Table 2.1: Comparing the estimated results of penetrating UWB system using RSSI and TOA method.

Parameter	Actual value	RSSI-based method	TOA- based method	Error of RSSI method	Error of TOA method
η	3	3.3568	2.9959	0.3568 (11.9%)	0.0041 (0.2%)
d_1 [m]	0.5	0.4384	0.4713	0.0616 (12.3%)	0.0287 (5.7%)
d_2[m]	0.6	0.6923	0.6551	0.0923 (15.4%)	0.0551 (9.1%)
R[m]	0.05	0.1270	0.0919	0.077 (152%)	0.0419 (8.4%)
Z_{ob} [m]	0.6	0.6830	0.6532	0.083 (13.8%)	0.0532 (8.9%)

According to Table 2.1 and Fig. 2.5, it can be seen that by using the Gauss-Newton nonlinear estimation method for the RSSI and TOA of the penetration UWB system, the path loss exponent of propagation medium and the location of the buried object can be determined. The

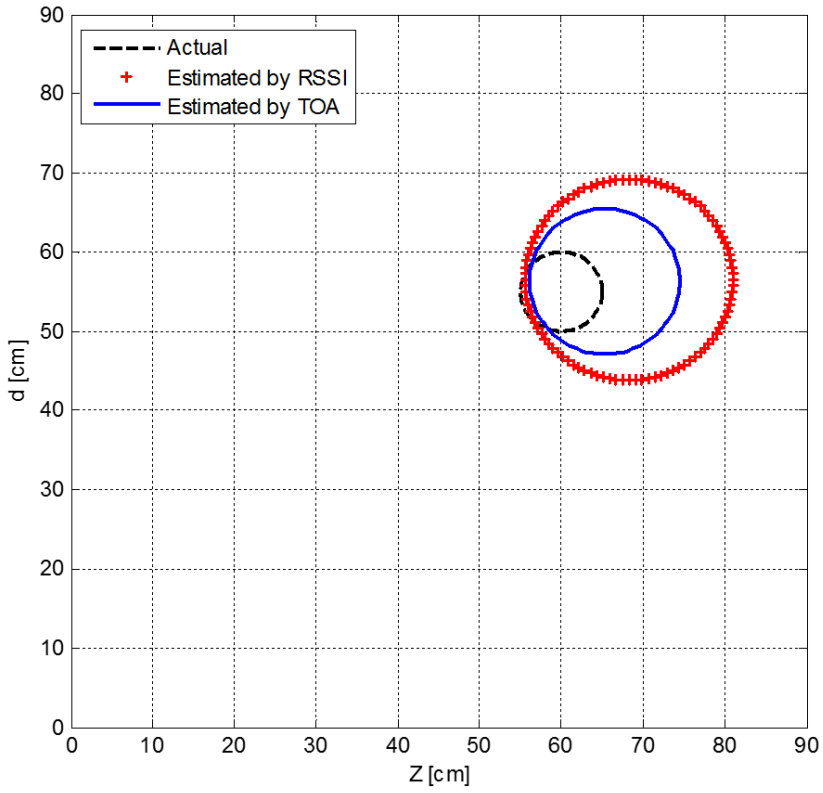

Figure 2.5: The estimated values by RSSI and TOA.

simulation results are in accordance with the evaluation of RSSI and TOA-based methods to determine the propagation distances in free space in [90]. In addition, due to low cost, low power consumption and simple hardware, the development of RSSI method is simpler and unnecessary to strictly synchronize as for TOA method. However, RSSI should be applied to short distance, and the dry and homogeneous investigated environment because the UWB signal attenuates rapidly.

The distance estimation based on RSSI and TOA methods is applied to the homogeneous medium. However, with the heterogeneous medium, the reflected UWB signal's shapes are significantly changed

compared with the transmitted signals. Besides, in the multi-path transmission environment, the difficulty in distance measurement is due to the fact that many incoming reflection paths in different time periods affect the estimation of TOA parameter. In order to accurately estimate TOA parameter, the first incoming signal path was used to determine TOA [93] [21]. In additional, to increase the ability of the correct detection of the reflected UWB signal, modulation techniques for the UWB signal are applied, including the pulse position modulation UWB-PPM. The PPM modulation is widely applied to the UWB system, in communication, PPM means the pulse position carries the information transmitted. However, in distance measuring and positioning UWB-PPM systems, to create the UWB-PPM signal, the UWB signal is modulated by the PN sequence. The accuracy of UWB-PPM positioning system depends significantly on the system parameters, such as pulse shift, the movement of device, investigated distance, etc. Hences, to improve the accuracy of UWB-PPM system, the pulse position modulation technique with an optimal pulse shift is proposed. This technique is described in detail in the Section 2.3.

2.3. Proposal of UWB-PPM with an additional time shift

The conventional UWB-PPM signal is given as in Eq. (2.13) with p_i being the i^{th} component of a PN sequence, and $p_i \in \{0, 1\}$.

$$s(t) = \sum_{i=1}^{N} g(t - iT_r - p_i T_{PPM}), \tag{2.13}$$

with T_r is the repetitive period of the pulse, and T_{PPM} is the time shift associated with PPM signal.

It can be seen that the time shift T_{PPM} directly affects the quality of UWB-PPM systems, the performance of system can be improved by selecting the appropriate value of the time shift. In order to increase the accuracy of the distance estimation by using the UWB-PPM system, the time shift in the UWB-PPM scheme should be selected so that the ability of correct detecting the reflected UWB pulse is the best. To accomplish this task, in UWB-PPM systems with the invariant time shift T_{PPM}, this time shift is adjusted with a certain time constant to achieve its optimal value. The optimal value of T_{PPM} is known as the value at which the UWB-PPM system gives the smallest error of distance estimation. Hences, a UWB pulse position modulation with the additional time shift (UWB-PPM-ATS) technique is proposed to improve the accuracy of the UWB system. In the proposed technique, the pulse position is changed with a time constant denoted by ζ. The signal of UWB-PPM-ATS is given as:

$$s(t) = \sum_{i=1}^{N} g(t - iT_r - p_i(T_{PPM} + \zeta)), \tag{2.14}$$

The sign '+' in Eq. (2.14) means the algebraic additions so ζ can take either positive or negative values. The effect of ζ on the quality of the system will be evaluated later.

Examples of the conventional UWB, UWB-PPM and UWB-PPM-ATS signal shapes are illustrated in Fig. 2.6. This figure shows a UWB signal modulated by PN sequence with 7 samples of 1001110, it adopts the fourth derivative of the Gaussian function $g_4(t)$. Whereby, when the value of p_i is 0, the transmitter sends out a pulse $g_{40}(t)$ as the original

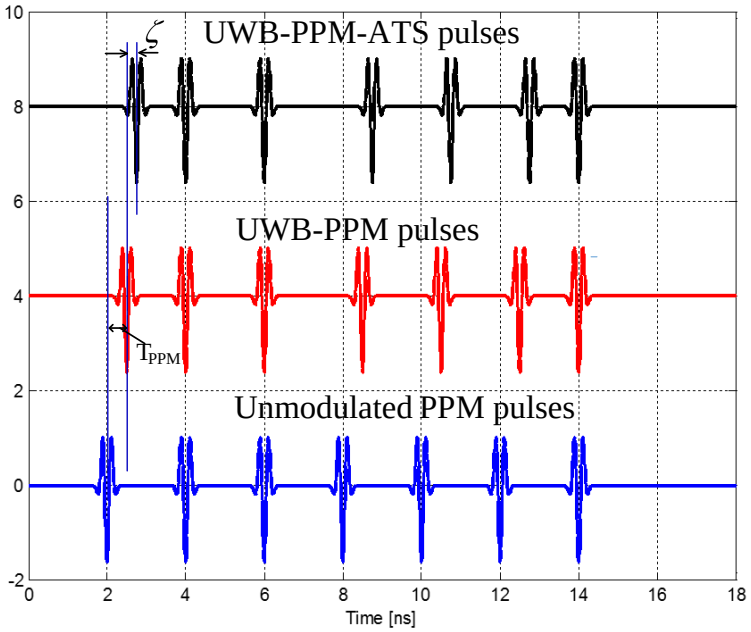

Figure 2.6: Pulse position of modulated UWB signal with PN=1001110.

pulse (without any change from the un-modulated pulse), when the value of p_i is 1, the transmitter sends out a pulse $g_{41}(t)$ which is the original pulse with a time shift of T_{PPM}. For the proposed UWB-PPM-ATS, the new shift level is set to $(T_{\text{PPM}} + \zeta)$ instead of the normal T_{PPM} time shift.

2.3.1. Distance estimation procedure

The propagation distance is estimated based on the correlation function by Eq. (1.16). With the conventional UWB-PPM scheme, the template waveform at the receiver is $g_4(t) - g_4(t - T_{\text{PPM}})$, and in the UWB-PPM-ATS scheme, the template waveform is $g_4(t) - g_4(t - T_{\text{PPM}} - \zeta)$.

The correlation of those scheme is:

$$R_0(\tau) = \int_{-\infty}^{\infty} r(t)\Big[g_4(t) - g_4(t - T_{\mathrm{PPM}})\Big]dt, \tag{2.15}$$

$$R_1(\tau) = \int_{-\infty}^{\infty} r(t)[g_4(t) - g_4(t - T_{\mathrm{PPM}} - \zeta)]dt. \tag{2.16}$$

The autocorrelation function of the fourth-order Gaussian monocycle denoted by $R_{G4}(\tau)$ is defined as the following:

$$R_{G4}(\tau) = \int_{-\infty}^{\infty} g_4(t)g_4(t - \tau)dt. \tag{2.17}$$

So

$$R_0(\tau) = R_{G4}(\tau) - R_{G4}(\tau - T_{\mathrm{PPM}}), \tag{2.18}$$

$$R_1(\tau) = R_{G4}(\tau) - R_{G4}(\tau - T_{\mathrm{PPM}} - \zeta). \tag{2.19}$$

The shapes of $R_{G4}(\tau)$,$R_0(\tau)$ and $R_1(\tau)$ are shown in Fig. 2.7. This figure indicates the autocorrelation function of the fourth-order Gaussian monocycle $R_{G4}(\tau)$ (a) and correlation functions $R_0(\tau)$ of UWB-PPM, and $R_1(\tau)$ of UWB-PPM-ATS system (b). These functions are compared together at the value of $\tau = 0$. In the Fig. 2.7 (b), the values of $R_0(\tau)$, $R_1(\tau)$ with $\zeta = -0.08$ ns, and $R_1(\tau)$ with $\zeta = +0.08$ ns are presented. It can be observed that the choice of $\zeta = -0.08$ ns makes $R_1(\tau)$ gets the maximum value at $\tau = 0$ and this value is greater than $R_1(0)$ with the value of $\zeta = +0.08$ ns, and also $R_0(0)$. Thus, the correlation function of the received signal changes according to the different values of ζ.

From Fig. 2.7 (b) and Eqs. (2.20), (2.21), ζ is selected to adjust the maximum value of $R_1(\tau)$ beyond the maximum value of $R_0(\tau)$. Thus ζ

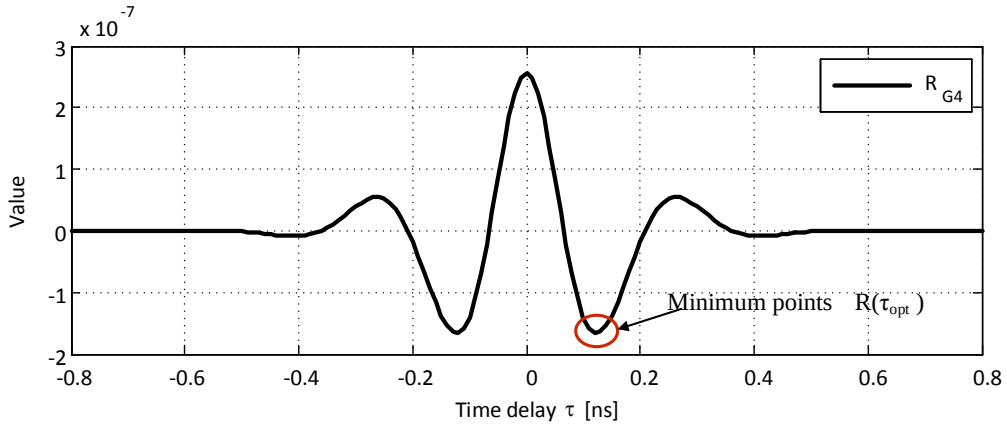

(a)

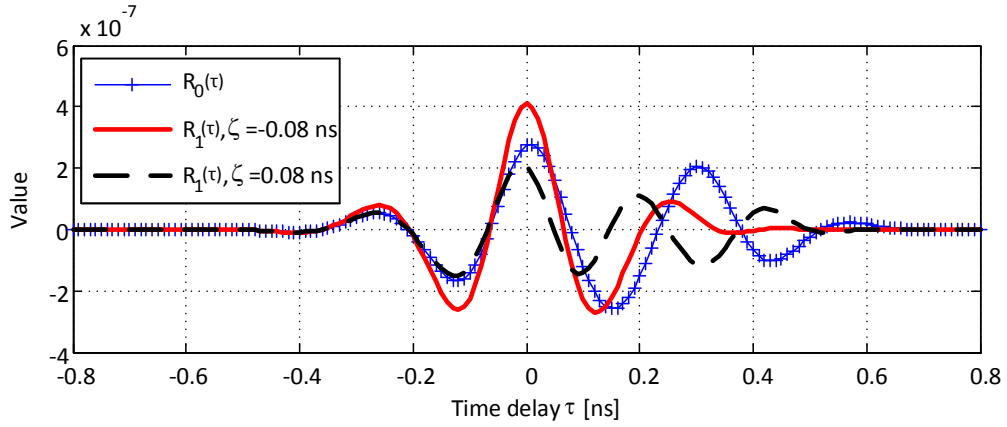

(b)

Figure 2.7: Correlation functions of the conventional UWB-PPM (a) and UWB-PPT-ATS schemes with different time shifts (b).

should be chosen so that the value of $R_{G4}(\tau - T_{\text{PPM}} - \zeta)$ is the minimum of the $R_{G4}(\tau)$ function, which denoted by $R(\tau_{opt})$ as shown in Fig. 2.7 (a). At $\tau = 0$, $R_{G4}(0)$ has the maximum value, and at $\tau = \tau_{opt}$, $R_{G4}(\tau_{opt})$ has the minimum value equal to $R(\tau_{opt})$. Therefore, for $R_1(\tau)$ maximized at $\tau = 0$, ζ is chosen so that $T_{PPM} + \zeta = \tau_{opt}$. The variation of the correlation function with the different values of ζ is illustrated in Fig. 2.8. In this figure, the different values of ζ leads to the different shapes of the correlation function, the optimal value of ζ in this case is $\zeta_{opt} = -0.08$

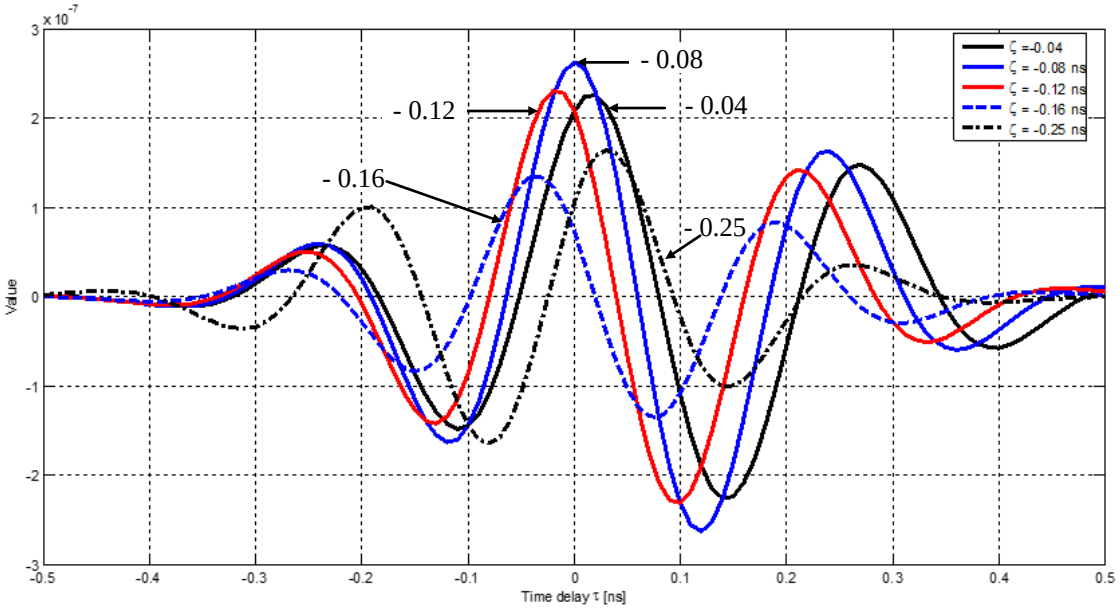

Figure 2.8: Correlation functions with the different additional time shifts.

ns which makes $R_1(0)$ obtains the maximum value. When the value of the ζ increases close to the pulse width ($\zeta = -0.16$ ns, and -0.25 ns in Fig. 2.8), the corresponding correlation functions do not reach the global maximum near the value of $\tau = 0$ and its local maximum points have the values close to the global maximum. This is similar for the unmodulated UWB signal, and it leads to the higher error of determining the global maximum point of these functions. Therefore, depending on the specific parameter configuration of each UWB-PPM system, the value of ζ should be selected so that $R_1(0)$ receives the largest value. The traveling time and therefore the propagation distance are estimated by the values of these correlation function (see Eqs. (1.17), and (1.18)) as shown in Section 1.2, Chapter 1.

2.3.2. Evaluation of the UWB-PPM-ATS technique

The performance of UWB-PPM-ATS technique is assessed by mathematical analysis and Matlab simulation. The UWB-PPM-ATS technique is compared with other modulation techniques including UWB-OOK and UWB-PPM according to the accuracy of distance estimation in heterogeneous medium. Our trials indicated that the UWB-PPM pulses shifted by a certain time constant can be used to improve the accuracy of estimating the distance. Here, the accuracy of these systems is evaluated by the average error between estimated distance and the true value as presented in Eqs. (1.20), (1.21) in Chapter 1:

$$\Delta d = \frac{1}{K}\sum_{k=1}^{K} \mid \hat{d}_k - d_0 \mid,$$

$$\delta d(\%) = \frac{1}{K}\sum_{k=1}^{K} \frac{\mid \hat{d}_k - d_0 \mid}{d_0} \times 100\%.$$

To evaluate the UWB-PPM-ATS system, consider the diagram with heterogeneous medium in Fig. 2.1. In this figure, the propagation environment is assumed to have three layers: sand (dry), sandy soil (dry) and granite (dry), and their relative permittivities $\varepsilon_1, \varepsilon_2, \varepsilon_3$ are 2.5, 3, 5, respectively. Those layers are assumed to be dry to reduce the attenuation of environment, so propagation velocity in those layers are 18.97 cm/ns, 17.32 cm/ns, 13.42 cm/ns, and the attenuation is 0.1 dB/cm [50] with sand (dry) at the frequency of $f = 10$ GHz. The UWB-OOK, UWB-PPM and UWB-PPM-ATS systems are used to estimate the total depth $d = d_1 + d_2 + d_3$ when d varies between 0 and 3 m. The performance of these systems are assessed by the average error between the results

obtained from the simulations and the actual value of the parameters. Based on the PSD plot of the Gaussian impulses shown in Fig. 1.6, most of the numerical results presented in this section are based on analysis using the fourth-order Gaussian monocycle. An example of the shape of the correlation function used to estimate the total depth d of UWB-PPM-ATS system is shown in Fig. 2.9.

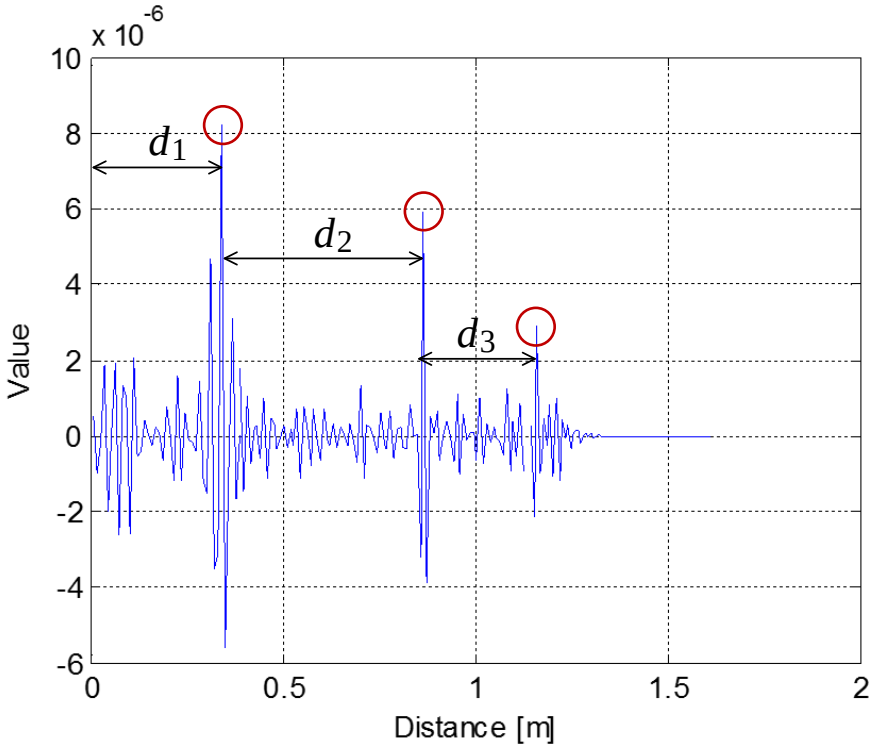

Figure 2.9: The correlation values are used to determine distances d_1, d_2, d_3 by the UWB-PPM-ATS system.

The errors of estimated values are illustrated in Fig. 2.10 for OOK, PPM and ATS systems with $\zeta = -0.08$ ns and $\zeta = -0.16$ ns.

Observe that the relative error of the UWB-OOK system is about 24%, of UWB-PPM is about 11%, while those of UWB-PPM-ATS with $\zeta = -0.08$, and -0.16 ns are about 7%, and 13%, respectively. There-

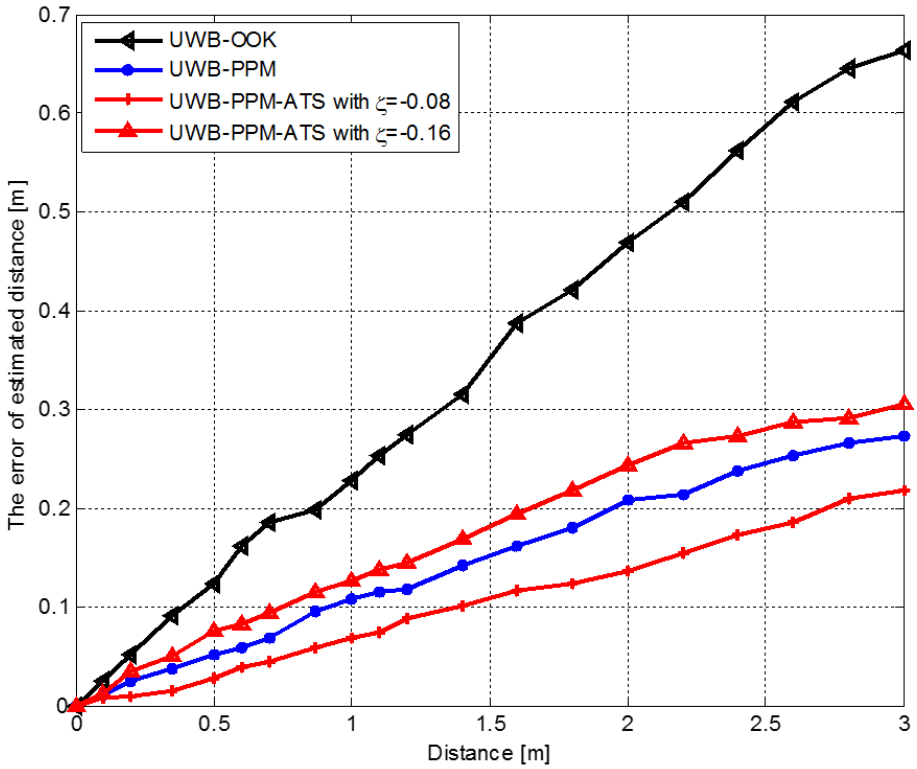

Figure 2.10: Comparison of distance estimation errors between OOK, PPM and the proposed UWB-PPM-ATS modulation techniques.

fore, the UWB-PPM- ATS with $\zeta = -0.08$ ns performs better for all simulated distance values. This can be explained by comparing the correlation functions in Figs. 2.7 and 2.8. It is observed that $R_1(0)$ is significantly greater than $R_0(0)$ for $\zeta = -0.08$ ns, and $R_0(0)$ is not the maximum value of $R_0(\tau)$. Therefore, the average error in the PPM-ATS with $\zeta = -0.08$ ns is smaller than in the UWB-PPM. However, with $\zeta = -0.16$ ns, $R_1(0)$ is less than $R_0(0)$ thus the PPM outperforms the PPM-ATS. Furthermore, the UWB-OOK is one of the amplitude modulation techniques, thus it is affected by the transmission environment, and more difficult to separate the received signal from noise interfer-

ences in comparison with the PPM techniques which have a constant amplitude.

The results in Fig. 2.10 indicate that the time shift ζ directly affects the performance of UWB-PPM systems. The value of $(T_{PPM} + \zeta)$ with suitable value of ζ, the accuracy of the UWB system was improved (such as $\zeta = -0.08$ ns in this case). Otherwise, with other values of ζ, it is possible to make the error of distance estimation of the UWB-PPM system higher than that of the conventional UWB-PPM. Due to the performance of the UWB-PPM system depends on the selection of the time shift, a suitable value of ζ must be chosen according to the specific pulse shape and pulse width employed in a particular UWB application.

2.3.3. Comparison of the computational complexity

The complexity of the UWB-PPM-ATS technique is investigated by the number of floating point operations (FLOPS) performed for the correlation function in the receiver side. Assume that a FLOP stands for a real multiplication, a real summation, or a real subtraction. Ignoring the operations of generating UWB signals, the computational complexity is evaluated based on the number of FLOPS in Eqs. (2.17) and (2.18), and illustrated in Table 2.2. In Eqs (2.17), (2.18), the correlation function of the n^{th} pulse is taken from $-NT_r/2$ to $NT_r/2$, the sampling rate of the correlation function is chosen by $T_{PPM}/20$ with UWB-PPM system, and $\zeta/20$ with UWB-PPM-ATS system, and by $\mu_p/20$ with UWB-OOK system. The parameters for the UWB system are following [2] as: $T_r = 50$ ns,$T_{PPM} = 0.2$ ns, $N = 100, \mu_p = 0.2877$ ns. It can be seen that the

proposed UWB-PPM-ATS system has higher computational complexity than that of the conventional UWB-PPM system. This is also a limitation of our proposal.

Table 2.2: The computational complexity.

Modulation Technique	Number of FLOPS for the N^{th} pulse	Specific values of FLOPS
UWB-OOK	$60 \times N \times T_r/\mu_p$	105×10^4
UWB-PPM	$60 \times N \times T_r/T_{PPM}$	150×10^4
UWB-PPM-ATS with $\zeta = -0.08$ ns	$60 \times N \times T_r/(\zeta)$	375×10^4
UWB-PPM-ATS with $\zeta = -0.16$ ns	$60 \times N \times T_r/(\zeta)$	187.5×10^4

2.4. Summary

In this chapter, the method of applying RSSI combined with Gauss-Newton algorithm for IR-UWB system to determine the propagation distance and the position of a buried object is proposed. However, due to the rapid attenuation of the signal, this method is only applicable for short-range detection and homogeneous medium. In the heterogeneous medium, to increase the ability of correct detection of the received UWB signal and thereby increase the accuracy of distance estimation, the UWB PPM ATS method is proposed. In the UWB PPM ATS method, the position of UWB pulse is modulated by PN sequence with an optimal additional time shift. This makes the error of distance estimation significantly reduced. Performance comparisons between the proposed system and the related ones are provided using numerical and simulation results especially in lossy transmission environments. The results of this chapter are published in [C1], [J2], [J4].

Chapter 3
CORRELATION FUNCTION SEPARATION AND SHIFTED PULSE-BASED BURIED OBJECTS LOCATING METHODS

Range-based position estimation techniques in free space are classified into lateration, triangulation, and multilateration, where the multilateration technique is more attractive than other techniques because it provides the better result than other [90]. However, these methods are not applicable to locating buried objects in in environments such as underground, concrete, etc. Meanwhile, many practical applications need to determine the position of multi-buried objects in various transmission environments. The Gauss-Newton method presented in Chapter 2 can be applied to positioning the buried object. However, this algorithm may converge slowly or not at all if the initial guess is far from the minimum, and causes large estimation errors, so to increase the accuracy of location estimation, the Levenberg-Marquardt algorithm is applied. This method is used to determine the relative permittivity of environment, and also the position of buried objects.

To increase the accuracy of locating multiple buried objects which are close to each other in the homogeneous and heterogeneous environments, in this chapter, the correlation function separation technique (CFST) combined with the Levenberg-Marquardt algorithm [J5] and UWB pulse

shifting technique [J3] with named UWB-PST are proposed. The multi-buried objects positioning method here is based on a single buried object positioning and applied to each individual buried object. Firstly, the correlation function values at the receiver of a single buried object case are calculated, and these values are used as the sample set. Then, the next buried object's position was determined using this sample set. The distinguishable distance between different objects according to the buried depth is also calculated, and the error is used to assess the two proposed methods in several scenarios. The chapter's results are published in the papers [J3], [J4], [J5].

3.1. A proposed method of positioning a single buried object

3.1.1. Estimation algorithm

The existence detection and location of the buried objects are performed based on analysis of the received UWB signal in penetration systems. For simplicity in the positioning problem, in this chapter, the position of the buried object is defined at the upper middle point of the object, which is considered as the reflected wave point. The nonlinear algorithm estimation called Levenberg-Marquardt Fletcher (LMF) [94] was applied into calculations of distances, the relative permittivity and the position of buried object in the case of unknown propagation environment. In the simplest case, there is a buried object in a homogeneous environment with a single layer as shown in Fig. 3.1. Here, the position of the object is considered in the two-dimensional space (2-D), and is regarded as a reflection point of propagation.

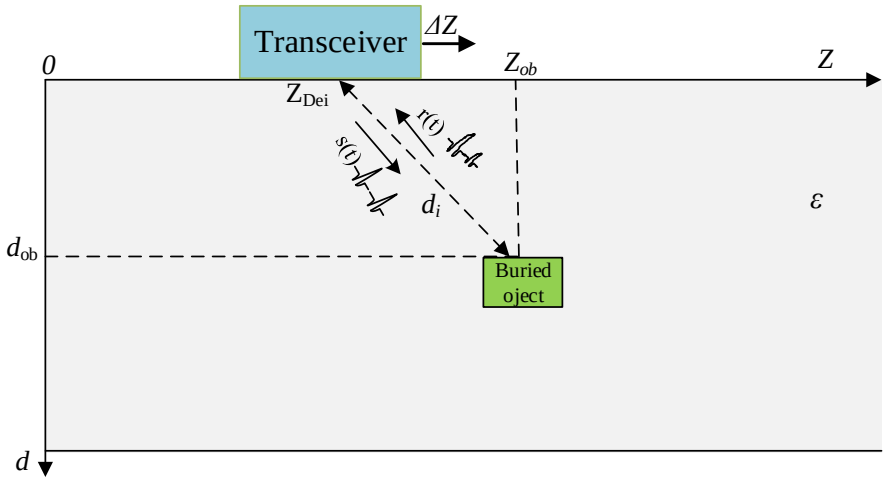

Figure 3.1: System model for positioning a single buried object in the homogeneous environment.

To determine the environment parameters and estimate the location of the buried objects, the transceiver moves horizontally (Z direction) and emits UWB pulses after every movement step of ΔZ. In the proposed method, the values of d_{ob}, ε, and Z_{ob} are estimated based on the traveling time τ_i and the position Z_{Dei} of the device. Here, Z_{Dei} is the position of the device at the i^{th} movement, and τ_i is the delay time corresponding to the distance d_i from the device to the buried object at the position of Z_{Dei}. These parameters are presented as follows.

$$Z_{Dei} = i \times \Delta Z; d_i = \sqrt{(Z_{ob} - Z_{Dei})^2 + d_{ob}^2}, \tag{3.1}$$

$i = (0 \div M)$. Hence, the traveling time τ_i is given by:

$$\tau_i = 2\frac{\sqrt{\varepsilon\left[(Z_{ob} - Z_{Dei})^2 + d_{ob}^2\right]}}{c}, \tag{3.2}$$

τ_i is calculated according to Eq. (1.17). In Eq. (3.2), the value of τ_i, c, and Z_{Dei} are known, the remaining parameters are estimated by the

estimation algorithm LMF. The unknown parameter vectors are denoted by

$$\mathbf{X} = (\varepsilon, d_{ob}, Z_{ob}). \tag{3.3}$$

With the known pairs (Z_{Dei}, τ_i), $\mathbf{X}$ is determined so that the deviation function in Eq. (3.4) reaches the minimum value.

$$E(\widehat{\mathbf{X}}) = \sum_{i=1}^{M} [\tau_i - f(Z_{Dei}, \widehat{\mathbf{X}})]^2, \tag{3.4}$$

where M is the number of movements of the transceiver, and

$$f(Z_{Dei}, \widehat{\mathbf{X}}) = 2\frac{\sqrt{\widehat{\varepsilon}\left[\widehat{d}_{ob}^2 + (Z_{Dei} - \widehat{Z}_{ob})^2\right]}}{c}. \tag{3.5}$$

The $\widehat{(.)}$ denotes the estimated values of the parameters. Thus, the equation of determining the value of the parameters can be rewritten as follows.

$$\widehat{\mathbf{X}} = Arg\min_{\widehat{\mathbf{X}}} E(\widehat{\mathbf{X}}) = Arg\min_{\widehat{\mathbf{X}}} \sum_{i=1}^{M} [\tau_i - f(Z_{Dei}, \widehat{\mathbf{X}})]^2. \tag{3.6}$$

The necessary conditions for E to be minimum are:

$$\frac{\partial E}{\partial \varepsilon} = 0, \frac{\partial E}{\partial Z_{ob}} = 0, \frac{\partial E}{\partial d_{ob}} = 0. \tag{3.7}$$

Rewriting Eq. (3.7) according to Eqs. (3.4) and (3.5) with $X_1 = \sqrt{\varepsilon}$, $X_2 = d_{ob}^2$, $X_3 = Z_{ob}$, the following formulas are obtained.

$$\frac{\partial E}{\partial X_1} = \sum_{i=1}^{M} 2\left[\tau_i - 2\frac{X_1\sqrt{X_2 + (Z_{Dei} - X_3)^2}}{c}\right]\left[-2\frac{\sqrt{X_2 + (Z_{Dei} - X_3)^2}}{c}\right] = 0, \tag{3.8}$$

$$\frac{\partial E}{\partial X_2} = \sum_{i=1}^{M} 2\left[\tau_i - 2\frac{X_1\sqrt{X_2 + (Z_{Dei} - X_3)^2}}{c}\right]\left[\frac{-1}{c\sqrt{X_2 + (Z_{Dei} - X_3)^2}}\right] = 0, \tag{3.9}$$

$$\frac{\partial E}{\partial X_3} = \sum_{i=1}^{M} 2\left[\tau_i - 2\frac{X_1\sqrt{X_2 + (Z_{Dei} - X_3)^2}}{c}\right]\left[\frac{-2X_1(Z_{Dei} - X_3)}{c\sqrt{X_2 + (Z_{Dei} - X_3)^2}}\right] = 0. \tag{3.10}$$

The values of $\widehat{\mathbf{X}} = (X_1, X_2, X_3)$ can be calculated by solving the Eqs. (3.8), (3.9) and (3.10). However, this calculation is very complicated, especially with the large values of M. So, in the proposed method, by using LMF, vector $\widehat{\mathbf{X}}$ is determined by the iteration steps as shown in Fig. 3.2, and described in detail through the following steps.

Step 1: Assign any arbitrary initialization values to $\mathbf{X}$ (usually zero values), denoted by $\mathbf{X}_{int}$.

Step 2: Replace the value of $\mathbf{X}$ with new ones $(\mathbf{X} + \delta)$, here δ is an updated step vector, hence:

$$E(\mathbf{X} + \delta) \approx [\tau - f(\mathbf{X})]^T[\tau - \mathbf{f}(\mathbf{X})] - \mathbf{2}[\tau - \mathbf{f}(\mathbf{X})]^{\mathbf{T}}\mathbf{J}\delta + \delta^{\mathbf{T}}\mathbf{J}^{\mathbf{T}}\mathbf{J}\delta; \tag{3.11}$$

with $\mathbf{J}$ is a Jacobian matrix of size $[3 \times M]$ with:

$$J_{i\times j} = \frac{\partial f(Z_{Dej}, \mathbf{X})}{\partial X_i}. \tag{3.12}$$

Step 3: To determine the minimum value of the sum E, the update step vector δ is calculated so that the derivative of $E(\mathbf{X}+\delta)$ with respect to δ is equal to zero, so δ can be determined satisfying:

$$[\mathbf{J}^T\mathbf{J} + \lambda \text{diag}(\mathbf{J}^T\mathbf{J})]\delta = \mathbf{J}^T[\tau - f(\mathbf{X})], \tag{3.13}$$

where the factor λ (non-negative) is adjusted at each iteration. If E reduces rapidly, a smaller value of λ can be used, whereas if in an iteration in which E does not reduce, λ can be increased.

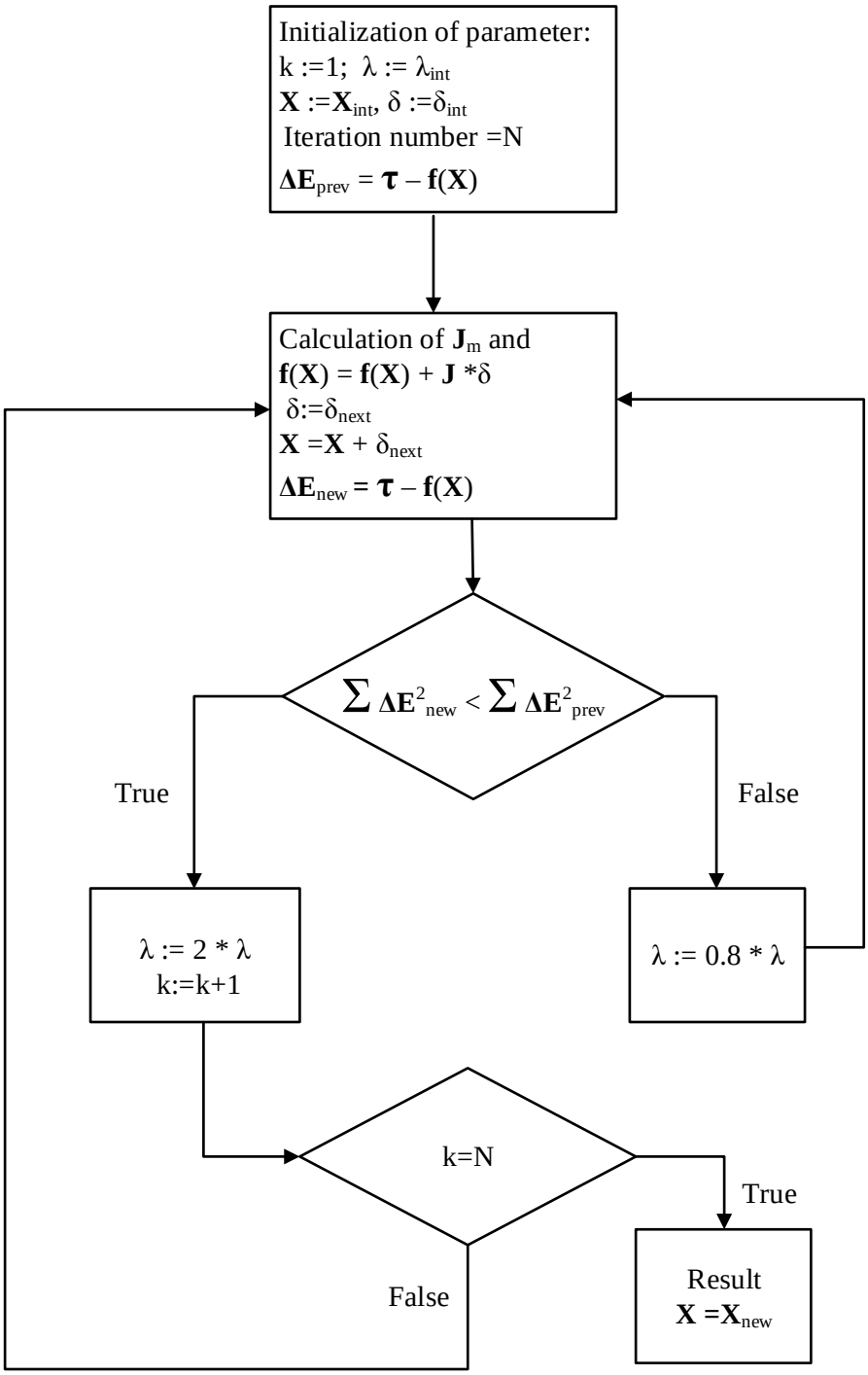

Figure 3.2: The flowchart of estimated algorithms LMF.

The update step vector is computed as follows:

$$\delta = [\mathbf{J}^T\mathbf{J} + \lambda \mathrm{diag}(\mathbf{J}^T\mathbf{J})]^{-1}\mathbf{J}^T[\tau - f(\mathbf{X})]; \qquad (3.14)$$

The algorithm repeats Steps 2 and 3 until the constraint condition in Eq. (3.6) is satisfied. The output of LMF algorithm are the final estimated values. For the convergence of this algorithm, the results are achieved after N iterations in Matlab simulation.

3.1.2. The results of positioning a single buried object

In the UWB systems, the pulse shape has a strong influence on the performance of them. The proposed method is evaluated with different UWB signal types: the IR-UWB signal generated by the 2^{nd}, 3^{rd}, 4^{th} order Gaussian monocycle, and the modulated UWB signal with OOK, PPM, and PPM-ATS techniques. Here, the order of the monocycle is the order of Gaussian pulse derivative. The 2^{nd}, 3^{rd} and 4^{th} Gaussian mono-

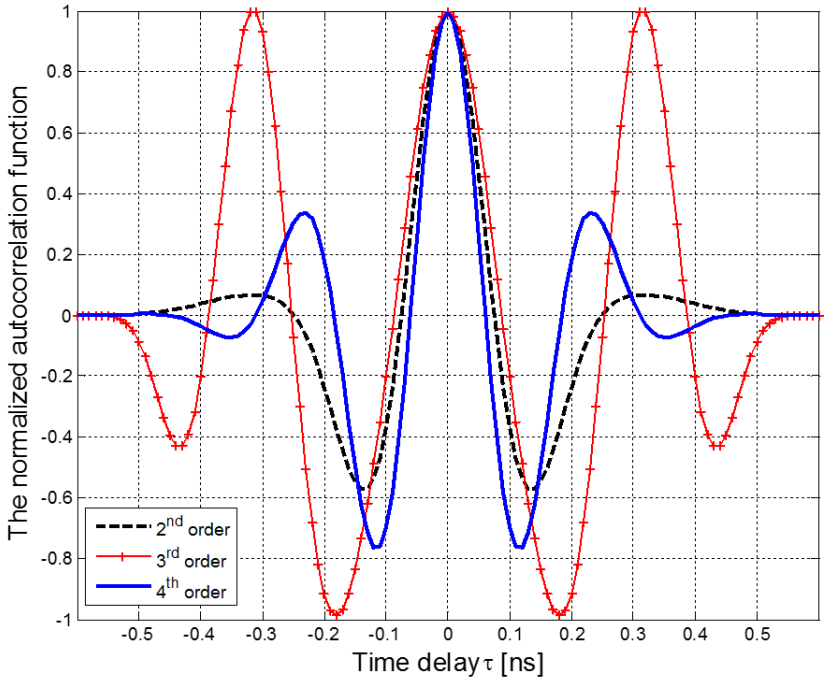

Figure 3.3: The autocorrelation function of the Gaussian pulses as a function of time.

cycles have autocorrelation functions as shown in Fig. 3.3. According

to the shapes of the autocorrelation function, it can be seen that the system using different types of pulses provides different performances.

The parameters of system model and the initialization vectors of the LMF algorithm are listed in Table 3.1, in which the environment is homogeneous and has a buried object. The transceiver moves horizontally (Z direction) and emits UWB pulses after every movement step of ΔZ and gets the reflected signal from the surface of the buried object (the scattered signals are omitted). The traveling time of received signals are

Table 3.1: Initialization parameters of the model [2], [3].

Parameter	Notation	Value
Transmitted power	P_{Tx}	-5.4 dBm
Time normalization factor of pulse	μ_p	0.2877 ns
Center frequency, Bandwidth	$f_c, \Delta F$	6.85 GHz, 3.5 GHz
Number of pulses	N_p	100
Noise power	$N_0/2$	-77 dBm
Time shift of PPM	T_{PPM}	0.2 ns
Additional time shift	ζ	-0.08 ns
Relative permittivity	ε	3.5
Damping factor	λ	3
Z-coordinate of buried object	Z_{ob}	0.6 m
The depth of buried object	d_{ob}	0.5 m
Movement step of the device	ΔZ	0.1 m

determined by the matched filter. The relative permittivity of propagation medium and the position of buried object are estimated by the LMF presented as above. The calculation results by Matlab software are shown in Table 3.2 and Figs. 3.4, and 3.5.

In Figs. 3.4 (a) and 3.5 (a), the dashed black lines denote the curve of τ versus Z_{De} with the actual values of Z_{ob}, d_{ob}, and ε. The remaining

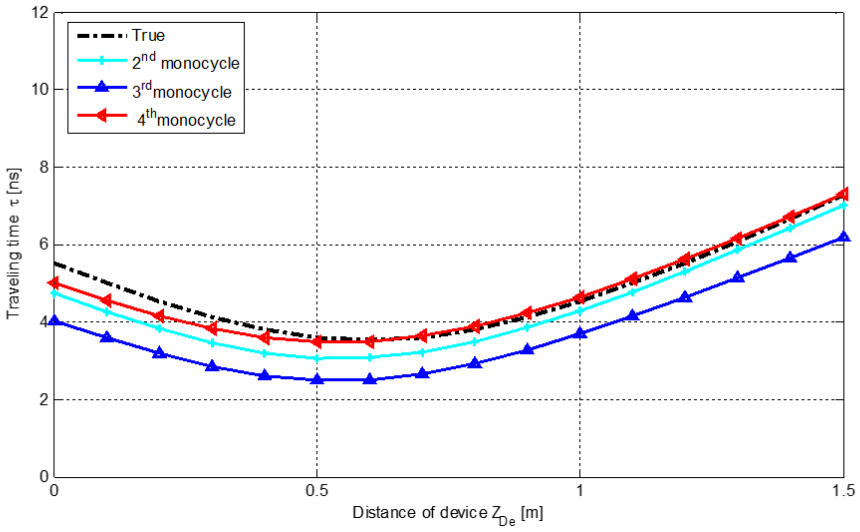

(a)

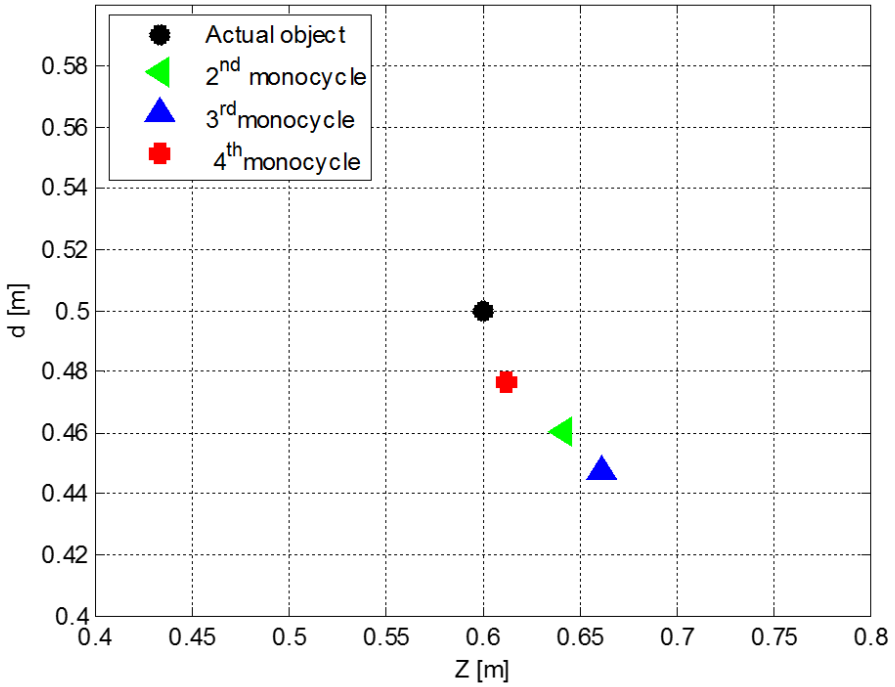

(b)

Figure 3.4: The actual and estimated locations by different types of Gaussian monocycles in the case of a single buried object; the traveling time changes according to the position of device (a) and the estimated positions of the buried object (b).

curves show the relationship between the estimated values with different types of UWB signal. Fig. 3.4 (a) shows the dependency curve of the traveling time τ of the reflected signal on the location of the device Z_{De}. This parameter is determined by the UWB system using the UWB signals generated from different Gaussian pulse monocycles. Similarly, different UWB signal modulation techniques are compared in Fig. 3.5 (a). Figs. 3.4 (b), 3.5 (b) show the locations of buried objects in the two-dimensional (2-D) space. These estimated results achieved after $N = 50$ iterations of LMF.

Table 3.2: The results of the estimated parameters.

Parameter/Notation	Z_{ob} [m]	d_{ob} [m]	ε
The actual value	0.6	0.5	4.5
The estimated location by the 2^{nd}-order Gaussian and relative error	0.6412 (6.9%)	0.4605 (7.9%)	4.2809 (4.9%)
The estimated location by the 3^{rd}-order Gaussian and relative error	0.6612 (10.2%)	0.4477 (10.5%)	4.1323 (8.3%)
The estimated location by the 4^{th}-order Gaussian and relative error	0.6118 (2%)	0.4763 (4.7%)	4.3266 (3.9%)
Value estimated by UWB-OOK and relative error	0.8969 (49.5%)	0.7884 (57.7%)	5.7261 (27.2%)
Value estimated by UWB-PPM and relative error	0.7546 (25.8%)	0.6288 (25.7%)	3.3590 (25.3%)
Value estimated by UWB-PPM-ATS and relative error	0.6212 (3.5%)	0.4642 (7.2%)	4.8167 (7%)

Table 3.2 presents the estimated results by the different UWB signals. In the IR-UWB systems, their performance for using the fourth-order Gaussian monocycle is better than those for the others in terms of the

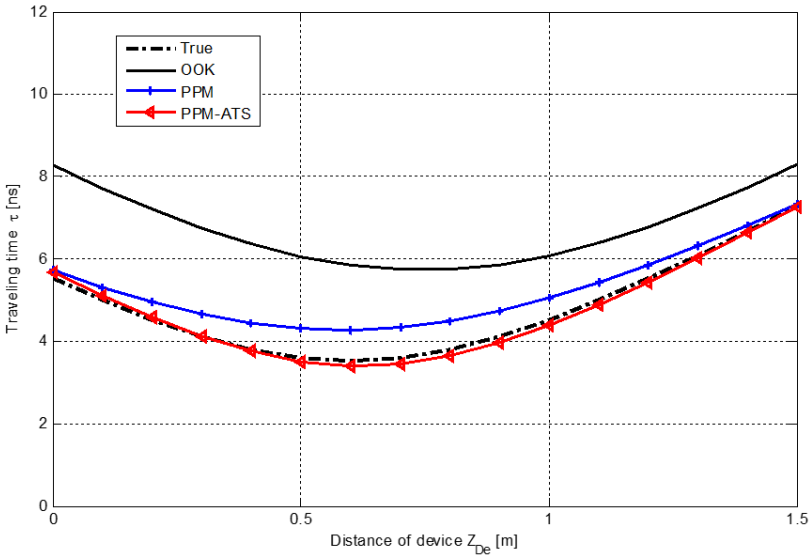

(a)

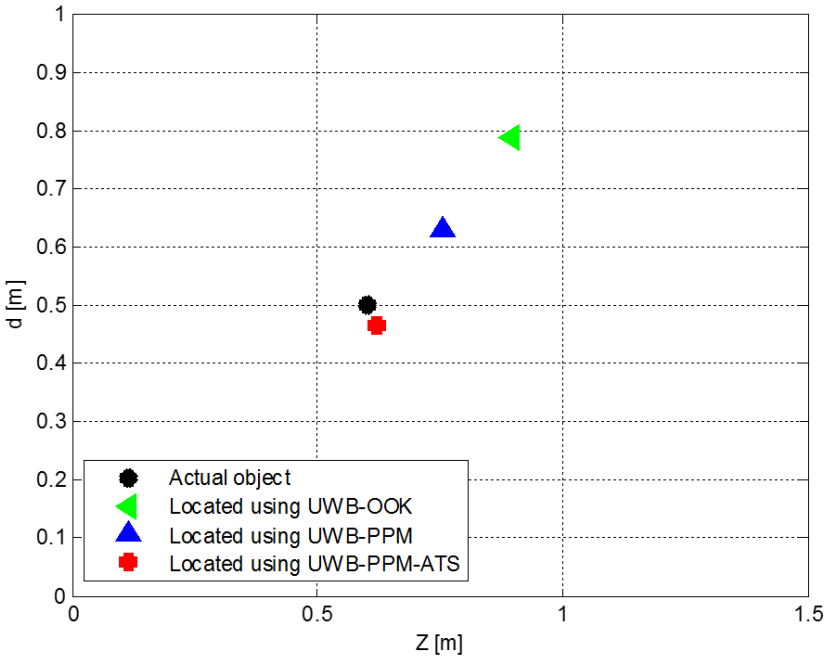

(b)

Figure 3.5: The actual and estimated locations for different modulated UWB signals in the case of a single buried object; the traveling time changes according to the position of device (a) and the estimated positions of the buried object (b).

positioning error. A reason can be explained through comparing the autocorrelation functions of Gaussian monocycles as shown in Fig. 3.3. The accuracy of the IR- UWB system depends primarily on determining the traveling time, which is calculated based on the maximum value of the correlation function (see Eq. (1.17)).

It can be seen from Fig. 3.3 that the shape of the autocorrelation function of the third-order Gaussian monocycle has maximum points at $\tau = 0.32$ ns and $\tau = 0$ ns while the second-order and fourth-order Gaussian monocycles have only one extreme point at $\tau = 0$ ns. This leads to determining the traveling time based on the correlation function of the third-order Gaussian monocycle with larger error than using other monocycles. Furthermore, the autocorrelation shape of the fourth-order monocycle has a narrower width around the maximum point than the second-order monocycle, so the accuracy when using the fourth-order monocycle is higher than using the second-order monocycle. Therefore, in detailed analysis, the error of the parameter estimation (distance) using the fourth-order pulses in this scenario has an average value about 2.4 cm, while for the second-order, and the third-order pulses, these values are 4.5 cm, and 5.4 cm, respectively.

In addition, the UWB-PPM-ATS modulation configuration proposed in Chapter 2 outperforms the UWB-OOK and UWB-PPM systems for all parameters of the model. This behavior results directly from the features of the correlation functions of different signals shown in Figs. 2.7 and 2.8. When using UWB-PPM-ATS technique with the optimal value of ζ, the estimated values of the traveling time have a smaller error than

using UWB-OOK and UWB-PPM techniques, so the calculated results from the LMF of the PPM-ATS system give the higher accuracy than conventional PPM systems.

3.2. Positioning multi-buried objects in a homogeneous environment

3.2.1. Positioning system model

Consider a positioning system model with multiple buried objects in a homogeneous environment as illustrated in Fig. 3.6. The transmission medium has a relative permitivity of ε, receive and transmit antennas are placed in the same position. To determine those buried objects' position, the transceiver moves along Z direction and transmits UWB signal at every ΔZ movement.

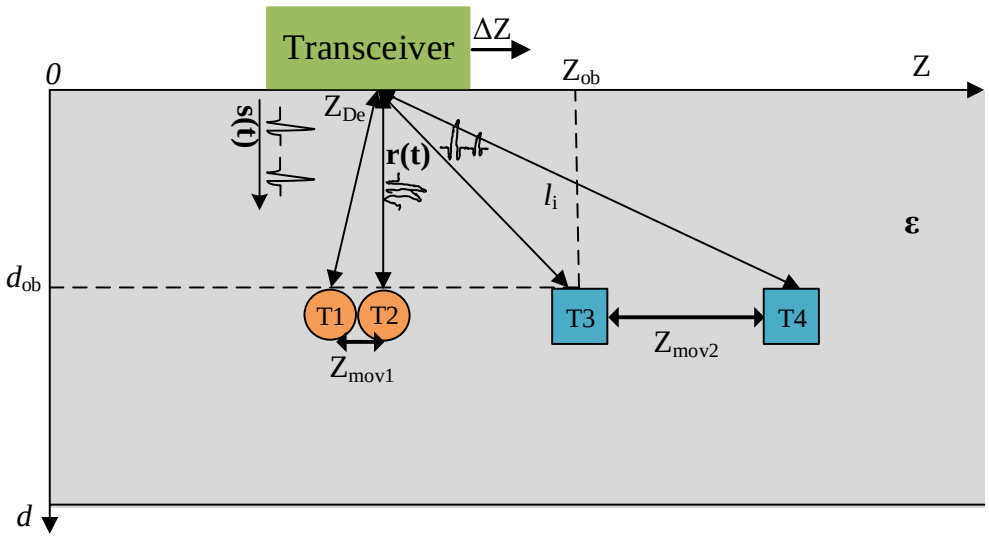

Figure 3.6: System model for positioning multi-buried objects in a homogeneous environment.

The transmitted IR-UWB signal takes the form as in Eq. (2.1), and

the received signal is described in Eq. (1.4).

The template signal at the receiver is $g(t)$ [44], the traveling time and the correlation function at the receiver side are determined as presented in Section 3.1. The propagation velocity in the system [46] is

$$V = \frac{c}{\sqrt{\varepsilon}}, \tag{3.15}$$

The distance from the device to the i^{th} buried object with assumption of the homogeneous medium:

$$d_i = \frac{1}{2} V \tau_i. \tag{3.16}$$

In this model, the two cases are considered. In the first case, two buried objects are assumed to be very close to each other, it means that the distance between them is approximately a resolution of the system. In the other case, two buried objects are far away from each other, and the distance between them is much greater than the resolution of the system.

In addition, as described in Section 3.1, the position of buried objects and characteristic of propagation environment (the relative permittivity) depend on the traveling time, which is determined from the values of the correlation function of system. Depending on the specific distance between two buried objects, different methods for determining the correlation functions are used.

3.2.2. Proposed multi-buried objects positioning method in homogeneous environments

With the system model as shown in Fig. 3.6, the received signal is the sum of reflected signals from the 1^{st} and the 2^{nd} buried objects with

attenuated amplitudes due to the propagation environment and noise components, which are denoted by $r_1(t)$ and $r_2(t)$, respectively. The shapes of received and transmitted signals in the cases of a single buried object and two nearby buried objects in the investigated environment are shown in Figs. 3.7 and 3.8, respectively.

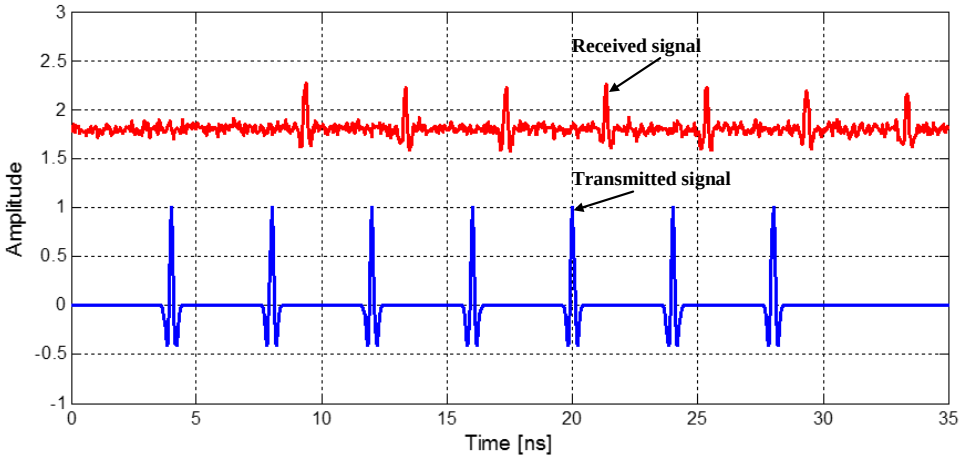

Figure 3.7: The transmitted and received signals with added noises in case of a single buried object.

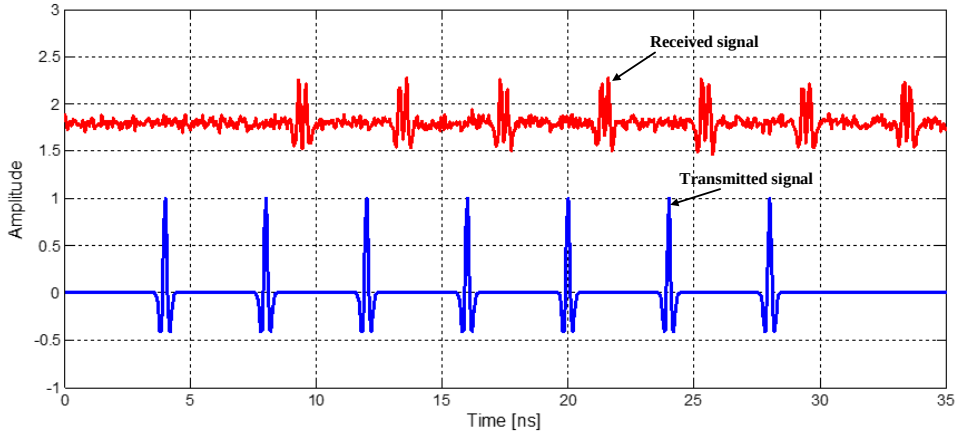

Figure 3.8: The transmitted and received signals with added noises in case of two closely buried objects.

Consider the system model in Fig. 3.6 with two buried objects far

from each other, such as 'T3' and 'T4' in Fig. 3.6. The reflected signals $r_1(t)$ and $r_2(t)$ do not overlap, consequently the procedure of locating a single object have been applied as presented in Section 3.1. However, in case that the buried objects close to each other, such as 'T1' and 'T2' in Fig. 3.6, the reflected signals $r_1(t)$ and $r_2(t)$ overlap (see Fig. 3.8). In this scenario, as shown in Fig. 3.9, the correlation function shapes are changed with different cases of the buried objects: one buried object, two closely buried objects and two apart buried objects with the distance between them equal to Z_{mov}.

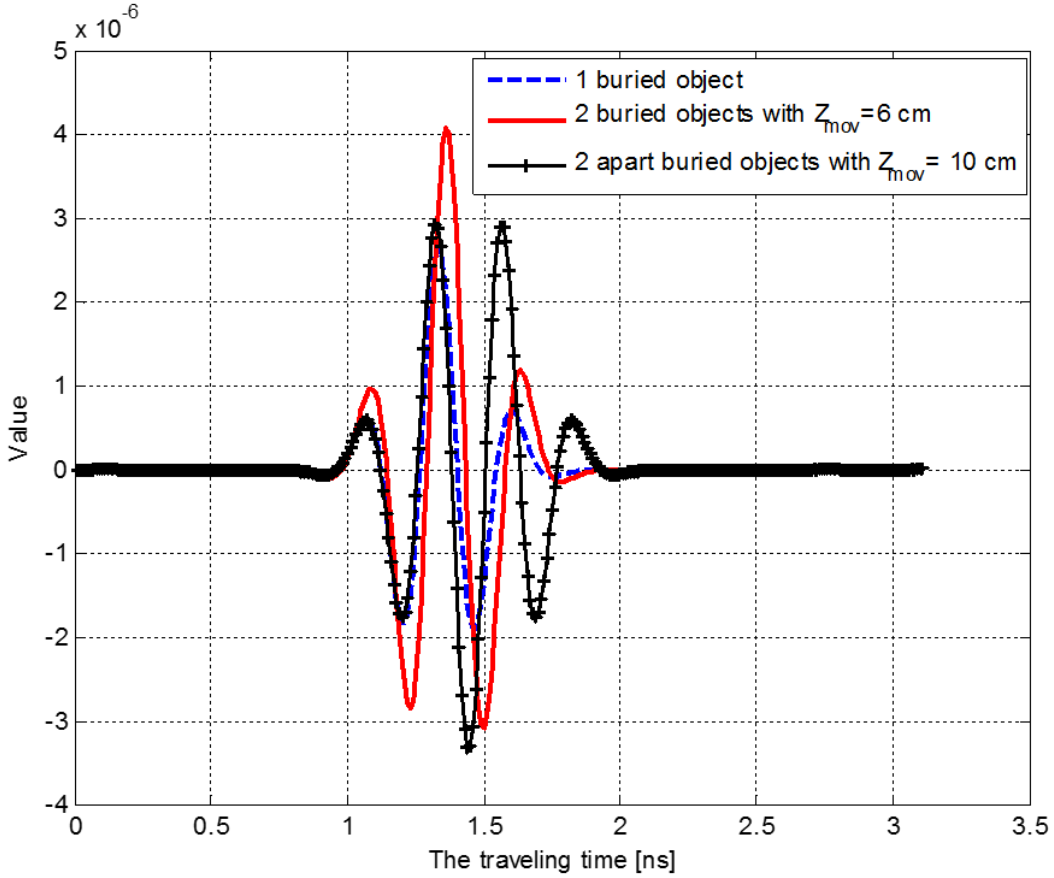

Figure 3.9: The correlation function shapes with different distances between buried objects.

It can be seen that, in the case of two apart buried objects, it is entirely possible to apply the method in Section 3.1.1 to locate one-by-one buried object. In the case of two objects close to each other, the thesis proposes a method to determine the second object by using the correlation function values and the position of the first object determined according to Section 3.1.1. The equation of correlation function is rewritten as follows.

$$R_{\Sigma}(\delta) = \int_{-\infty}^{\infty} r_{\Sigma}(t)p(t-\delta)dt \tag{3.17}$$

$$= \int_{-\infty}^{\infty} \big[r_1(t) + r_2(t)\big]p(t-\delta)dt \tag{3.18}$$

$$= R_1(\delta) + R_2(\delta), \tag{3.19}$$

and the traveling time can be calculated as:

$$\tau_{\Sigma} = \mathrm{Arg}\max_{\delta}\{\mathrm{R}_{\Sigma}(\delta)\}. \tag{3.20}$$

According to the received signal $r_{\Sigma}(t)$, the traveling time from the second object to the device is denote by τ_2, and can be computed as

$$\tau_2 = \delta_{op} = \big[\mathrm{Agr}\max_{\delta}\{\mathrm{R}_{\Sigma}(\delta) - \mathrm{R}_1(\delta)\}\big], \tag{3.21}$$

or

$$\tau_2 = \delta_{op} = \left[\mathrm{Agr}\max_{\delta}\left\{\frac{\mathrm{R}_{\Sigma}(\delta)}{\mathrm{R}_1(\delta)}\right\}\right]. \tag{3.22}$$

The determination of the traveling time τ_2 using Eqs. (3.21) and (3.22) is named the correlation function separation technique (CFST). Fig. 3.10 illustrates examples of the correlation function shapes of the received signal with the reference wave when there are two closely buried objects

in the homogeneous environment. These types of correlation functions are determined by Eqs. (3.17), (3.21) and (3.22). Hence, based on the values of the correlation function in the case of positioning a single object, the traveling time τ_2 can be estimated according to Eqs. (3.21) and (3.22), and the position of the second object can be located in the same way as presented in the Section 3.1.1 by using the LMF algorithm in which τ is replaced by τ_2.

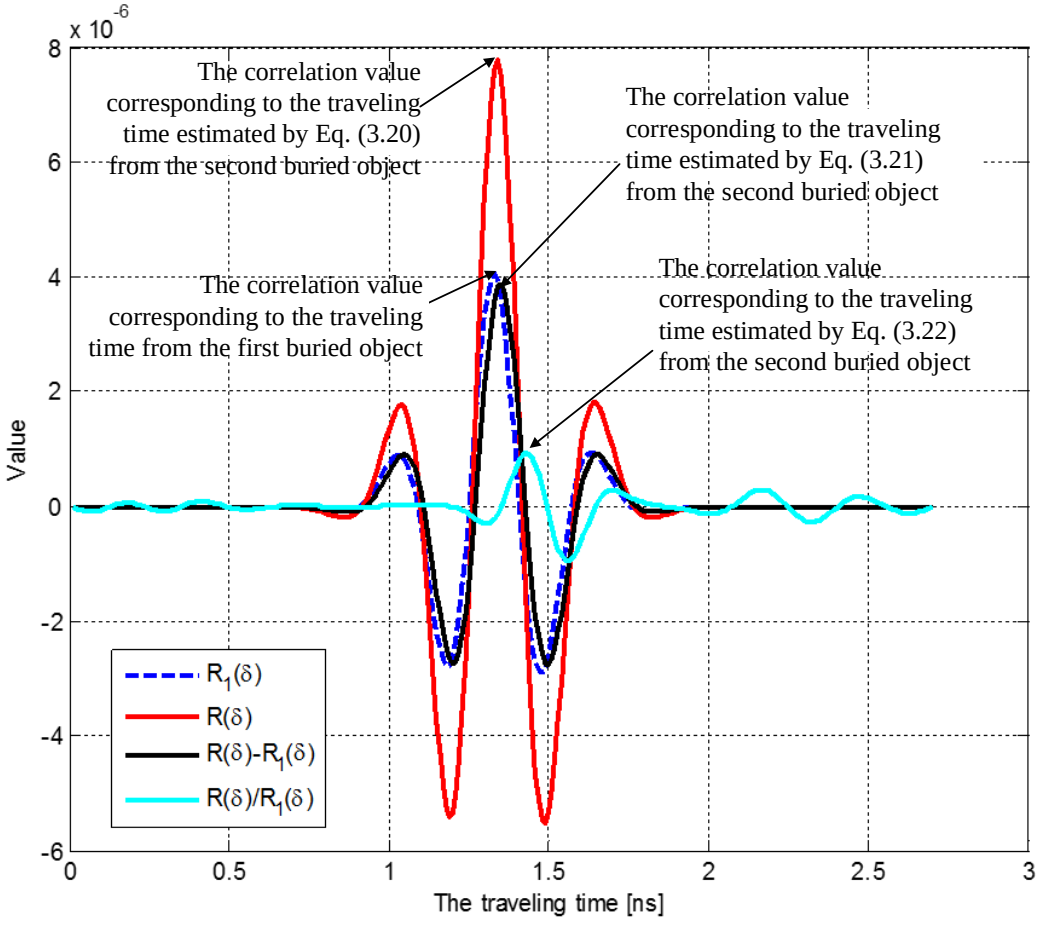

Figure 3.10: The correlation function shapes with the first buried object at $(Z_{ob1}, d_{ob1}) = (0.3, 0.2)$m; $Z_{mov} = 0.04$m; the transceiver at $Z_{Dei} = 0.3$ m.

3.2.3. The performance of CFST

The localization technique is based on the TOA method and the root mean squared error (RMSE) of the CFST is determined by the Eq. (3.23) and compared with the Cramer-Rao lower bound (CRLB) in Eq. (3.24).

The root mean squared error (RMSE) of the CFST in determining the traveling time τ_2:

$$RMSE = \sqrt{\frac{1}{N}\sum_{k=1}^{N}\left(\hat{\tau}_{2k} - \tau_2\right)^2}. \tag{3.23}$$

The CRLB [95] on the standard deviation of an unbiased TOA estimator $\hat{\tau}$ is given by:

$$\sqrt{Var(\hat{\tau})} \geq \frac{1}{2\sqrt{2}\pi\sqrt{SNR}\Delta F}, \tag{3.24}$$

where SNR, ΔF are signal to noise ratio and effective bandwidth, respectively. The change of RMSE vs. SNR for SCF, DCF and Total methods in estimating the traveling time τ_2 are illustrated in Fig. 3.11 with the case of two adjacent buried objects in the homogeneous environment, the first buried object at a depth of 30 cm, and the second buried object is 4 cm away from the first one.

Based on the sample set of the correlation values in the case of positioning a single buried object, the results of locating two objects are illustrated in Fig. 3.12 and Fig. 3.13. The former figure illustrates the case of two objects far from each other, the distance between two objects Z_{mov2} is 100 cm, whereas the latter figure presents the case of two objects close to each other, and the distance between them Z_{mov1} is 2 cm.

In the first case, because the distance between the two buried objects

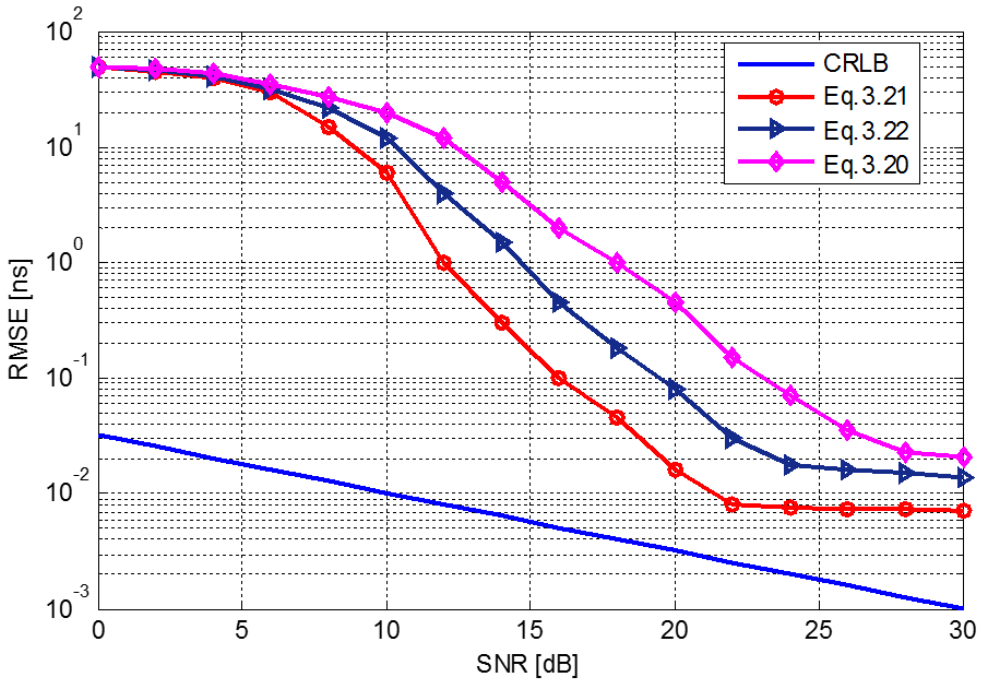

Figure 3.11: RMSE vs. SRN for CFST method and CRLB.

is large, so the reflected signals from these objects do not overlap. Therefore, locating of two buried objects is carried out in turn for each object as in the case of positioning a single buried object.

In the second case, the location of the second buried object is determined by CFST using Eqs. (3.2), (3.21) and (3.22) with the fourth-order Gaussian monocycle. Fig. 3.13 depicts the estimated traveling time of reflected signal from the second buried object according to Eq. (3.2), and its position is determined by using the CFST based on the estimated values of the first buried object and the relative permittivity.

As seen in Fig. 3.13, the estimated error by Eq. (3.21) is smaller than by Eq. (3.22). The results can be explained by analyzing Fig. 3.10 and Eqs. (3.21) and (3.22), the error of estimating traveling time de-

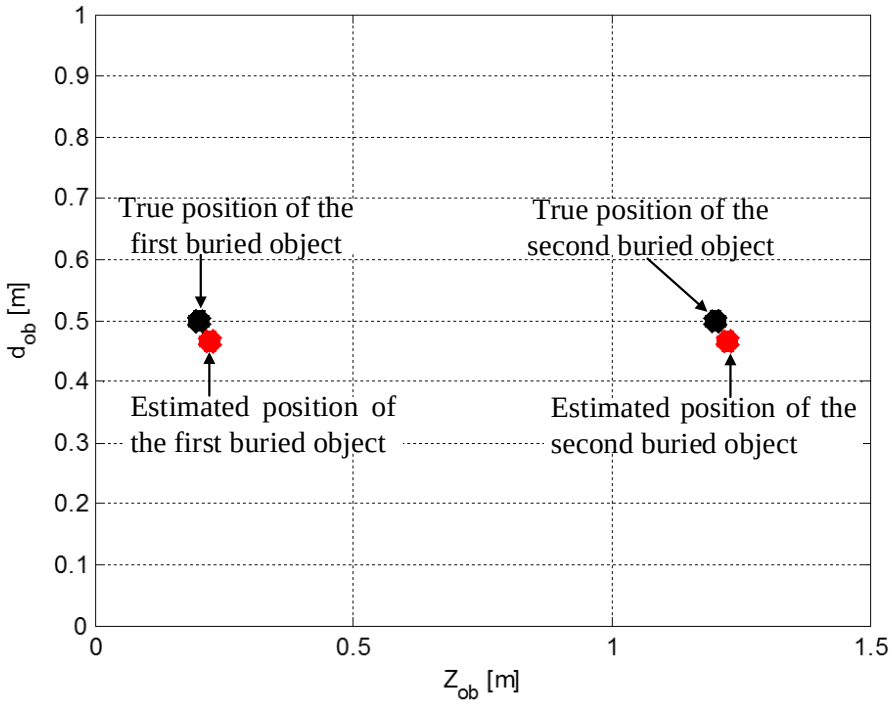

Figure 3.12: Two buried objects are far from each other.

pends on the values of the correlation function which are proportional to the amplitude of received signal, hence the estimation error depends on the amplitude of received signal. Moreover, comparing Eqs. (3.21) and (3.22), it is observed that in Eq. (3.22), the amplitude of the reflected signal from the second object reduces by the amplitude of the received signal from the first object. Hence, the value of the correlation function by Eq. (3.22) also reduces, causing higher errors when determining traveling time rather than using Eq. (3.21). Thus, with the acceptable errors, the CFST based on both the subtraction (see Eq. (3.21)) and division (see Eq. (3.22)) are applied to locate two closely buried objects.

To determine the resolution of the CFST, the first object is buried at (0.3 m, 0.15 m), and the second object is moved to the position at (0.5

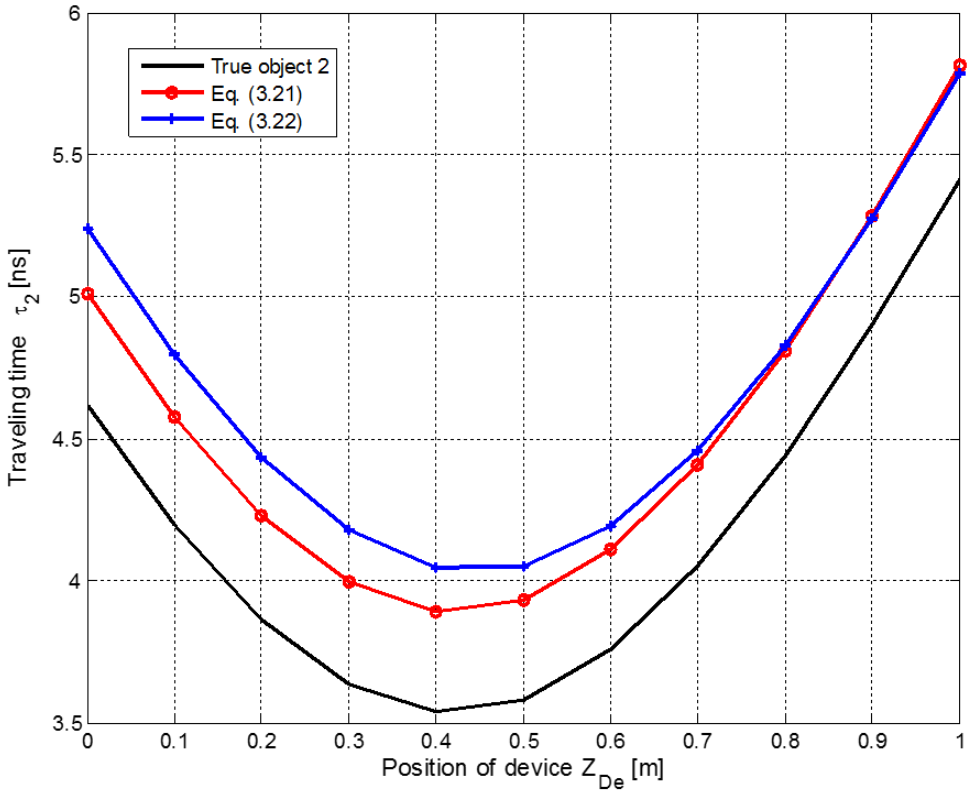

(a)

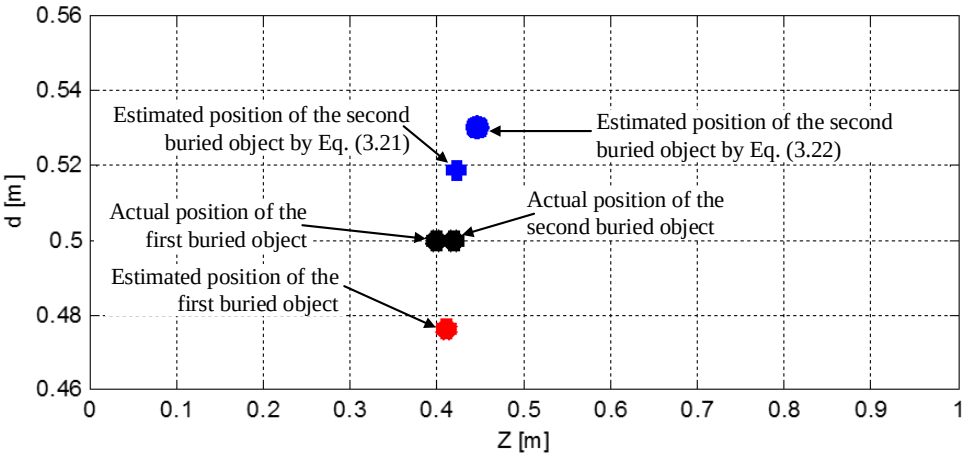

(b)

Figure 3.13: Two buried objects are close to each other; the traveling time changes according to the device's position (a) and the estimated positions of the buried objects by the CFST (b).

m, 0.15 m) with a movement step of 1 cm. The movement distance of the second object from the first object is estimated by the CFST. The error of estimating the movement distances of the second buried object is indicated in Fig. 3.14. It can be seen that when the traveling time

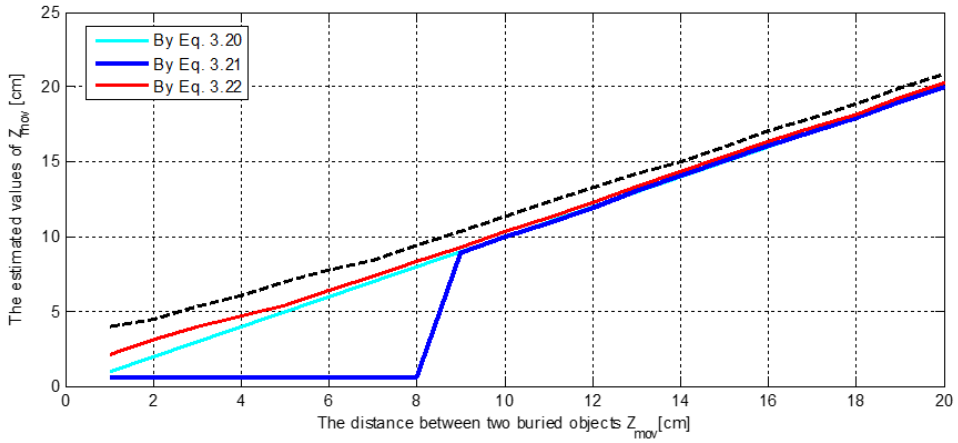

(a)

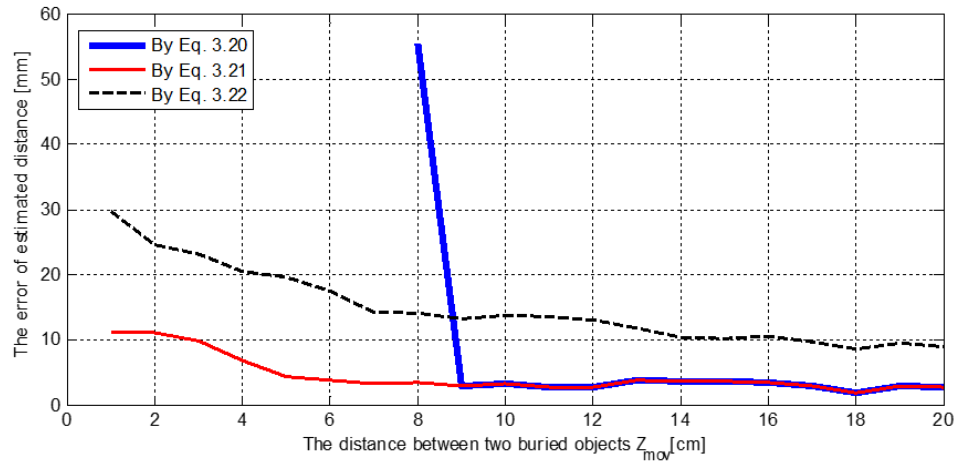

(b)

Figure 3.14: The estimated values (a) and the errors (b) according to the movement of the second buried object.

is calculated by Eq. (3.20), it is impossible to distinguish two buried objects with the distance between them less than or equal to 8 cm (de-

noted by the blue dash with Z_{mov} from 1 cm to 8 cm in Fig. 3.14). This can be explained by the correlation function shapes as illustrated in Figs. 3.9 and 3.10. Accordingly, when the deviation between traveling times from two buried objects less than a half of normalization time T_p, the received signals $r_1(t)$ and $r_2(t)$ overlap, thus the correlation function of these signals gets the maximum value at the same traveling time with the correlation function of $r_1(t)$. Hence, Eq. (3.20) gives an unique traveling time value, and two objects could be considered as a single object. Furthermore, the received signals are completely separated when the deviation between traveling times is greater or equal to a half of normalization time T_p. This means that, to distinguish the two objects, the smallest distance between two buried objects denoted by Z_{sma} ($\min\{Z_{mov}\}$) is derived from the following formula.

$$\frac{T_P}{2} = \frac{\sqrt{d_{ob1}^2 + Z_{sma}^2}}{V} - \frac{d_{ob1}}{V}. \tag{3.25}$$

Here, for simplicity, the transceiver is assumed to be located at $Z_{De} = 0.3$ m, and d_{ob1} is the depth of the first object. From Eq. (3.25), Z_{sma} is determined as:

$$Z_{sma} = \sqrt{\left(\frac{T_P \times V}{2}\right)^2 + d_{ob1} \times T_P \times V}, \tag{3.26}$$

with $d_{ob1} = 0.15$ m and the parameters T_p, c, and ε as listed in Table 3.1, $Z_{sma} = 8.2$ cm.

So at a depth of 0.15 m, when using Eq. (3.20) to determine traveling time, two objects are distinguished from each other when the distance between them is greater than or equal to 9 cm. Meanwhile, with the proposed method, the traveling time is determined using Eqs. (3.21) and

(3.22), as indicated in Figs. 3.9 and 3.10, these objects are completely distinguishable even if the distance between them is 1 cm with an average error of 0.45 cm (Eq. (3.21) is used) and 1.5 cm (Eq. (3.22) is used). When the distance between two objects is greater than Z_{sma}, the received signals $r_1(t)$ and $r_2(t)$ are non-overlapping, so the estimation results by Eqs. (3.21) and (3.20) have the same value. Thus with the proposed CFST method, two buried objects can be fully distinguished when the distance between them is close to the possible resolution of the system ($\Delta r = 2.1$ cm). For comparison, as reported in [61], the buried pipes can be located with a range resolution of 10 cm at a depth 0.5 m by using wide band chaotic ground penetrating radar in the dry sand medium. Using the Eq. (3.26) for dry sand with ε of 2.5 and d_{ob1} of 0.5 m, the value of Z_{sma} is 16.7 cm, which is the range resolution when using Eq. (3.20). However, using Eqs. (3.21) and (3.22), the range resolution can be reduced to the value compared with the theoretical resolution of the system.

Figs. 3.15 and 3.16 indicate the results of the CFST with three buried objects in different directions relative to the motion of the transceiver. Accordingly, the position of the first buried object and the relative permittivity of the environment are determined at first, then, the location of the second object, and the third object is located by CFST method. If there are more buried objects in the environment, each next buried object will be located in turn as the way to determine these three objects.

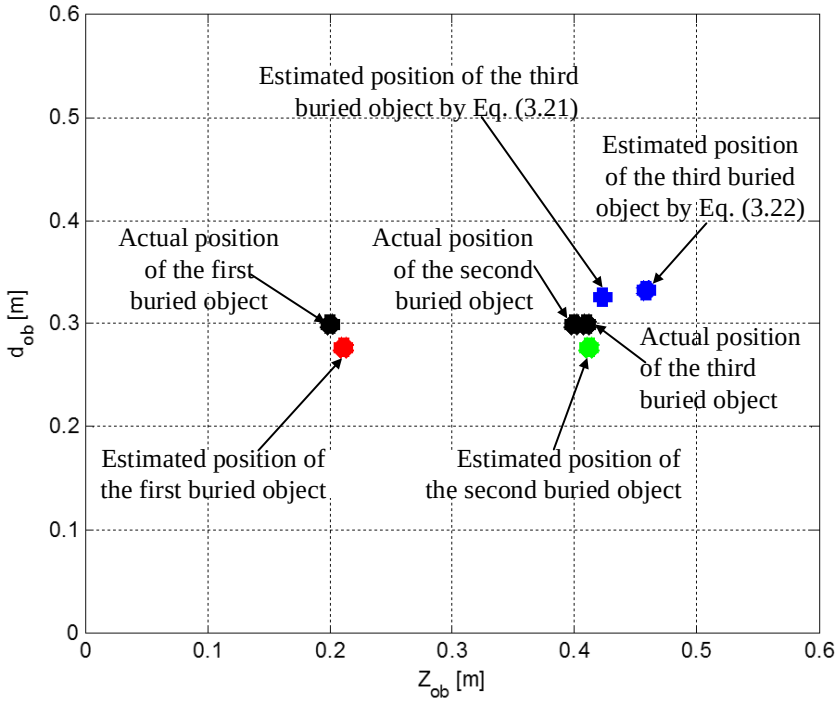

Figure 3.15: The actual and estimated locations of multi-buried objects by the CFST.

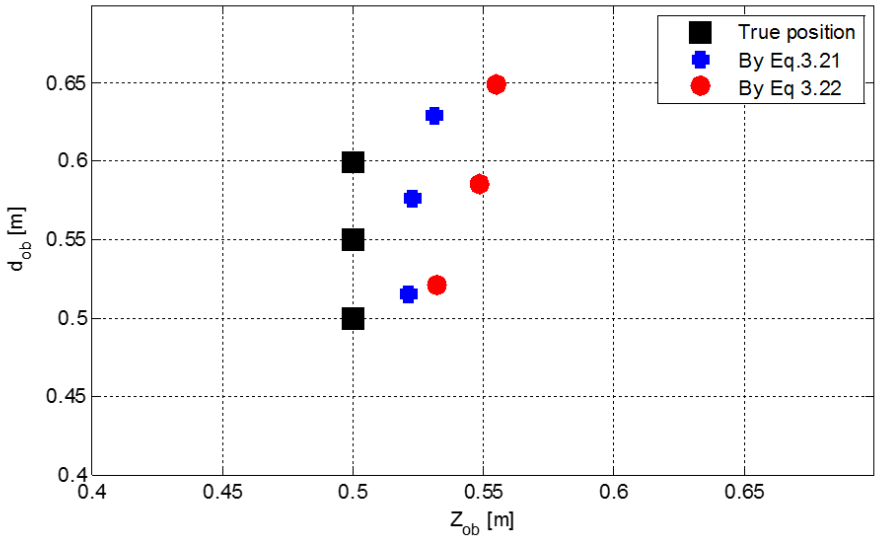

Figure 3.16: The actual and estimated locations of three buried objects placed in a straight line together with the transceiver by the CFST.

3.3. A proposed method of positioning multi-buried objects in the heterogeneous environments

3.3.1. System model

A positioning system in a heterogeneous environment is illustrated in Fig. 3.17. Similarly in the case of a single buried object, the location of each buried object is defined in the 2-D space via the horizontal parameter of Z_{ob} and the buried depth of d_{ob}.

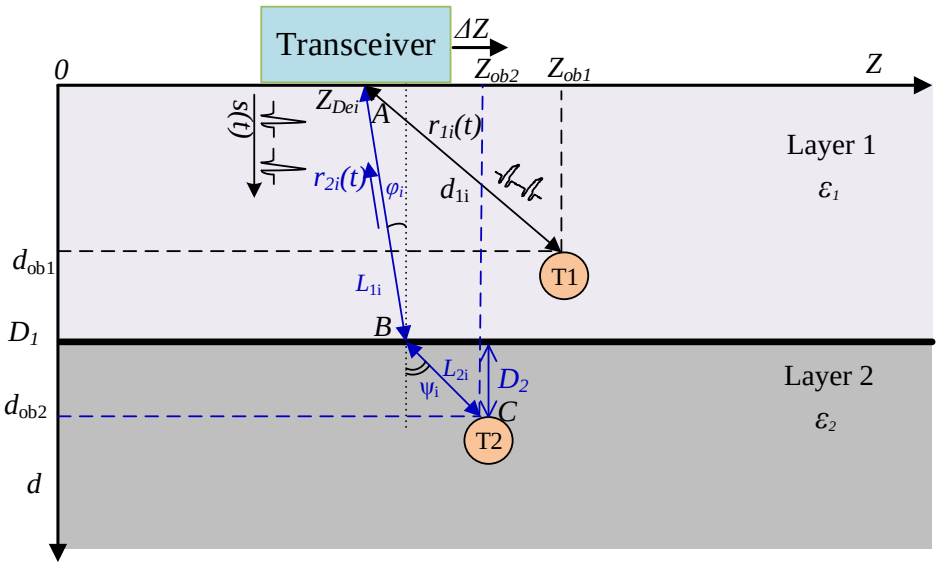

Figure 3.17: System model for positioning multi-buried objects in the heterogeneous environment.

The transmission medium has two layers with the relative permittivities of ε_1 and ε_2, respectively. The signal $s(t)$ passes through the first layer, partly reflected at the boundary, the rest is transmitted to the second layer, reflected at the second buried object, and returned to the transceiver according to the direction $C \rightarrow B \rightarrow A$. The incidence and refraction angles when the device is at position Z_{Dei} are denoted by φ_i

and ψ_i, respectively. To locate the position of 'T1', 'T2', the values of $Z_{ob1,2}$, $d_{ob1,2}$, $\varepsilon_{1,2}$, and D_1 need to be calculated.

Here, IR-UWB signal is mainly used, the modulated UWB signals (TH-BPSK and TH-PPM UWB) are used for comparison. With the system model shown in Fig. 3.17, the signals reflected from the first buried object, the boundary and the second buried object at the i^{th} displacement of the device have the following forms.

$$r_{1i}(t) = A_1(d_{1i})s(t - \tau_{1i}) + n_1(t), \tag{3.27}$$

$$r_{21i}(t) = A_1(L_{1i})A_{21}s(t - \tau_{21}) + n_{21}(t), \tag{3.28}$$

$$r_{22i}(t) = A_2(L_{2i})(1 - A_{21})s(t - \tau_{22}) + n_{22}(t), \tag{3.29}$$

where A_1, A_2 are the attenuation factors relative to the distance of the environment with Layer 1 and Layer 2, respectively; A_{21} is the reflection factor from the boundary between two layers; $n(t)$ is AWGN. At the i^{th} displacement of the transceiver, d_{1i}, L_{1i} are the propagation distances from the device to the first buried object, and the boundary, and L_{2i} is propagation distance from the boundary to the second buried object, respectively.

The distance from the device to the buried objects:

$$d_{1i} = \frac{1}{2}V_1\tau_{1i}, \tag{3.30}$$

$$d_{2i} = L_{1i} + L_{2i}, \tag{3.31}$$

where V_i is the wave velocity in the i^{th} layer of the environment.

3.3.2. Positioning method

In heterogeneous transmission environments, with the different layers' properties, the received signals are ones reflected from the buried object and from the boundary between the layers. Hences, the detection and separation of the reflected signals are very complicated. The reflected signals are easier to be detected when they have the different times of arrival. Therefore, to change the time of arrival of the reflected signals and to increase the accuracy of detecting them, a method of shifting transmitted pulses with UWB signal named UWB-PST (UWB Pulse Shifting Technique) is proposed to locate multi-buried objects in heterogeneous environments. Accordingly, the i^{th} pulse in the sequence of N_p transmitted pulses is delayed by $i \times T_r/N_p$, where T_r is the repetitive period.

The transmitted signal in Eq. (2.1) is rewritten in the UWB-PST as follows.

$$s_{IRs}(t) = \sqrt{P}\sum_{i=0}^{N_p} g(t - iT_r - \frac{iT_r}{N_p}), \tag{3.32}$$

which is similar to the forms of TH-BPSK and TH-PPM signals. The traveling time is determined according to the correlation values of N_p pulses as follows.

$$\tau = \frac{1}{N_p}\sum_{i=0}^{N_p}\tau_i = \frac{1}{N_p}\sum_{i=0}^{N_p} Arg\max_{x}\int_{-\infty}^{\infty} r_i\left(t - \frac{iT_r}{N_p}\right)\omega(t-x)dt, \tag{3.33}$$

where $r_i(t)$ is the received signal of the i^{th} pulse. With the estimated values of traveling time from the device to the buried object, the location of the object can be determined by LMF. In Fig. 3.17, to locate the

position of buried objects 'T1' and 'T2', the device is moved along the Z direction and emits a sequence of shifted pulses after every movement step of ΔZ. The parameters ε_1, Z_{ob1}, d_{ob1}, D_1, ε_2, Z_{ob2}, d_{ob2} are estimated based on the traveling time values τ_{1i}, τ_0, τ_{2i} and the position Z_{Dei} of the device. The relationship between the system parameters are expressed in the following equations.

$$\tau_{1i} = 2\frac{\sqrt{\varepsilon_1\Big(d_{ob1}^2 + (Z_{Dei} - Z_{ob1})^2\Big)}}{c}, \tag{3.34}$$

$$\tau_0 = 2\frac{D_1\sqrt{\varepsilon_1}}{c}, \tag{3.35}$$

$$\tau_{2i} = 2\Big(\frac{L_{1i}}{V_1} + \frac{L_{2i}}{V_2}\Big), \tag{3.36}$$

$$\sqrt{\varepsilon_1} \times sin\varphi_i = \sqrt{\varepsilon_2} \times sin\psi_i. \tag{3.37}$$

where $Z_{Dei} = i\Delta Z$ is the position of device at the i^{th} moving times. To simplify the representation of the parameters, the geometry of the system model in the Fig. 3.17 is illustrated in Fig. 3.18. The relationship of the parameters in Fig. 3.18 is described by the following expressions.

$$x + y = |Z_{ob2} - Z_{Dei}|, \tag{3.38}$$

$$\frac{x}{\sqrt{D_1^2 + x^2}} = \Gamma.\frac{D_2}{\sqrt{D_2^2 + y^2}}, \tag{3.39}$$

$$\Gamma = \frac{\sqrt{\varepsilon_2}}{\sqrt{\varepsilon_1}}, \tag{3.40}$$

$$\tau_{2i} = 2\Big(\frac{L_{1i}}{V_1} + \frac{L_{2i}}{V_2}\Big). \tag{3.41}$$

Let $b_1 = |Z_{ob2} - Z_{Dei}|$, Eq. (3.37) is equivalent to

$$x^4 - 2b_1x^3 + (D_2^2 + b_1^2 - \Gamma^2D_2^2)x^2 - \Gamma^2D_1^2D_2^2 = 0. \tag{3.42}$$

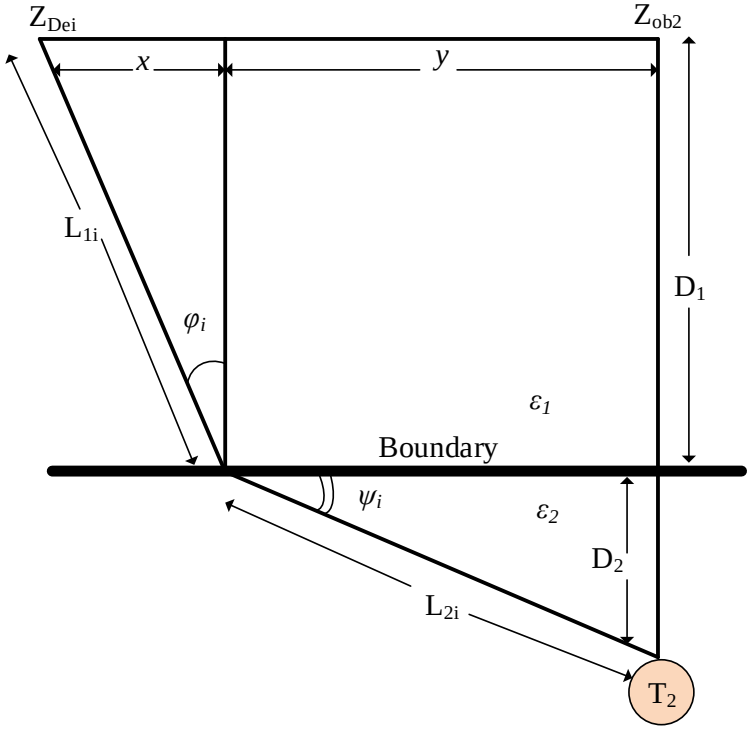

Figure 3.18: The geometry of the system model in the Fig. 3.17.

The Eq. (3.42) is rewritten as:

$$x^4 - 2b_1x^3 + b_2x^2 + b_3 = 0, \tag{3.43}$$

where $b_2 = (D_2^2 + b_1^2 - \Gamma^2 D_2^2)$, $b_3 = -\Gamma^2 D_1^2 D_2^2$. Solving Eq. (3.43) with x by Ferrari method [96], x is received as a positive solution, and given by:

$$x = \frac{b_1}{2} + S + \frac{1}{2}\sqrt{-4S^2 - 2p - \frac{q}{S}}, \tag{3.44}$$

where:

$$p = b_2 - \frac{3}{2}b_1^2, q = b_1^3 + b_1 b_2, \tag{3.45}$$

$$S = \frac{1}{2}\sqrt{-\frac{2}{3}p + \frac{1}{3}\left(Q + \frac{\Delta_0}{Q}\right)}, \tag{3.46}$$

$$Q = \sqrt[3]{\frac{\Delta_1 + \sqrt{\Delta_1^2 - 4\Delta_0^3}}{2}}, \tag{3.47}$$

$$\Delta_0 = b_2^2 + 12b_3, \tag{3.48}$$

$$\Delta_1 = 2b_2^3 + 108b_1^2 b_3 - 72b_2 b_3. \tag{3.49}$$

From Eqs. (3.39) and (3.45), the traveling time of the reflected signal from the second buried object is presented in the following formula.

$$\tau_{2i} = 2\left(\frac{\sqrt{\varepsilon_1\left(D_1^2 + x^2\right)}}{c} + \frac{\sqrt{\varepsilon_2\left[D_2^2 + \left(|Z_{ob2} - Z_{Dei}| - x\right)^2\right]}}{c}\right). \tag{3.50}$$

According to the LMF estimation method presented in the Section 3.1.1, the parameters of the model are calculated such that the deviation function in Eqs. (3.51) and (3.50) reaches the minimum value.

$$E_1 = \sum_{i=1}^{M}[\tau_{1i} - f_1(Z_{Dei})]^2, \tag{3.51}$$

$$E_2 = \sum_{i=1}^{M}[\tau_{2i} - f_2(Z_{Dei})]^2, \tag{3.52}$$

where M is the number of movements of transceiver. In Eq. (3.51), E_1 is a function of variables ε_1, Z_{ob1} and d_{ob1}, and in Eq. (3.50), E_2 is a function of variables ε_2, Z_{ob2} and D_2. The values of τ_{1i}, τ_0 and τ_{2i} are estimated from the correlation function values, and $f_1(Z_{Dei})$ and $f_2(Z_{Dei})$

are respectively computed:

$$f_1(Z_{Dei}) = 2\frac{\sqrt{\varepsilon_1\left(d_{ob1}^2 + (Z_{Dei} - Z_{ob1})^2\right)}}{c}, \tag{3.53}$$

$$f_2(Z_{Dei}) = 2\left(\frac{\sqrt{\varepsilon_1\left(D_1^2 + x^2\right)}}{c} + \frac{\sqrt{\varepsilon_2\left[D_2^2 + \left(|Z_{ob2} - Z_{Dei}| - x\right)^2\right]}}{c}\right). \tag{3.54}$$

The LMF algorithm is implemented to calculate the parameters ε_1, d_{ob1}, and Z_{ob1} using Eqs. (3.49) and (3.51). In addition, as seen in Fig.

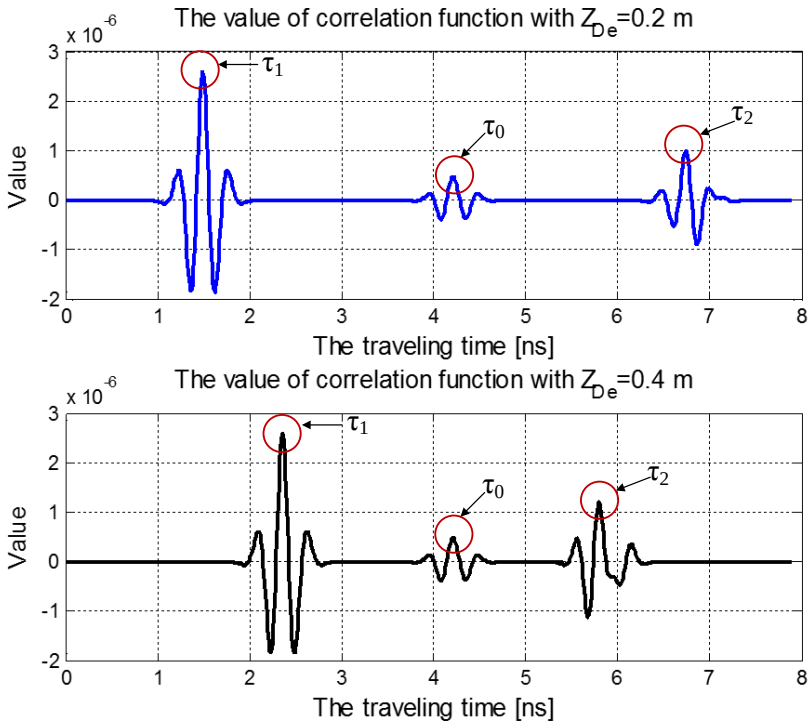

Figure 3.19: The correlation shapes of received signals in the IR-UWB system as described in Fig. 3.17 with different positions of the device.

3.19 and Eq. (3.33), the value of D_1 and therefore the value of τ_0 are constant when the device is moved, so with the estimated values of ε_1 and τ_0, D_1 is completely determined.

With the estimated values of ε_1 and D_1, the LMF algorithm is again applied to estimate the values of ε_2, D_2 and Z_{ob2} using Eqs. (3.50) and (3.52). The depth of the second buried object is $d_{ob2} = (D_1 + D_2)$.

3.3.3. Numerical results and comparisons

The UWB-PST is evaluated in terms of the errors of determining transmission distances in a well-known homogeneous medium and locating multi-buried objects in a heterogeneous medium.

The homogeneous environment is assumed to be dry sand with the relative permittivity of $\varepsilon = 2.5$, the parameters of an example UWB system are listed in Table 3.1 and Table 3.3, the buried objects move within a distance of 0-1 m on the d direction. The performance of conventional IR-UWB, TH-BPSK, TH-PPM UWB and UWB-PST are indicated in Fig. 3.20.

Table 3.3: Simulation parameters [2], [3].

Parameter	**Notation**	**Value**
Center frequency, Bandwidth	$f_c, \Delta F$	6.85 GHz, 3.5 GHz
Impulse Width	PW	0.7 ns
Time normalization factor	μ_p	0.2877 ns
Time shift of PPM	T_{PPM}	0.2 ns
Chip Width	T_c	0.9 ns
Number of pulses	N_p	100
Movement step of the device	ΔZ	0.1 m

As seen, with the same system parameters, the TH-BPSK and PPM UWB give smaller errors than the IR-UWB system. The UWB-PST outperforms the conventional with the mean relative error about 1.9 % with shifted-TH-BPSK, 2.6 % with shifted-TH-PPM, and 3.2 % with

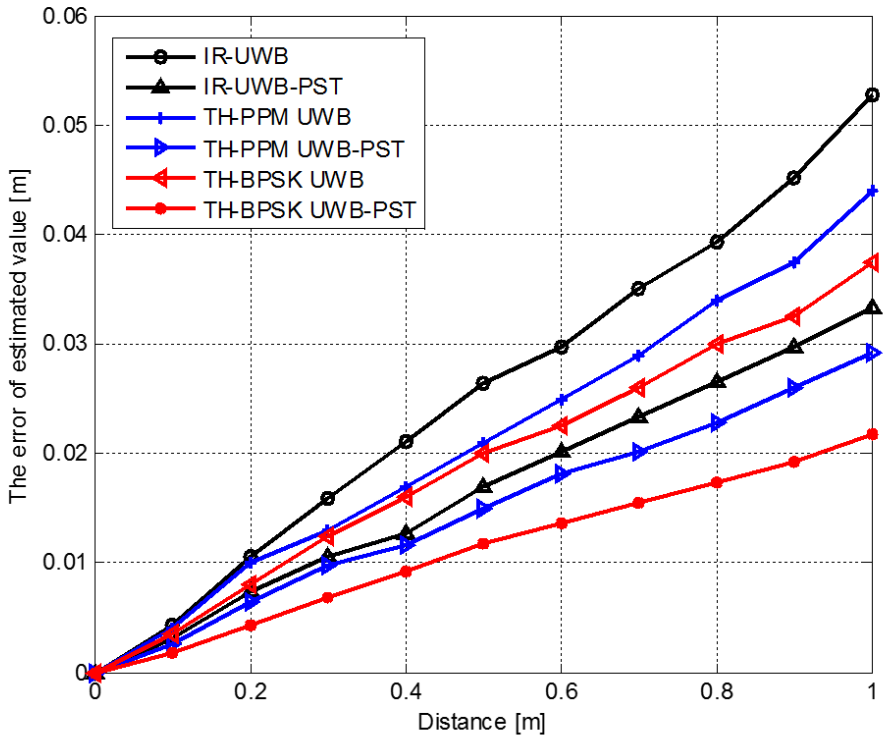

Figure 3.20: The errors of estimated values of IR, TH-BPSK, TH-PPM UWB and proposed systems.

shifted-IR UWB. While, with conventional IR-UWB, TH-PPM UWB and TH-BPSK, the values of average relative errors are 4.8 %, 4%, and 3.5 %, respectively. These results can be explained from the Eqs. (3.2), (3.4), (3.32), and (3.33), when UWB pulses are modulated by TH code, the detection of received pulses is better than that of the IR system. The antipodal BPSK modulated pulses also provide better detection in comparison with the PPM modulated pulses. In addition, the transmitted pulses are shifted by a specific time of $(i \times T_r/N_p)$, which helps to detect incoming reflected signals more accurately. Because, by changing the transmitted time of the pulses, there is a reflected pulse with the

traveling time closest to the actual propagation time value.

To determine the relative permittivity and location of the buried objects, the transceiver is moved from position 0, in the Z-axis direction (as illustrated in Fig. 3.17). At each movement step $\Delta Z = 10$ cm, the transceiver emits a sequence of N_p pulses using UWB-PST, receives the reflected signals, and calculates the traveling time of signals from the object 'T1', boundary with the depth of D_1 and from the object 'T2'. After that, the LMF algorithm is used to determine the location of those buried objects. Table 3.4, Figs. 3.21 and 3.22 indicate the results for estimating the model parameters.

Table 3.4: Estimated results.

Parameter	Actual value	By IR-UWB	By TH-PPM	By TH-BPSK	By UWB-PST IR-UWB	By UWB-PST TH-PPM	By UWB-PST TH-BPSK
ε_1	2.5	3.0132	2.8687	2.6462	2.631	2.6201	2.3415
Z_{ob1} [m]	0.4	0.3658	0.3795	0.3806	0.3818	0.3838	0.4146
d_{ob1} [m]	0.2	0.2395	0.1813	0.2270	0.2160	0.1883	0.2058
D_1 [m]	0.4	0.4282	0.4273	0.4231	0.3805	0.4187	0.4153
ε_2	4.5	4.2316	4.2852	4.3214	4.3106	4.3683	4.4125
Z_{ob2} [m]	0.6	0.5013	0.5248	0.5373	0.5487	0.5521	0.6307
d_{ob2} [m]	0.6	0.6787	0.5483	0.6418	0.6358	0.5695	0.6263

The parameters ε_1, Z_{ob1} and d_{ob1} are computed at first, then D_1 is determined based on τ_0 and $\widehat{\varepsilon_1}$; then, with τ_0 and τ_2, the parameters ε_2, Z_{ob2} and d_{ob2} are also estimated. Fig. 3.21 shows the curves of the estimated traveling time according to the device position (see Eq. (3.34)) for the first buried object ('T1'), Fig. 3.22 shows the locations estimated by the UWB-PST. It is similar to those shown in Fig. 3.20, the estimated results of TH-BPSK-UWB-PST have the highest accuracy among the compared systems. For comparison, as reported in [3], the average

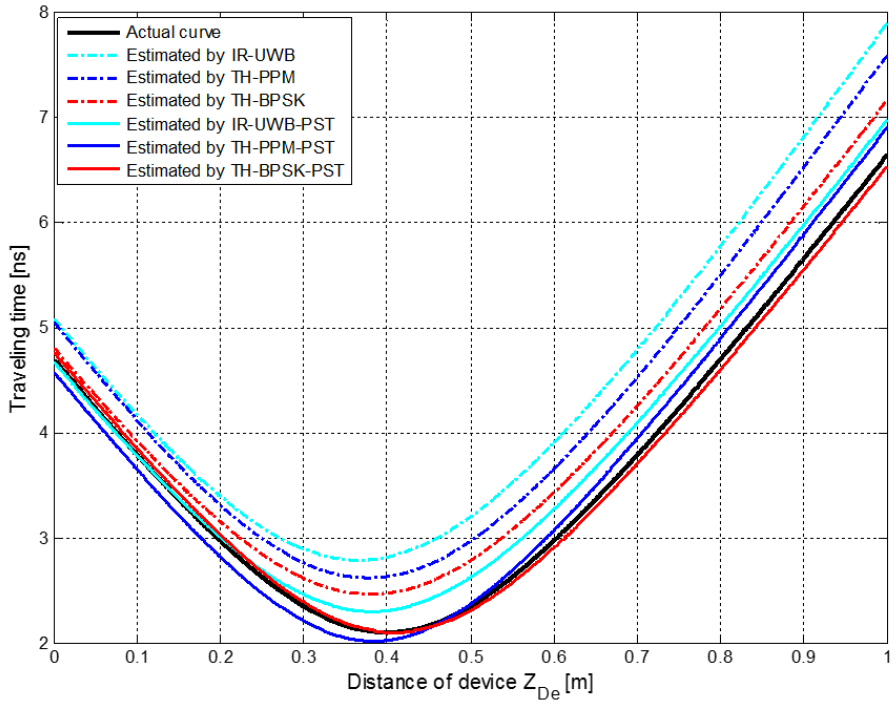

Figure 3.21: The curves of traveling time according to the position of transceiver.

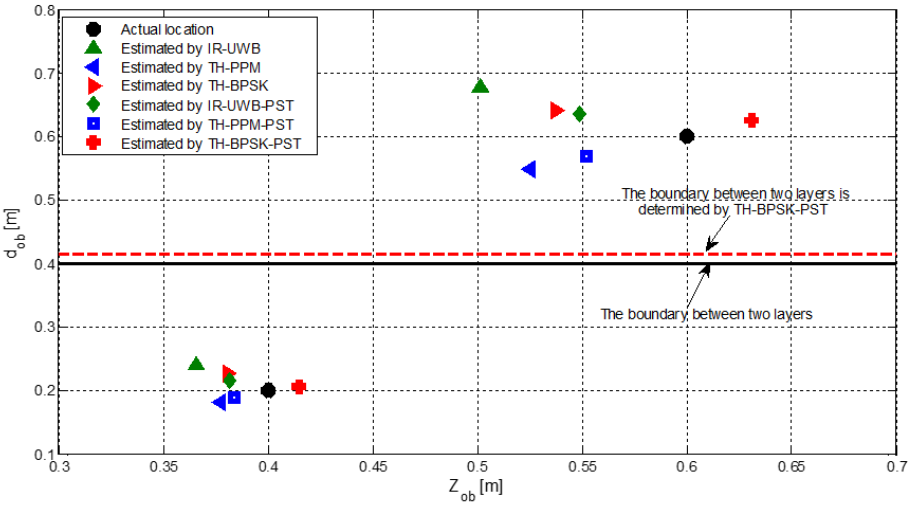

Figure 3.22: The location of buried objects estimated by UWB-PST.

estimate value of ε_1 by the MSE method is 2.76. Moreover, the evaluation is based on the mean absolute error of the estimated distance

between different methods indicated in Table 3.5. It can be seen that the distance error of the TH-BPSK UWB-PST is smaller than the others. This reason can be explained that the conventional methods based on processing GPR images (Multiresolution Monogenic Signal Analysis [97], Wide-band chaotic [61]) have problems with nearby and tangent hyperbolas (when buried objects are close) and with background noise. Therefore, the distance error of the proposed UWB-PPM-ATS and TH-BPSK-UWB-PST methods is smaller than in the conventional methods. In the UWB-CFST, the error mainly depends on the determination of the correlation function's peak, so the accuracy of this method is less than that of the power spectral density [84] based approach.

Table 3.5: The comparison of results.

Method used in GPR system	Distance Error [cm]
The Multiresolution Monogenic Signal Analysis [97]	5.8
Wideband chaotic [61]	10
The power spectral density [84]	2.03
UWB-PPM-ATS	2.86
UWB-CFST	3.52
TH-BPSK-UWB-PST	1.85

3.4. Summary

In this chapter, the methods used to locate the buried objects by the correlation function separation technique, called CFST and pulse shifting technique, named UWB-PST, for UWB systems are proposed. Our analysis indicates that, based on the values of the correlation function of the received UWB signals and the nonlinear estimation method LMF, the characteristics of the environment and the location of buried

objects can be determined. The CFST method may be applied to locate the single buried object, and multi-buried objects are close to each other. In addition, the accuracy of positioning multi-buried objects in the heterogeneous medium can be improved by using the UWB-PST. The performance of the UWB systems is assessed by positioning errors. The proposed methods have significantly improved the accuracy of locating buried objects. However, the environment under consideration is limited as the dry medium, and has two layers. The results of this chapter are published in [J3], [J4], [J5].

CONCLUSIONS AND SUGGESTIONS FOR FUTURE STUDIES

This section summarizes the contributions of the thesis and presents some open problems for future studies.

A. Conclusions

With the ultra-wide bandwidth and good material penetration, the UWB signal is a potential candidate for non-destructive testing systems, locating buried object, etc. In terms of ranging and locating, the UWB system is more powerful than others. The main advantages of UWB systems are the usage of ultra-short pulses, either for communication or for ranging systems. The use of ultra-short pulses of the UWB system in positioning can provide an accuracy of centimeter-level, which is higher than in the NB system. Besides, the UWB wireless positioning cost is relatively cheap.

The thesis presented the essential contents of UWB technology used in measuring distance and positioning buried objects using non-destructive techniques. Based on the analysis of the potential applications of the UWB systems, the dissertation has the following main contributions.

- Distance measuring techniques in free space such as RSSI, TOA, and the method of changing the impulse width, and the length of PN sequence are proposed for determining the penetration depth of

penetrating UWB systems [C1], [J1]. These researches are applied to the homogeneous environment.

- A novel CFST combined with LFM algorithm method for locating nearby buried objects in the homogeneous medium is proposed to improve the accuracy and resolution in determining distances and locating buried objects. The CFST can be used to locate and distinguish the adjacent buried objects and improve the resolution of the penetrating systems [J5].
- The UWB-PPM-ATS [J4] and UWB-PST [J3] are introduced for locating the multi-buried objects in the heterogeneous medium. By those methods, the positioning accuracy is significantly improved.

Our proposed methods are different from the existing methods in four ways. Firstly, the bandwidth of the used UWB signals is adaptively chosen according to the investigated distance. Secondly, using UWB-PPM-ATS with the additional time shifts are selected following the used Gaussian impulse shapes. With this technique, the accuracy of positioning a single buried object in a multi-layer medium is significantly improved. Thirdly, the objects buried adjacent to each other in a single-layer medium are distinguished, and located using analysis of the correlation function of the received signal in IR-UWB system. Finally, the multi-buried objects in a heterogeneous environment are located by shifting the position of the transmitted pulse with different movements.

The performance of proposed methods is assessed based on positioning errors calculated by using Matlab simulations. The simulation results

show that with the proposed UWB signal processing methods, the accuracy and resolution of the UWB systems are significantly improved. However, the dissertation still exists some limitations. Fist, due to the rapid attenuation of the UWB signals, the UWB penetration systems operate well in a short range and dry environment. Second, the surveyed environments must have some certain assumptions. And the computational complexity is higher when the positioning accuracy is increased.

B. Future Studies

Although the penetrating UWB systems were studied widely in the literature, there are still several possible open problems which require further investigations in order to have a full understanding about their applicability as follows.

- Developing identification algorithms used for buried object based on UWB technology: Building a sample set of reflected signals from some typical buried object shapes such as round, square, rectangular cylinders, etc; constructing a neural network model, optimizing the number of hidden layers of the model to training with sample set, and appling it to real identification problems.

- Building algorithm of positioning simultaneously many buried objects in heterogeneous environments.

- Locating the moving objects using penetration UWB systems by generating an adaptive reference waveform at the receiver side.

PUBLICATIONS

[J1] **N. T. Huyen**, P.T.Hiep, V.V.Son, D.D.Ha, "A variable impulse width method for improving the ranging accuracy of IR-UWB penetrating systems," *Journal of Science and Technology*, No.196, pp.103-114, Feb., 2019.

[J2] P.T.Hiep,**N.T.Huyen**, "Locating the buried object in the non-destructive structures using TH-BPSK UWB system," *Journal of Science and Technology*, No.198, pp.87-97, May., 2019.

[J3] **N.T.Huyen**, D.D.Ha, and P.T.Hiep, "Buried Objects Detection in Heterogeneous Environment using UWB Systems Combined with Curve Fitting Method," *ICT Express Journal, (SCIE, Q1, IF=4.317, SJR=0.73)*, Vol. 6, Issue 4, Dec. 2020, pp. 348-352, doi: https://doi.org/10.1016/j.icte.2020.06.006.

[J4] **N.T.Huyen**, N.L.Cuong, P.T.Hiep, "Proposal of UWB-PPM with Additional Time Shift for Positioning Technique in Non-destructive Environments," *Applied Sciences Journal (ISSN 2076-3417), (SCI-ISI, Q1, IF= 2.679, SJR=0.44)*, vol. 10, Issue 17, 6011, 9/2020, doi: https://doi.org/10.3390/app10176011.

[J5] **N.T.Huyen**, D.D.Ha, P.T.Hiep, "Positioning the Adjacent Buried Objects Using UWB Technology Combine with Levenberg-Marquardt

Algorithm," *Advances in Electrical and Electronic Engineering Journal, (Scopus, Q3, IF= 0.93, SJR=0.23)*, vol. , no. , pp., 20xx.(Under Review).

[C1] **Nguyen Thi Huyen**, Pham Thanh Hiep, "Application of RSSI to ground penetrating radar using ultra wideband technology," *International Conference on Advanced Technologies for Communications (ATC) 2018*, .137-141, Oct., 2018 (Scopus).

[C2] **Nguyen Thi Huyen**, Pham Thanh Hiep, "Proposing adaptive PN sequence length scheme for testing non-destructive structure using DS-UWB," *The 3rd International Conference on Recent Advances in Signal Processing, Telecommunications & Computing (SigTelCom) 2019*, pp.10-14, Mar., 2019.

BIBLIOGRAPHY

[1] S. Gezici and H. V. Poor, "Position estimation via ultra-wide-band signals," *Proceedings of the IEEE*, vol. 97, no. 2, pp. 386–403, 2009.

[2] B. Hu and N. C. Beaulieu, "Accurate evaluation of multiple-access performance in TH-PPM and TH-BPSK UWB systems," *IEEE Transactions on Communications*, vol. 52, no. 10, pp. 1758–1766, 2004.

[3] L. Li, A. E.-C. Tan, K. Jhamb, and K. Rambabu, "Buried object characterization using ultra-wideband ground penetrating radar," *IEEE Transactions on Microwave Theory and Techniques*, vol. 60, no. 8, pp. 2654–2664, 2012.

[4] Y. Gao, M. Brennan, P. Joseph, J. Muggleton, and O. Hunaidi, "On the selection of acoustic/vibration sensors for leak detection in plastic water pipes," *Journal of Sound and Vibration*, vol. 283, no. 3-5, pp. 927–941, 2005.

[5] M. Brennan, P. Joseph, J. Muggleton, and Y. Gao, "The use of acoustic methods to detect water leaks in buried water pipes," *Water and Sewerage Journal*, no. 1, pp. 11–14, 2006.

[6] W. Cong and L. Zhou, "Three dimensional acoustic imaging technology of buried object detection," in *MATEC Web of Conferences*,

vol. 283. EDP Sciences, 2019.

[7] X. Li and Y. Wu, "Feature extraction for acoustic scattering from a buried target," *Journal of Marine Science and Application*, vol. 18, no. 3, pp. 380–386, 2019.

[8] I. Stoianov, L. Nachman, S. Madden, and T. Tokmouline, "PIPENETa wireless sensor network for pipeline monitoring," in *Proceedings of the 6th international conference on Information processing in sensor networks*, 2007, pp. 264–273.

[9] M. Choi, K. Kang, J. Park, W. Kim, and K. Kim, "Quantitative determination of a subsurface defect of reference specimen by lock-in infrared thermography," *Ndt & E International*, vol. 41, no. 2, pp. 119–124, 2008.

[10] S. Saha, S. Mukhopadhyay, U. Mahapatra, S. Bhattacharya, and G. Srivastava, "Empirical structure for characterizing metal loss defects from radial magnetic flux leakage signal," *Ndt E International*, vol. 43, no. 6, pp. 507–512, 2010.

[11] D. Rifai, A. N. Abdalla, R. Razali, K. Ali, and M. A. Faraj, "An eddy current testing platform system for pipe defect inspection based on an optimized eddy current technique probe design," *Sensors*, vol. 17, no. 3, p. 579, 2017.

[12] B. Park, J. Kim, J. Lee, M.-S. Kang, and Y.-K. An, "Underground object classification for urban roads using instantaneous phase anal-

ysis of ground-penetrating radar (GPR) data," *Remote Sensing*, vol. 10, no. 9, p. 1417, 2018.

[13] M. Salucci, L. Tenuti, L. Poli, and A. Massa, "Buried object detection and imaging through innovative processing of GPR data," in *2017 11th European Conference on Antennas and Propagation (EUCAP)*. IEEE, 2017, pp. 1703–1706.

[14] Q. Hoarau, G. Ginolhac, A. M. Atto, and J.-M. Nicolas, "Robust adaptive detection of buried pipes using GPR," *Signal Processing*, vol. 132, pp. 293–305, 2017.

[15] P. Chaturvedi and R. G. Plumb, "Electromagnetic imaging of underground targets using constrained optimization," *IEEE Transactions on Geoscience and Remote sensing*, vol. 33, no. 3, pp. 551–561, 1995.

[16] M. E. Requena-Pérez, A. Albero-Ortiz, J. Monzó-Cabrera, and A. Díaz-Morcillo, "Combined use of genetic algorithms and gradient descent optmization methods for accurate inverse permittivity measurement," *IEEE Transactions on Microwave Theory and Techniques*, vol. 54, no. 2, pp. 615–624, 2006.

[17] T. Zwick, J. Haala, and W. Wiesbeck, "A genetic algorithm for the evaluation of material parameters of compound multilayered structures," *IEEE Transactions on Microwave Theory and Techniques*, vol. 50, no. 4, pp. 1180–1187, 2002.

[18] G. R. Chandra, K. Rajiv, and B. B. Rao, "Detecting radius of pipe in GPR images and comparing with 3D synthetic data," in *2019 Fifth*

International Conference on Image Information Processing (ICIIP). IEEE, 2019, pp. 7–10.

[19] Y. Guzel, M. A. Alper, I. Ozturk, and A. Nassib, in *2017 IEEE International Conference on Power, Control, Signals and Instrumentation Engineering (ICPCSI)*. IEEE, 2017, pp. 152–156.

[20] C. A. Balanis, *Antenna theory: analysis and design*. John wiley & sons, 2016.

[21] S. Gezici, Z. Sahinoglu, A. F. Molisch, H. Kobayashi, and H. V. Poor, "A two-step time of arrival estimation algorithm for impulse radio ultra wideband systems," in *2005 13th European Signal Processing Conference*. IEEE, 2005, pp. 1–6.

[22] F. FCC, "Report and order 02-48," 2002.

[23] W. Webb, "Ultra wideband-the final few regulatory processes," 2006.

[24] S. A. Mitilineos, D. M. Kyriazanos, O. E. Segou, J. N. Goufas, and S. C. Thomopoulos, "Indoor localisation with wireless sensor networks," *Progress In Electromagnetics Research*, vol. 109, pp. 441–474, 2010.

[25] J. Xiao, Z. Liu, Y. Yang, D. Liu, and X. Han, "Comparison and analysis of indoor wireless positioning techniques," in *2011 International Conference on Computer Science and Service System (CSSS)*. IEEE, 2011, pp. 293–296.

[26] R. Mautz and S. Tilch, "Optical indoor positioning systems," in *Proceedings of the 2011 International Conference on Indoor Positioning and Indoor Navigation (IPIN)*, 2011.

[27] J. Kemper and H. Linde, "Challenges of passive infrared indoor localization," in *2008 5th Workshop on Positioning, Navigation and Communication*. IEEE, 2008, pp. 63–70.

[28] S. Gezici, Z. Tian, G. B. Giannakis, H. Kobayashi, A. F. Molisch, H. V. Poor, and Z. Sahinoglu, "Localization via ultra-wideband radios: a look at positioning aspects for future sensor networks," *IEEE Signal Processing Magazine*, vol. 22, no. 4, pp. 70–84, 2005.

[29] M. Z. Win and R. A. Scholtz, "Impulse radio: How it works," *IEEE Communications letters*, vol. 2, no. 2, pp. 36–38, 1998.

[30] S. Ingram, D. Harmer, and M. Quinlan, "Ultrawideband indoor positioning systems and their use in emergencies," in *PLANS 2004. Position Location and Navigation Symposium (IEEE Cat. No. 04CH37556)*. IEEE, 2004, pp. 706–715.

[31] I. Guvenc, S. Gezici, and Z. Sahinoglu, "Ultra-wideband range estimation: Theoretical limits and practical algorithms," in *2008 IEEE International Conference on Ultra-Wideband*, vol. 3. IEEE, 2008, pp. 93–96.

[32] X. Chen and S. Kiaei, "Monocycle shapes for ultra wideband system," in *2002 IEEE International Symposium on Circuits and Sys-*

tems. Proceedings (Cat. No. 02CH37353), vol. 1. IEEE, 2002, pp. I–I.

[33] G. T. F. De Abreu, C. J. Mitchell, and R. Kohno, "On the orthogonality of hermite pulses for ultra wideband communications systems," *rn*, vol. 1000, p. 22, 2003.

[34] D. Benedetto, *Understanding ultra wide band radio fundamentals*. Pearson Education India, 2008.

[35] X. Gao, *UWB indoor localization system*. Ph.D. dissertation, The George Washington University, 2018.

[36] M. L. Welborn, "System considerations for ultra-wideband wireless networks," in *Proceedings RAWCON 2001. 2001 IEEE Radio and Wireless Conference (Cat. No. 01EX514)*. IEEE, 2001, pp. 5–8.

[37] C. R. Nassar, F. Zhu, and Z. Wu, "Direct sequence spreading UWB systems: Frequency domain processing for enhanced performance and throughput," in *Communications, 2003. ICC'03. IEEE International Conference on*, vol. 3. IEEE, 2003, pp. 2180–2186.

[38] H. Khalesi and V. Ghods, "QPSK modulation scheme based on orthogonal gaussian pulses for IR-UWB communication systems," *Journal of Circuits, Systems and Computers*, vol. 28, no. 01, p. 1950008, 2019.

[39] D. Leon, S. Balkır, M. Hoffman, and L. Perez, "Pseudo-chaotic PN-sequence generator circuits for spread spectrum communications,"

IEE Proceedings-Circuits, Devices and Systems, vol. 151, no. 6, pp. 543–550, 2004.

[40] S. Xu, Y. Chen, and P. Zhang, "Integrated radar and communication based on DS-UWB," in *Ultra wideband and Ultrashort Impulse Signals, The Third International Conference*. IEEE, 2006, pp. 142–144.

[41] Y. Nakayama and R. Kohno, "Novel variable spreading sequence length system for improving the processing speed of DS-UWB radar," in *2008 8th International Conference on ITS Telecommunications*. IEEE, 2008, pp. 357–361.

[42] C. N. C. Ginsburg, "Evaluating global positioning system (GPS) accuracy and precision among receivers," Ph.D. dissertation, Texas Tech University, 2002.

[43] J. Yan, D. Lin, K. Tang, G. Yang, and Q. Ye, "High precision indoor positioning method based on UWB," in *International Conference on Ad Hoc Networks*. Springer, 2019, pp. 201–207.

[44] A. Taha and K. M. Chugg, "A theoretical study on the effects of interference UWB multiple access impulse radio," in *Conference Record of the Thirty-Sixth Asilomar Conference on Signals, Systems and Computers, 2002.*, vol. 1. IEEE, 2002, pp. 728–732.

[45] M. Z. Win and R. A. Scholtz, "Ultra-wide bandwidth time-hopping spread-spectrum impulse radio for wireless multiple-access commu-

nications," *IEEE Transactions on Communications*, vol. 48, no. 4, pp. 679–689, 2000.

[46] I. M. Gottlieb, *Practical RF power design techniques.* Tab Books, 1993.

[47] K. V. Finkelstein, M.I. and V. Zolotarev, *The Use of Radar Subsurface Probing in Engineering Geology.* NEDRA, Moscow. (in Russian), 1986.

[48] S. G. Kang, Y. Lee, J. Kim, D. Chong, J. Baek, and S. Yoon, "A distance measuring scheme based on repeated use of PN sequence," in *Communications (APCC), 2011 17th Asia-Pacific Conference on.* IEEE, 2011, pp. 872–874.

[49] K. M. Strohm, H.-L. Bloecher, R. Schneider, and J. Wenger, "Development of future short range radar technology," in *European Radar Conference, 2005. EURAD 2005.* IEEE, 2005, pp. 165–168.

[50] S. Hubbard, J. Peterson Jr, E. Majer, P. Zawislanski, K. Williams, J. Roberts, and F. Wobber, "Estimation of permeable pathways and water content using tomographic radar data," *The leading EDGE*, vol. 16, no. 11, pp. 1623–1630, 1997.

[51] K. Siwiak and D. McKeown, "Ultra-wideband radio technology. 2004," *John Wiley&Sons Ltd.*

[52] M. Z. Win, D. Dardari, A. F. Molisch, W. Wiesbeck, and W. Jinyun Zhang, "History and applications of UWB." Institute of Electrical and Electronics Engineers, 2009.

[53] V. Aranchuk, I. Aranchuk, B. Carpenter, and C. Hickey, "Laser Doppler multi-beam differential vibration sensor for acoustic detection of buried objects," in *Applications of Lasers for Sensing and Free Space Communications*. Optical Society of America, 2019, pp. LM4B–2.

[54] A. Gharamohammadi, F. Behnia, and A. Shokouhmand, "Machine learning based identification of buried objects using sparse whitened NMF," *arXiv preprint arXiv:1910.07180*, 2019.

[55] Y. Long, Y. Gong, Z. Xiao, and Q. Liu, "Accurate object localization in remote sensing images based on convolutional neural networks," *IEEE Transactions on Geoscience and Remote Sensing*, vol. 55, no. 5, pp. 2486–2498, 2017.

[56] J. Wang, L. Sang, and B. Li, "The detection of buried objects in shallow sea with low frequency electromagnetic waves," in *2018 OCEANS-MTS/IEEE Kobe Techno-Oceans (OTO)*. IEEE, 2018, pp. 1–6.

[57] G. Borgioli, L. Capineri, P. Falorni, S. Matucci, and C. G. Windsor, "The detection of buried pipes from time-of-flight radar data," *IEEE Transactions on Geoscience and Remote Sensing*, vol. 46, no. 8, pp. 2254–2266, 2008.

[58] X. Zhou, H. Chen, and T. Hao, "Efficient detection of buried plastic pipes by combining GPR and electric field methods," *IEEE Trans-*

actions on Geoscience and Remote Sensing, vol. 57, no. 6, pp. 3967–3979, 2019.

[59] T. Roackaway and J. A. Rivard, "Application of ground penetrating radar in the urban environment," in *Proceedings of the XIII Internarional Conference on Ground Penetrating Radar*. IEEE, 2010, pp. 1–4.

[60] H. Liu, Z. Long, B. Tian, F. Han, G. Fang, and Q. H. Liu, "Two-dimensional reverse-time migration applied to GPR with a 3-D-to-2-D data conversion," *IEEE Journal of Selected Topics in Applied Earth Observations and Remote Sensing*, vol. 10, no. 10, pp. 4313–4320, 2017.

[61] J. Li, T. Guo, H. Leung, H. Xu, L. Liu, B. Wang, and Y. Liu, "Locating underground pipe using wideband chaotic ground penetrating radar," *Sensors*, vol. 19, no. 13, p. 2913, 2019.

[62] H. Zeine, S. Ebadi, D. W. Williams, and A. Alfarra, "Techniques for determining distance between radiating objects in multipath wireless power delivery environments," Feb 6 2020, US Patent No 16/598,147.

[63] S. Sharma, A. Gupta, and V. Bhatia, "A simple modified peak detection based UWB receiver for WSN and IoT applications," in *2017 IEEE 85th Vehicular Technology Conference (VTC Spring)*. IEEE, 2017, pp. 1–6.

[64] N. B. Benotmane, S. A. Elahmar, I. Dayoub, and W. Hamouda, "Improved eigenfilter design method for channel shortening equalizer in TH-UWB," *IEEE Transactions on Vehicular Technology*, vol. 67, no. 8, pp. 7749–7753, 2018.

[65] L. Zhao and A. M. Haimovich, "Capacity of M-ary PPM ultra-wideband communications over AWGN channels," in *IEEE 54th Vehicular Technology Conference. VTC Fall 2001. Proceedings (Cat. No. 01CH37211)*, vol. 2. IEEE, 2001, pp. 1191–1195.

[66] V. Venkatesan, H. Liu, C. Nilsen, R. Kyker, and M. E. Magana, "Performance of an optimally spaced PPM ultra-wideband system with direct sequence spreading for multiple access," in *2003 IEEE 58th Vehicular Technology Conference. VTC 2003-Fall (IEEE Cat. No. 03CH37484)*, vol. 1. IEEE, 2003, pp. 602–606.

[67] J. Wu, H. Xiang, and Z. Tian, "Weighted noncoherent receivers for UWB PPM signals," *IEEE Communications Letters*, vol. 10, no. 9, pp. 655–657, 2006.

[68] J. M. Almodovar-Faria and J. McNair, "Optimal integration time for energy-detection PPM UWB systems," in *2012 IEEE Global Communications Conference (GLOBECOM)*. IEEE, 2012, pp. 4054–4059.

[69] H. B. Yin, J. A. Yang, and W. D. Wang, "A randomly permuted fourier measurement matrix for UWB-PPM signals," in *Applied Me-*

chanics and Materials, vol. 556. Trans Tech Publ, 2014, pp. 2646–2649.

[70] V. Yajnanarayana and P. Händel, "Joint estimation of TOA and PPM symbols using Sub-Nyquist sampled IR-UWB signal," *IEEE Communications Letters*, vol. 21, no. 4, pp. 949–952, 2017.

[71] M. Jabbar, "Improving PSD of PPM-IR for UWB signal using Turbo Encoder," *Ind Eng Manage S*, vol. 3, pp. 2169–0316, 2018.

[72] V. Goyal and B. Dhaliwal, "Improving ultra wideband (UWB) system by modified random combination of pulses," *Engineering Review*, vol. 38, no. 2, pp. 189–203, 2018.

[73] D. J. Daniels, "Ground penetrating radar," *Encyclopedia of RF and Microwave Engineering*, 2005.

[74] J. Blanco-Murillo, D. Lluveras, V. Y. Jiménez, J. Anaya, F. Casajús-Quirós, M. Izquierdo, J. Menéndez, M. Hernández, and A. Herrera, "Combined US and UWB-RF imaging of concrete structures for identification and location of embedded materials," *Construction and Building Materials*, vol. 152, pp. 693–701, 2017.

[75] Y. Cao, J. Labuz, and B. Guzina, "Evaluation of pavement system based on ground-penetrating radar full-waveform simulation," *Transportation Research Record*, vol. 2227, no. 1, pp. 71–78, 2011.

[76] H. H. Karim and A. M. Al-Qaissi, "Assessment of the accuracy of road flexible and rigid pavement layers using GPR," *Engineering*

and Technology Journal, vol. 32, no. 3 Part (A) Engineering, pp. 788–799, 2014.

[77] P. Dabove, V. Di Pietra, M. Piras, A. A. Jabbar, and S. A. Kazim, "Indoor positioning using ultra-wide band (UWB) technologies: Positioning accuracies and sensors' performances," in *2018 IEEE/ION Position, Location and Navigation Symposium (PLANS)*. IEEE, 2018, pp. 175–184.

[78] E. R. Santos, H. Azpurua, P. A. Rezeck, M. F. Corrêa, M. A. Vieira, G. M. Freitas, and D. G. Macharet, "Localization using ultra wideband and IEEE 802.15. 4 radios with nonlinear Bayesian filters: a comparative study," *Journal of Intelligent & Robotic Systems*, pp. 1–17, 2020.

[79] B. Mukhopadhyay, S. Sarangi, and S. Kar, "Novel RSSI evaluation models for accurate indoor localization with sensor networks," in *2014 Twentieth National Conference on Communications (NCC)*. Ieee, 2014, pp. 1–6.

[80] A. Pal, "Localization algorithms in wireless sensor networks: Current approaches and future challenges." *Netw. Protoc. Algorithms*, vol. 2, no. 1, pp. 45–73, 2010.

[81] X. Li, "Signal strength differentiation based navigation of mobile robot in wireless sensor networks," in *2013 IEEE 8th Conference on Industrial Electronics and Applications (ICIEA)*. IEEE, 2013, pp. 1908–1913.

[82] W. Xie, X. Li, and X. Long, "Underground operator monitoring platform based on ultra-wide band WSN," *International Journal of Online and Biomedical Engineering (iJOE)*, vol. 14, no. 10, pp. 219–229, 2018.

[83] Y. Qin, J. Wan, J. Yang, L. Qiao, C. Zhu, and Q. Wang, "Using spectral residual method to identification buried objects from GPR B-Scan image," in *2018 Progress in Electromagnetics Research Symposium (PIERS-Toyama)*. IEEE, 2018, pp. 1381–1385.

[84] A. Saghafi, S. Jazayeri, S. Esmaeili, and C. P. Tsokos, "Real-time object detection using power spectral density of ground-penetrating radar data," *Structural Control and Health Monitoring*, vol. 26, no. 6, p. e2354, 2019.

[85] V. H. Tang, S. L. Phung, F. H. C. Tivive, and A. Bouzerdoum, "A sparse Bayesian learning approach for through-wall radar imaging of stationary targets," *IEEE Transactions on Aerospace and Electronic Systems*, vol. 53, no. 5, pp. 2485–2501, 2017.

[86] V. H. Tang, A. Bouzerdoum, and S. L. Phung, "Wall clutter mitigation for radar imaging of indoor targets: A matrix completion approach," in *2017 21st Asia Pacific Symposium on Intelligent and Evolutionary Systems (IES)*. IEEE, 2017, pp. 116–121.

[87] M.-T. Pham and S. Lefèvre, "Buried object detection from B-scan ground penetrating radar data using Faster-RCNN," in *IGARSS*

2018-2018 IEEE International Geoscience and Remote Sensing Symposium. IEEE, 2018, pp. 6804–6807.

[88] Vo Xung Ha, Phuong Van Quang, Tran Manh Quy, Bui Thanh Hong, "Researching the solution for expanding the bandwidth of half-wavelength dipole antennas applied in ground-penetrating radar systems," *Journal of Military Science and Technology Research*, no. 74, pp. 59–64, 2021.

[89] P. Tarrío, A. M. Bernardos, and J. R. Casar, "Weighted least squares techniques for improved received signal strength based localization," *Sensors*, vol. 11, no. 9, pp. 8569–8592, 2011.

[90] H. P. Mistry and N. H. Mistry, "RSSI based localization scheme in wireless sensor networks: a survey," in *2015 Fifth International Conference on Advanced Computing & Communication Technologies*. IEEE, 2015, pp. 647–652.

[91] I. Immoreev, "Main features of UWB radars and differences from common narrowband radars," *book "Ultra wideband Radar Technology". Edited Taylor, JD; CRC Press, Boca Raton, London, New Work, Washington*, 2000.

[92] Å. Björck, *Numerical methods for least squares problems*. SIAM, 1996.

[93] I. Guvenc and Z. Sahinoglu, "Threshold-based toa estimation for impulse radio uwb systems," in *2005 IEEE International Conference on Ultra-Wideband*. IEEE, 2005, pp. 420–425.

[94] C. Kanzow, N. Yamashita, and M. Fukushima, "Withdrawn: Levenberg–Marquardt methods with strong local convergence properties for solving nonlinear equations with convex constraints," *Journal of Computational and Applied Mathematics*, vol. 173, no. 2, pp. 321–343, 2005.

[95] S. G. Soganci, Hamza and H. V. Poor, "Accurate positioning in ultra-wideband systems," *IEEE Wireless Communications*, vol. 18, no. 2, pp. 19–27, 2011.

[96] S. H. Lee, S. M. Im, and I. S. Hwang, "Quartic functional equations," *Journal of Mathematical Analysis and Applications*, vol. 307, no. 2, pp. 387–394, 2005.

[97] L. Qiao, Y. Qin, X. Ren, and Q. Wang, "Identification of buried objects in GPR using amplitude modulated signals extracted from multiresolution monogenic signal analysis," *Sensors*, vol. 15, no. 12, pp. 30 340–30 350, 2015.